

Preimplantation genetic testing for aneuploidy: a comparison of live birth rates in patients with recurrent pregnancy loss due to embryonic aneuploidy or recurrent implantation failure

Takeshi Sato¹, Mayumi Sugiura-Ogasawara^{1,*}, Fumiko Ozawa¹, Toshiyuki Yamamoto², Takema Kato³, Hiroki Kurahashi³, Tomoko Kuroda⁴, Naoki Aoyama⁴, Keiichi Kato⁴, Ryota Kobayashi⁵, Aisaku Fukuda⁵, Takafumi Utsunomiya⁶, Akira Kuwahara⁷, Hidekazu Saito⁸, Toshiyuki Takeshita⁹, and Minoru Irahara⁷

¹Department of Obstetrics and Gynecology, Graduate School of Medical Sciences, Nagoya City University, Nagoya, Japan ²Institute of Medical Genetics, Tokyo Women's Medical University, Tokyo, Japan ³Division of Molecular Genetics, Institute for Comprehensive Medical Science, Fujita Health University, Toyoake, Japan ⁴Kato Ladies Clinic, Tokyo, Japan ⁵IVF Osaka Clinic, Osaka, Japan ⁶St. Luke Clinic, Oita, Japan ⁷Department of Obstetrics and Gynecology, Tokushima University, Tokushima, Japan ⁸Center for Maternal-Fetal, Neonatal and Reproductive Medicine, National Center for Child Health and Development, Tokyo, Japan ⁹Department of Obstetrics and Gynecology, Nippon Medical School, Tokyo, Japan

*Correspondence address. E-mail: og.mym@med.nagoya-cu.ac.jp

Submitted on July 3, 2019; resubmitted on September 17, 2019; editorial decision on September 25, 2019

STUDY QUESTION: Can preimplantation genetic testing for aneuploidy (PGT-A) improve the live birth rate and reduce the miscarriage rate in patients with recurrent pregnancy loss (RPL) caused by an abnormal embryonic karyotype and recurrent implantation failure (RIF)?

SUMMARY ANSWER: PGT-A could not improve the live births per patient nor reduce the rate of miscarriage, in both groups.

WHAT IS KNOWN ALREADY: PGT-A use has steadily increased worldwide. However, only a few limited studies have shown that it improves the live birth rate in selected populations in that the prognosis has been good. Such studies have excluded patients with RPL and RIF. In addition, several studies have failed to demonstrate any benefit at all. PGT-A was reported to be without advantage in patients with unexplained RPL whose embryonic karyotype had not been analysed. The efficacy of PGT-A should be examined by focusing on patients whose previous products of conception (POC) have been aneuploid, because the frequencies of abnormal and normal embryonic karyotypes have been reported as 40–50% and 5–25% in patients with RPL, respectively.

STUDY DESIGN, SIZE, DURATION: A multi-centre, prospective pilot study was conducted from January 2017 to June 2018. A total of 171 patients were recruited for the study: an RPL group, including 41 and 38 patients treated respectively with and without PGT-A, and an RIF group, including 42 and 50 patients treated respectively with and without PGT-A. At least 10 women in each age group (35–36, 37–38, 39–40 or 41–42 years) were selected for PGT-A groups.

PARTICIPANTS/MATERIALS, SETTING, METHODS: All patients and controls had received IVF-ET for infertility. Patients in the RPL group had had two or more miscarriages, and at least one case of aneuploidy had been ascertained through prior POC testing. No pregnancies had occurred in the RIF group, even after at least three embryo transfers. Trophectoderm biopsy and array comparative genomic hybridisation (aCGH) were used for PGT-A. The live birth rate of PGT-A and non-PGT-A patients was compared after the development of blastocysts from up to two oocyte retrievals and a single blastocyst transfer. The miscarriage rate and the frequency of euploidy, trisomy and monosomy in the blastocysts were noted.

MAIN RESULT AND THE ROLE OF CHANCE: There were no significant differences in the live birth rates per patient given or not given PGT-A: 26.8 versus 21.1% in the RPL group and 35.7 versus 26.0% in the RIF group, respectively. There were also no differences in the miscarriage rates per clinical pregnancies given or not given PGT-A: 14.3 versus 20.0% in the RPL group and 11.8 versus 0% in the RIF group, respectively. However, PGT-A improved the live birth rate per embryo transfer procedure in both the RPL (52.4 vs 21.6%, adjusted OR 3.89; 95% CI 1.16–13.1) and RIF groups (62.5 vs 31.7%, adjusted OR 3.75; 95% CI 1.28–10.95). Additionally, PGT-A was shown to reduce biochemical pregnancy loss per biochemical pregnancy: 12.5 and 45.0%, adjusted OR 0.14; 95% CI 0.02–0.85 in the RPL group and 10.5 and 40.9%, adjusted OR 0.17; 95% CI 0.03–0.92 in the RIF group. There was no difference in the distribution of genetic abnormalities between RPL and RIF patients, although double trisomy tended to be more frequent in RPL patients.

LIMITATIONS, REASONS FOR CAUTION: The sample size was too small to find any significant advantage for improving the live birth rate and reducing the clinical miscarriage rate per patient. Further study is necessary.

WIDER IMPLICATION OF THE FINDINGS: A large portion of pregnancy losses in the RPL group might be due to aneuploidy, since PGT-A reduced the overall incidence of pregnancy loss in these patients. Although PGT-A did not improve the live birth rate per patient, it did have the advantage of reducing the number of embryo transfers required to achieve a similar number live births compared with those not undergoing PGT-A.

STUDY FUNDING/COMPETING INTEREST(S): This study was supported by the Japan Society of Obstetrics and Gynecology and grants from the Japanese Ministry of Education, Science, and Technology. There are no conflicts of interest to declare.

TRIAL REGISTRATION NUMBER: N/A

Key words: preimplantation genetic testing for aneuploidy/recurrent miscarriage/recurrent pregnancy loss/recurrent implantation failure/live birth rate

Introduction

Preimplantation genetic screening (PGS) by blastomere biopsy and fluorescence *in situ* hybridisation (FISH) analysis was initiated as a means of preventing miscarriages in patients with unexplained recurrent pregnancy loss (RPL, Munné *et al.*, 2005). PGS has been performed worldwide, although there has been controversy regarding whether it can improve the live birth rate and prevent miscarriage in patients with RPL or infertile patients (Mastenbroek *et al.*, 2011).

Recently, several molecular techniques, such as array comparative genomic hybridisation (aCGH), the digital polymerase chain reaction (dPCR), single-nucleotide polymorphism (SNP) array, real-time quantitative PCR (qPCR) and next generation sequencing (NGS), have been utilised for preimplantation genetic testing for aneuploidy (PGT-A) (American Society of Reproductive Medicine, 2018). Furthermore, trophectoderm (TE) biopsy of blastocysts has been found to be superior to cleavage-stage embryo biopsy (Scott Jr *et al.*, 2013a).

After the improvement of these techniques, several randomised control trials (RCT) revealed that PGT-A improved the live birth rate in limited infertile populations with a favourable prognosis (Yang *et al.*, 2012; Scott Jr *et al.*, 2013b; Forman *et al.*, 2013; Rubio *et al.*, 2017). However, several RCTs were unable to demonstrate any benefit to the live birth rate from PGT-A (Kang *et al.*, 2016; Kushnir *et al.*, 2016; Verpoest *et al.*, 2018; Murphy *et al.*, 2019). The largest RCT showed that the chance of having a baby with and without PGT-A was similar in infertile women of an advanced maternal age (Verpoest *et al.*, 2018). In addition, the use of PGT-A is not recommended for all infertile women (ESHRE, 2017; ASRM, 2018).

Identifiable causes of RPL include antiphospholipid syndrome (APS), uterine anomalies, parental chromosomal abnormalities and abnormal embryonic karyotypes (Sugiura-Ogasawara *et al.*, 2004; Sugiura-Ogasawara *et al.*, 2010; Sugiura-Ogasawara *et al.*, 2012; ESHRE Early Pregnancy Guideline Development Group, 2017; Popescu *et al.*, 2018). However, the actual cause in over half of RPL cases has been

considered unknown in patients when their products of conception (POC) have not been karyotyped. However, when the POC have been analysed, 40–50% have been found to be caused by an abnormal embryonic karyotype (Sugiura-Ogasawara *et al.*, 2012; Popescu *et al.*, 2018). When using PGT-A for unexplained RPL, only one retrospective cohort study has indicated a similar live birth rate (63 versus 68%) and similar miscarriage rate (18 versus 25%) between patients with IVF and PGT-A and those solely under expectant management (Murugappan *et al.*, 2016). The limitation of this study was that it included patients with embryonic euploidy because the embryonic karyotype is seldom analysed clinically.

Regarding recurrent implantation failure (RIF), exclusion criteria in studies of patients with a favourable outcome included patients with RIF and patients who were poor responders. RIF can involve complex pathological symptoms affected by numerous, frequently unknown factors. Aneuploidy might be one of the causes because it increases according to women's age and the rate of aneuploidy in blastocysts reaches 58% at 40 years of age (Franasiak *et al.*, 2014).

The present pilot study was therefore conducted to compare the live birth rates with and without the use of PGT-A in patients with RPL caused by embryonic aneuploidy and patients with RIF. To the best of our knowledge, this is the first study focusing on the live birth rates of these two groups of patients.

Materials and Methods

Design

Patients were recruited to participate in this multicentre, prospective study between January 2017 and June 2018. All patients were seen at Nagoya City University Hospital, Kato Ladies Clinic, IVF Osaka Clinic or St. Luke Clinic for investigation of the cause of the RPL or infertility.

At least 10 patients of each group, aged 35–36, 37–38, 39–40 and 41–42 years, were selected for inclusion in the group receiving PGT-A. Matched patients with the same inclusion and exclusion criteria were enrolled as controls who were not to undergo PGT-A (non-PGT-A group).

Whole genome amplification (WGA) and aCGH were performed in Nagoya City University, Tokyo Women's Medical University and Fujita Medical University.

Oocyte retrievals were performed for up to two cycles for each patient according to the number of obtained blastocysts and the couple's wishes. Cases in which blastocysts were not provided within 6 months after temporary registration were regarded as dropouts, and the subsequent full registration was not permitted.

A single ET of a thawed blastocyst was planned for each patient; in the PGT-A group, only euploid blastocysts were transferred.

Recurrent pregnancy loss caused by embryonic aneuploidy

Women included in the RPL protocol had no previous live birth but two or more previous clinical miscarriages, where at least one miscarriage was caused by embryonic aneuploidy, and where the pregnancies were the result of *in vitro* fertilisation and embryo transfer (IVF-ET), were included in the RPL protocol. All patients underwent a systematic examination, including 4D-ultrasound sonography and/or hysterosalpingography, chromosome analysis of both partners, diagnostic tests for APS including screening for lupus anticoagulant by activated partial thromboplastin time and dilute Russell's viper venom time and (β 2 glycoprotein I-dependent) anticardiolipin antibody and blood tests for hypothyroidism and diabetes mellitus, before a subsequent pregnancy was attempted. Exclusion criteria were an abnormal chromosome in either or both partners, a congenital uterine anomaly, APS and other severe complications.

Recurrent implantation failure

Patients with a history of three or more implantation failures after IVF-ET treatment were enrolled in the RIF protocol. The inclusion criterion was that no pregnancy had occurred after three or more good quality blastocyst transfers. Exclusion criteria were an abnormal chromosome in either or both partners, a congenital uterine anomaly and azoospermia.

Ethics statement

The protocol was approved by the Research Ethics Committee of the Japan Society of Obstetrics and Gynecology (JSOG) and Nagoya City University, Graduate School of Medical Sciences and all participating institutes. This study was registered at Clinical [Trials.gov](https://www.clinicaltrials.gov). as UMIN000026104. Couples provided their written informed consent to participate in this study.

Ovarian stimulation, oocyte retrieval, embryo culture and trophoctoderm biopsy

Patients underwent ovarian stimulation, oocyte retrieval and ET per standard protocol. Protocols used were based on the physician's preference. Ovarian stimulation was performed with a long protocol of gonadotropin-releasing hormone (GnRH) agonist, a short protocol

of GnRH agonist, a GnRH antagonist protocol or a clomiphene citrate (CC) protocol (Sawada *et al.*, 2018). Each protocol was selected according to the patient age and the ovarian reserve predicted by the serum anti-Mullerian hormone and/or basal follicular stimulating hormone (FSH) level on Day 3 of the menstrual cycle. Oocyte maturation using 5000 IU human chorionic gonadotropin (hCG) depended on the protocol employed when the leading follicle reached a diameter of more than 20 mm as measured by transvaginal ultrasonography. At 36 h after the injection of hCG, transvaginal ultrasonography-assisted oocyte retrieval was performed, and following the removal of cumulus cells, intracytoplasmic sperm injection (ICSI) was performed for oocytes at the MII stage. Normal fertilisation was assessed 16–18 h after ICSI by the presence of two pronuclei, and all zygotes were cultured to the blastocyst stage.

On Day 5 or 6 after oocyte retrieval, a TE biopsy was performed on a good quality blastocyst from that around five TE cells located apart from the inner cell mass (ICM) were aspirated gently and separated from the blastocyst by applying multiple pulses of a noncontact 1.48- μ m diode laser (Saturn 5 Active™, Cooper Surgical, Inc., CT, USA) through a zona pellucida opening created by the laser. The biopsied TE cells were washed three times in 1 \times phosphate buffered saline (PBS) (Life Technologies, NY, USA), transferred to a PCR tube containing 2.5 μ l 1 \times PBS and cryopreserved at -80°C until analysis. After the TE biopsy, blastocysts were vitrified using the Cryotop method as described previously (Kuwayama *et al.*, 2005).

Whole genome amplification and comprehensive chromosome screening using an array comparative genomic hybridisation technique

WGA of the biopsied TE samples and male and female Human Reference DNA (Agilent Technologies, Inc., CA, USA) was performed with the use of a PicoPLEX WGA Kit (Takara Bio USA Inc., CA, USA) in accordance with the manufacturer's guidelines (Lu *et al.*, 2012). The WGA products of the TE samples and male and female reference DNA were labelled with Cyanine3 (Cy3) or Cyanine5 (Cy5) fluorophores for 2 h at 37°C . Labelled DNA was purified using SureTag Purification Columns and then hybridised using a GenetiSure Pre-Screen Array Kit (Agilent Technologies, Inc., CA, USA) under cover slides for 16 h at 67°C . After hybridisation, microarray slides were washed, dried and scanned using a SureScan Microarray Scanner (Agilent Technologies, Inc., CA, USA). The scanning data were analysed by CytoGenomics Single Cell Analysis software (Agilent Technologies, Inc., CA, USA) for obtaining the copy number of each chromosome.

Blastocyst classification and single embryo transfer

According to the results of the analysis, blastocysts were classified into four groups: A, euploids; B, euploids with suspicious mosaicism; C, aneuploids; or D, undiagnosable. Blastocysts that had results showing small variations, but that couldn't be confirmed as aneuploids—for example, when mosaicism was suspected, were classified as belonging to group B. It was determined that the blastocysts in group A or B could be transferred. The blastocyst classification was determined by means of a web conference in that all researchers participated.

For patients with one or more blastocysts classified as group A or B, a single ET of a thawed euploid blastocyst of the best morphological quality was performed for each patient. The priority of transfer was higher for group A than group B. Cryopreserved blastocysts were thawed in accordance with the manufacturer's guidelines. In cases in that all the blastocysts were classified as group C or D, the ET was cancelled.

For patients in the non-PGT-A groups, a single ET of a thawed blastocyst with good quality was performed the same way.

Comparison and statistical analysis

The primary outcome was a live birth for each enrolled patient with one or two oocyte retrievals and one opportunity for ET in either of the two protocols. Secondary outcomes were live birth per ET, clinical pregnancy, biochemical pregnancy loss and clinical miscarriage. A case with a serum hCG level > 4 mIU/ml on the 10th day after ET but tissue that never progressed to a gestational sac as viewed by transvaginal ultrasonography was diagnosed with a biochemical pregnancy loss. A clinical pregnancy was diagnosed as such when a gestational sac was ascertained by a transvaginal ultrasonography. A clinical miscarriage was diagnosed as a miscarriage after a gestational sac was ascertained.

Student's t-test was used to analyse the difference between means. Multiple logistic regression analyses were conducted to compare the outcomes of PGT-A and non-PGT-A groups after controlling for covariables with $P < 0.10$.

The distribution of euploidy, trisomy, double (triple) trisomy and (at least one) monosomy was compared between patients with RPL and RIF. Euploidy with suspicious mosaicism was included as euploidy. Adjusted residuals as a post hoc test was determined after chi-squared tests were calculated.

All analyses were carried out using the statistical software SPSS, Version 21. A P value <0.05 was considered to denote statistical significance.

Results

A total of 79 patients with a history of RPL were enrolled in the study. Of these, 41 were selected for PGT-A and 38 were included as controls (Table I). The mean (SD) age and number of prior miscarriages were 39.2 (2.05) vs 39.3 (2.07) and 2.56 (0.78) vs 2.47 (0.92) for the PGT-A and non-PGT-A group, respectively. There were no differences in the baseline characteristics of the two groups. A total of 64 OR cycles were performed for the patients in the PGT-A group, and 174 good quality blastocysts were obtained from 33 patients. Among the 174 blastocysts, 161 (92.5%) were diagnosable by aCGH analysis. Of these, 47 (29.2%) were diagnosed as euploid, and 21 ETs were performed (Table II).

There was no difference in the live birth rate per patient between the PGT-A and non-PGT-A groups (26.8 vs 21.1%). There was also no difference in the miscarriage rate per clinical pregnancy (14.3 vs 20.0%). The live birth rate and clinical pregnancy rate per ET were significantly higher in the PGT-A group than in the non-PGT-A group (52.4 vs 21.6%, adjusted OR 3.89; 95% CI 1.16–13.1 and 66.7 vs 29.7%, 5.14; 1.52–17.3). The live birth rate per clinical pregnancy was similar in both groups. PGT-A reduced the biochemical pregnancy loss rate per biochemical pregnancy significantly (12.5 vs 45.0%, 0.14; 0.02–

0.85). The rate of total pregnancy loss per patient, which included both clinical miscarriage and biochemical pregnancy loss, was significantly lower in the PGT-A group than in the non-PGT-A group (4/41 = 9.8% vs 11/38 = 28.9%, 0.22; 0.06–0.82).

A total of 92 patients with a history of RIF were enrolled, of which 42 were chosen for PGT-A and 50 were included as controls (Table III). The mean (SD) age and number of prior ETs were 38.6 (2.06) vs 38.7 (2.15) and 5.00 (2.30) vs 4.34 (1.72) in the PGT-A and non-PGT-A groups, respectively. There were no differences in the baseline characteristics of the two groups. A total of 81 OR cycles were performed for patients in the PGT-A group, and 208 good quality blastocysts were obtained from 39 patients. Among the 208 blastocysts, 199 (95.7%) were diagnosable by aCGH analysis of that 42 (21.1%) were euploid, and 24 ETs were performed (Table IV).

There was no difference in the live birth rates per patient of the PGT-A and non-PGT-A groups (35.7 vs 26.0%). There was also no difference in the rate of miscarriage per clinical pregnancy (11.8 vs 0%). The live birth rate and clinical pregnancy rate per ET were significantly higher in the PGT-A group compared to the non-PGT-A group (62.5 vs 31.7%, 3.75; 1.28–10.95 and 70.8 vs 31.7%, 5.62; 1.82–17.3). The live birth rate per clinical pregnancy was similar in both groups. The rate of biochemical pregnancy loss per biochemical pregnancy was significantly lower in the PGT-A group compared to the non-PGT-A group (10.5 vs 40.9%, 0.17; 0.03–0.92).

There was no significant difference of the distribution of blastocysts with euploidy, at least a single monosomy, trisomy or double trisomy between the RPL and RIF groups (Fig. 1). The frequency of double trisomy tended to be higher in the RPL group (adjusted residuals; 1.6).

The euploidy rate decreased from 56 to 37, 31 and 9% in patients with RPL and from 44 to 23, 23 and 6% in patients with RIF according to age (Fig. 2a). The estimated minimum essential number of ORs to obtain at least one euploid blastocyst was calculated to be 0.6, 1.1, 1.1 and 4.8 in patients with RPL, while it was 0.63, 1.8, 4.8 and 9.0 in patients with RIF, in groups aged 35–36, 37–38, 39–40 and 41–42 years, respectively (Fig. 2b).

Only trisomy was obtained in previous POC (Supplementary Figure 1b); however, a 1:1 ratio of trisomy to monosomy was ascertained in blastocysts subjected to PGT-A of both groups (Supplementary Figure 1a). The frequency of aneuploidy in POC and blastocysts increased according to the chromosome number.

Six patients had no embryos of category A, five of whom requested ET using embryos of category B embryos. Three cases resulted in live births, but in two cases, there was no pregnancy.

Discussion

We failed to show that PGT-A improves the live birth rate per patient or reduces the rate of clinical miscarriage significantly in both groups. The efficacy of PGT-A, at least in RPL patients, was expected because the present study focused only on patients whose POC were ascertained to be aneuploid. Mosaicism might be speculated to be one of the reasons why PGT-A showed limited efficacy. Recently, concordance between TE and the ICM was established in 62.1% of embryos analysed by PGT-A (Popovic *et al.*, 2019). The reliability of the TE biopsy compared to the ICM biopsy in blastocysts is extremely high, but that of the cleavage-stage biopsy compared with the ICM biopsy is less so. The rate of false positive results between TE and ICM has

Table I Baseline demographics of PGT-A and non-PGT-A patients with recurrent pregnancy loss.

	PGT-A	Non-PGT-A	p-value
Number of enrolled patients	41	38	
Mean age (SD, range)	39.2 (2.05, 35–42)	39.3 (2.07, 35–42)	0.71
Mean BMI (SD)	21.1 (2.86)	21.7 (2.45)	0.36
Mean (SD) number of previous miscarriages	2.56 (0.78)	2.47 (0.92)	0.65
Mean (SD) number of previous pregnancies with the use of IVF-ET	2.00 (0.87)	1.53 (0.92)	0.021
Mean (SD) number of previous live births	0	0	
Smokers (n)	1	2	

Bold indicates statistical significance.

Table II Comparison of clinical outcomes between PGT-A and non-PGT-A patients with recurrent pregnancy loss.

	PGT-A (n = 41) ^a	Non-PGT-A (n = 38) ^b	Adjusted ORs (95% CI) [*] , p-value
Number of patients with at least one good quality blastocyst	21	38	
Diagnosed blastocysts/total number of blastocysts	161/174 (92.5%)	-	
Euploid blastocysts/diagnosed blastocysts	47/161 (29.2%)	-	
Embryo transfers/patients	21/41 (51.2%)	37/38 (97.3%)	0.03 (0.003–0.23), 0.001
Biochemical pregnancies/embryo transfers	16/21 (76.2%)	20/37 (54.1%)	2.45 (0.71–8.44), 0.16
Biochemical pregnancy losses/biochemical pregnancies	2/16 (12.5%)	9/20 (45.0%)	0.14 (0.02–0.85), 0.03
Clinical pregnancies/embryo transfers	14/21 (66.7%)	11/37 (29.7%)	5.14 (1.52–17.3), 0.008
Miscarriages/clinical pregnancies	2/14 (14.3%)	2/10 (20.0%)	0.68 (0.06–6.51), 0.68
	47,XX,+12[13]/46,XX[7] 46,XX (21wIUFD)	47,XX,+20 47,X?,+18	
Ectopic pregnancies/clinical pregnancies	1/14 (7.1%)	1/11 (9.1%)	5.67 (0.03–1014.5), 0.51
Live births/embryo transfers	11/21 (52.4%)	8/37 (21.6%)	3.89 (1.16–13.1), 0.028
Live births/patients	11/41 (26.8%)	8/38 (21.1%)	1.33 (0.45–3.91), 0.60

^{a,b}Both groups were followed up until the second oocyte retrieval and the first embryo transfer.

^{*}Adjusted for the number of previous pregnancies with the use of IVF-ET

Bold indicates statistical significance.

been reported as 7.5% (Lawrenz et al., 2019). Damage by biopsy might influence the outcome although only cleavage-stage biopsy and not TE biopsy has been reported to reduce the live birth rate (Franasiak et al., 2014).

Over 70% of embryos are reported to be at least partially aneuploid by Day 3 because of prevalent errors of both meiotic and mitotic origins. On the other hand, aneuploidy observed in miscarried POC has been thought to be due to division errors of meiotic origin (Nagaoka et al., 2013). Variation of the *PLK4* gene was found to be associated with mitotic errors in human embryos, and infertile women with the high-risk genotype contribute fewer blastocysts for testing at Day 5, suggesting that their embryos were less likely to survive to blastocyst formation (McCoy et al., 2015). Blastocysts with monosomy can not survive after implantation (Franasiak et al., 2014). The present study

indicated that natural selection or chromosome correcting pathways might be superior to PGT-A in the current situation.

Indeed, PGT-A has several ethical problems related to its use; false positives, due to mosaicism, and technical aspects of the process can lead to the abandonment of large numbers embryos that have the potential for live births (Rosenwaks et al., 2018). In the present study, we had 3 healthy babies from 5 transferred mosaic embryos and, in the first clinical trials, 100 such babies were reported (Greco et al., 2015; Rosenwaks et al., 2018).

PGT-A improved the live birth rate per ET both in the RPL and RIF groups. PGT-A has an advantage reducing the number of ETs (Forman et al., 2014). PGT-A also lowered the rate of biochemical pregnancy loss. This suggests that the cause of biochemical pregnancy loss might be speculated to be due to chromosome abnormality. Indeed, the

Table III Baseline demographics of PGT-A and non-PGT-A patients with recurrent implantation failure.

	PGT-A	Non-PGT-A	P-value
Number of enrolled patients	42	50	
Mean age (SD, range)	38.6 (2.06, 35–42)	38.7 (2.15, 35–42)	0.78
Mean BMI (SD)	21.6 (2.68)	21.7 (3.07)	0.88
Mean (SD) number of previous embryo transfers	5.00 (2.30)	4.34 (1.72)	0.119
Mean (SD) number of previous pregnancies with the use of IVF-ET	0	0	
Mean (SD) number of previous live births	0	0	
Smokers (n)	2	0	
Mean (SD) months of infertility	62.0 (39.1)	62.7 (47.5)	0.94
Cause of infertility % (n)			
Male	28.6% (12)	30.0% (15)	0.713
Female	35.7% (15)	28.0% (14)	
Unexplained	35.7% (15)	42.0% (21)	

Table IV Comparison of clinical outcomes between PGT-A and non-PGT-A patients with recurrent implantation failure.

	PGT-A (n = 42) ^a	Non-PGT-A (n = 50) ^b	Adjusted ORs (95% CI) [*] , p-value
Number of patients with at least one good quality blastocyst	24	42	
Diagnosed blastocysts/total number of blastocysts	199/208 (95.7%)	-	
Euploid blastocysts/diagnosed blastocysts	42/199 (21.1%)	-	
Embryo transfers/patients	24/42 (57.1%)	41/50 (82.0%)	0.29 (0.11–0.75), 0.01
Biochemical pregnancies/embryo transfers	19/24 (79.2%)	22/41 (53.7%)	3.28 (1.03–10.5), 0.05
Biochemical pregnancy losses/biochemical pregnancies	2/19 (10.5%)	9/22 (40.9%)	0.17 (0.03–0.92), 0.04
Clinical pregnancies/embryo transfers	17/24 (70.8%)	13/41 (31.7%)	5.62 (1.82–17.3) 0.003
Miscarriages/clinical pregnancies	2/17 (11.8%)	0/13 (0%)	-, 0.999
	46,XY not tested		
Ectopic pregnancies/clinical pregnancies	0/17 (0%)	0/13 (0%)	-
Live births/embryo transfers	15/24 (62.5%)	13/41 (31.7%)	3.75 (1.28–10.95) 0.016
Live births/patients	15/42 (35.7%)	13/50 (26.0%)	1.69 (0.68–4.20) 0.26

^{a,b}Both groups were followed up until the second oocyte retrieval and the first embryo transfer.

^{*}Adjusted for the number of previous pregnancies with the use of IVF-ET

Bold indicates statistical significance.

rate of chromosome abnormality decreases according to the developmental stage: 70–80% of clinical miscarriages (Ogasawara *et al.*, 2000; Azmanov *et al.*, 2007), 4% of stillbirths and 0.3% of newborn babies (Nagaoka *et al.*, 2013). Furthermore, trisomies and monosomies are equally prevalent in blastocysts; however, monosomies disappear after implantation (Franasiak *et al.*, 2014). This evidence suggests that chromosome abnormality might be more frequent and of greater severity in biochemical pregnancy losses in this earlier stage of development compared with clinical miscarriages.

There was no difference in the distribution of abnormalities, although the frequency of double trisomy tended to be higher in patients with RPL than in those with RIF (Fig. 1). The euploidy rate was much lower in both RPL (29.2%) and RIF (21.1%) patients than in 15 169 blastocysts of a previous study (38-year-old women, 52.1%, 39-year-old women, 47.1%) (Franasiak *et al.*, 2014). Thus, RPL caused by aneuploidy and RIF may be associated with a meiosis-specific genes. On the other hand, endometrial receptivity for euploid embryo implantation might be sufficiently high in both RPL and RIF patients since the clinical pregnancy

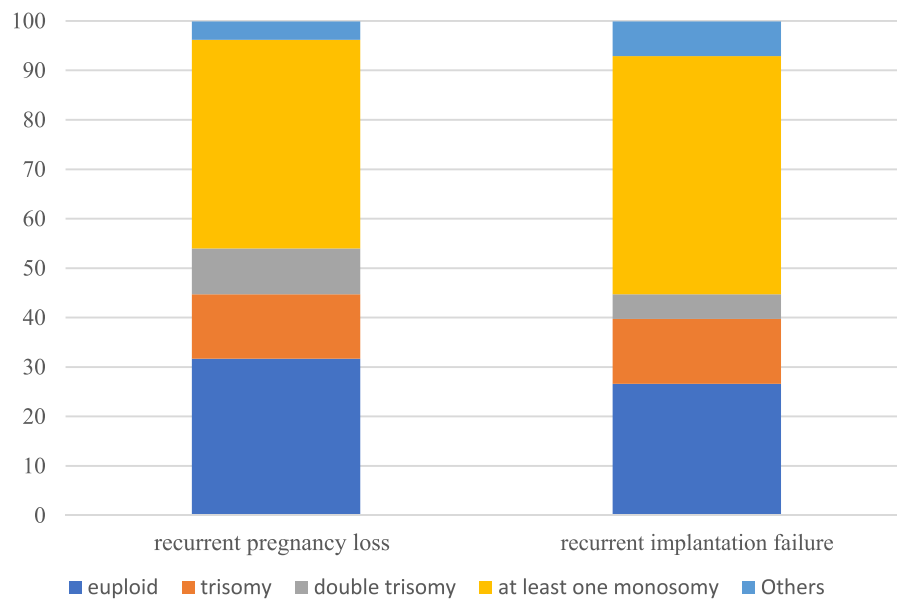


Figure 1 The distribution of blastocysts with euploidy, at least one monosomy, trisomy or double trisomy after PGT-A in patients in the recurrent pregnancy loss (RPL) and recurrent implantation failure (RIF) groups. There was no significant difference in the distribution of blastocyst with euploidy, at least a single monosomy, trisomy or double trisomy between the RPL and RIF groups. The frequency of double trisomy tended to be higher in RPL (adjusted residuals: 1.6). If a blastocyst contained both monosomy and trisomy, it was classified as 'at least one monosomy'.

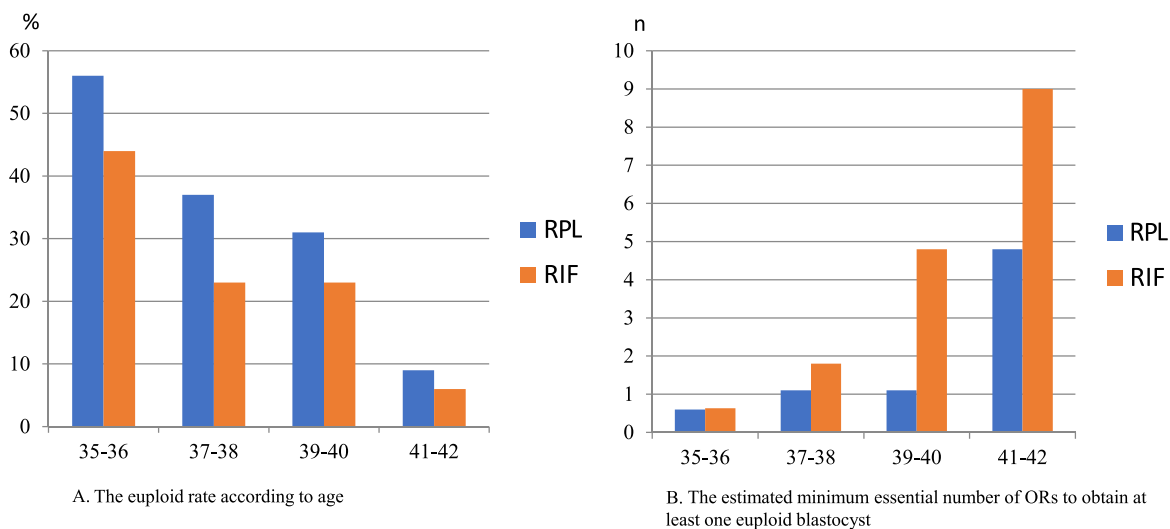


Figure 2 The euploidy rate and estimated minimum essential number of oocyte retrievals required to obtain at least one euploid blastocyst according to the woman's age. (A) The euploid rate decreased according to age from 56 to 37, 31 and 9% in patients with RPL and from 44 to 23, 23 and 6% in patients with RIF. (B) The estimated minimum essential number of oocyte retrievals required to obtain at least one euploid blastocyst in groups aged 35–36, 37–38, 39–40 and 41–42 years, respectively, was calculated to be 0.6, 1.1, 1.1 and 4.8 in patients with RPL and 0.6, 1.8, 4.8 and 9.0 in patients with RIF.

rate per embryo transfer after PGT-A was excellent (66.7 and 70.8%) compared with a previous study of women of advanced maternal age (38–41 years, 54.4%) (Rubio et al., 2017). The cause of RPL with aneuploidy might involve 'superfertility' due to high endometrial receptivity for aneuploidy embryo implantation (Teklenburg et al., 2010).

Monosomies disappeared in POC although both trisomies and monosomies were ascertained in blastocysts (Supplementary Figure S1). The frequency of aneuploidy increased according to the chromosome number. Embryos with both trisomy and monosomy in larger chromosomes might have difficulty in developing.

Regarding ethical considerations, there are no laws in Japan related to reproductive technology. The JSOG made a ruling on PGT in 1998 such that each case must be submitted to the JSOG and that the facilities can only initiate PGT after obtaining JSOG permission. PGT-A has been prohibited because the JSOG considered that the feelings of handicapped people might be resistant to PGT. In a total of 622 cases, PGT for monogenic/single gene defects was used for several extremely severe genetic disorders, and PGT for chromosomal structural rearrangements for RPL caused by a translocation was permitted from 2006 to December 2018. The maternal age has increased year by year and older women with RPL or infertility desire PGT-A in spite of a lack of evidence. Thus, the JSOG decided to conduct the present pilot study and ordered the present facilities to carry it out before conducting a RCT to examine the effect of PGT-A on the live birth rate while also considering ethical issues in a committee open to patients and media. The usefulness of PGT-A has been made public by its proponents not only in the USA but also in Japan (Rosenwaks *et al.*, 2018). Patients and physicians might have the misperception that PGT-A has advantages for all patients in spite of the lack of evidence. It also should be noted that physicians who administer the clinics or laboratories have a potential conflict of interest.

There were only two miscarriages (20.0%, 2/10) in the control group of the present RPL protocol. This was relatively low when compared with the 41.9% reported previously (in patients with a previous average of 2.9 miscarriages and who were 40 and older) (Sugijura-Ogasawara *et al.*, 2009). The reason might be speculated to be that the miscarriage rate in patients with RPL due to embryonic aneuploidy was lower than in those with a normal embryonic karyotype (38.3 vs 62.0%, mean age 32) (Ogasawara *et al.*, 2000). There has been no data on the miscarriage rate in patients with RPL whose POC were aneuploid and who have received IVF-ET. There was no bias between the PGT-A group and non-PGT-A group because of the same inclusion and exclusion criteria.

One limitation of this study is that the sample size was too small to find any significant advantage in improving the live birth rate and reducing the clinical miscarriage rate because this work was conducted as a pilot study to calculate the sample size for subsequent RCT. The JSOG decided not to continue this pilot study and not to conduct an RCT because of the difficulty involved. It did not change the ruling that PGT-A is prohibited. Thus, it was impossible for us to increase the sample size.

In the present study, patients received only one ET following one or two oocyte retrievals. It was found that 4.8 and 9.0 oocyte retrievals are necessary to obtain one euploid blastocyst in 41–42-year-old patients with RPL and RIF, respectively. Further study with a larger number of patients and determination of the cumulative live birth rate is necessary to confirm the present findings.

Supplementary data

Supplementary data are available at *Human Reproduction* online.

Authors' Roles

MSO designed the present study and analysed the data, and TS wrote the first draft of the manuscript. TS, TKu, NA, KK, RK, AF and TU were

responsible for IVF-ET, biopsy and clinical data acquisition, and TS, FO, TY, TKa and HK were responsible for the diagnosis of blastocysts. HS managed the data centre, and AK, TT and MI supervised the study. All authors interpreted the data, contributed to the writing of the manuscript and revised it critically for important intellectual content.

Funding

Japan Society of Obstetrics and Gynecology and the Japanese Ministry of Education, Science and Technology.

Conflict of Interest

The authors declare no conflicts of interest associated with this manuscript.

References

- American Society of Reproductive Medicine. Practice Committees of the American Society for Reproductive Medicine and the Society for Assisted Reproductive Technology. The use of preimplantation genetic testing for aneuploidy (PGT-A): a committee opinion. *Fertil Steril* 2018; **109**:429–436.
- Azmanov DN, Milachich TV, Zaharieva BM, Michailova GI, Dimitrova VG, Karagiozova ZH, Maznejkova VT, Chernev TA, Toncheva DI. Profile of chromosomal aberrations in different gestational age spontaneous abortions detected by comparative genomic hybridization. *Eur J Obstet Gynecol Reprod Biol* 2007; **131**:127–131.
- European Society of Human Reproduction and Embryology. Early pregnancy guideline development group. *Recurrent Pregnancy Loss Guideline* 2017; **11**:90–92.
- Forman EJ, Hong KH, Franiasiak JM, Scott RT Jr. Obstetrical and neonatal outcomes from the BEST Trial: single embryo transfer with aneuploidy screening improves outcomes after in vitro fertilization without compromising delivery rates. *Am J Obstet Gynecol* 2014; **210**:157.e1–157.e6.
- Franiasiak JM, Forman EJ, Hong KH, Werner MD, Upham KM, Treff NR, Scott RT Jr. The nature of aneuploidy with increasing age of the female partner: a review of 15,169 consecutive trophectoderm biopsies evaluated with comprehensive chromosomal screening. *Fertil Steril* 2014; **101**:656–663.
- Greco E, Minasi MG, Fiorentino F. Healthy babies after intrauterine transfer of mosaic aneuploid blastocysts. *N Engl J Med* 2015; **373**:2089–2090.
- Kang HJ, Melnick AP, Stewart JD, Xu K, Rosenwaks Z. Preimplantation genetic screening: who benefits? *Fertil Steril* 2016; **106**:597–602.
- Kushnir VA, Darmon SK, Albertini DF, Barad DH, Gleicher N. Effectiveness of in vitro fertilization with preimplantation genetic screening: a reanalysis of United States assisted reproductive technology data 2011–2012. *Fertil Steril* 2016; **106**:75–79.
- Kuwayama M, Vajta G, Kato O, Leibo SP. Highly efficient vitrification method for cryopreservation of human oocytes. *Reprod Biomed Online* 2005; **11**:300–308.
- Lawrenz B, El Khatib I, Liñán A, Bayram A, Arnanz A, Chopra R, De Munck N, Fatemi HM. The clinicians' dilemma with mosaicism—an insight from inner cell mass biopsies. *Hum Reprod* 2019; **34**:998–1010.


- Lu S, Zong C, Fan W, Yang M, Li J, Chapman AR, Zhu P, Hu X, Xu L, Yan L et al. Probing meiotic recombination and aneuploidy of single sperm cells by whole-genome sequencing. *Science* 2012;**338**:1627–1630.
- Mastenbroek S, Twisk M, van der F, Repping S. Preimplantation genetic screening: a systematic review and meta-analysis of RCTs. *Hum Reprod Update* 2011;**17**:454–466.
- McCoy RC, Demko Z, Ryan A, Banjevic M, Hill M, Sigurjonsson S, Rabinowitz M, Fraser HB, Petrov DA. Tripolar chromosome segregation drives the association between maternal genotype at variants spanning PLK4 and aneuploidy in human preimplantation embryos. *Science* 2015;**348**:235–238.
- Munné S, Chen S, Fischer J, Colls P, Zheng X, Stevens J, Escudero T, Oter M, Schoolcraft B, Simpson JL et al. Preimplantation genetic diagnosis reduces pregnancy loss in women aged 35 years and older with a history of recurrent miscarriages. *Fertil Steril* 2005;**84**:331–335.
- Murphy LA, Seidler EA, Vaughan DA, Resetskova N, Penzias AS, Toth TL, Thornton KL, Sakkas D. To test or not to test? A framework for counselling patients on preimplantation genetic testing for aneuploidy (PGT-A). *Hum Reprod* 2019;**34**:268–275.
- Nagaoka SI, Hassold TJ, Hunt PA. Human aneuploidy: mechanisms and new insights into an age-old problem. *Nat Rev Genet* 2013;**13**:493–504.
- Ogasawara M, Aoki K, Okada S, Suzumori K. Embryonic karyotype of abortuses in relation to the number of previous miscarriages. *Fertil Steril* 2000;**73**:300–304.
- Popescu F, Jaslow CR, Kutteh WH. Recurrent pregnancy loss evaluation combined with 24-chromosome microarray of miscarriage tissue provides a probable or definite cause of pregnancy loss in over 90% of patients. *Hum Reprod* 2018;**33**:579–587.
- Popovic M, Dhaenens L, Taelman J, Dheedene A, Bialecka M, De Sutter P, Chuva de Sousa Lopes SM, Menten B, Heindryckx B. Extended in vitro culture of human embryos demonstrates the complex nature of diagnosing chromosomal mosaicism from a single trophectoderm biopsy. *Hum Reprod* 2019;**34**:758–769.
- Rosenwaks Z, Handyside AH, Fiorentino F, Gleicher N, Paulson RJ, Schattman GL, Scott RT Jr, Summers MC, Treff NR, Xu K. The pros and cons of preimplantation genetic testing for aneuploidy: clinical and laboratory perspectives. *Fertil Steril* 2018;**110**:353–361.
- Rubio C, Bellver J, Rodrigo L, Castellón G, Guillén A, Vidal C, Giles J, Ferrando M, Cabanillas S, Remohí J et al. In vitro fertilization with preimplantation genetic diagnosis for aneuploidies in advanced maternal age: a randomized, controlled study. *Fertil Steril* 2017;**107**:1122–1129.
- Sawada Y, Sato T, Saito C, Ozawa F, Ozaki Y, Sugiura-Ogasawara M. Clinical utility of decorin in follicular fluid as a biomarker of oocyte potential. *Reprod Biol* 2018;**18**:33–39.
- Scott RT Jr, Upham KM, Forman EJ, Zhao T, Treff NR. Cleavage-stage biopsy significantly impairs human embryonic implantation potential while blastocyst biopsy does not: a randomized and paired clinical trial. *Fertil Steril* 2013a;**100**:624–630.
- Scott RT Jr, Upham KM, Forman EJ, Hong KH, Scott KL, Taylor D, Tao X, Treff NR. Blastocyst biopsy with comprehensive chromosome screening and fresh embryo transfer significantly increases in vitro fertilization implantation and delivery rates: a randomized controlled trial. *Fertil Steril* 2013b;**100**:697–703.
- Sugiura-Ogasawara M, Ozaki Y, Sato T, Suzumori N, Suzumori K. Poor prognosis of recurrent aborters with either maternal or paternal reciprocal translocations. *Fertil Steril* 2004;**81**:367–373.
- Sugiura-Ogasawara M, Ozaki Y, Kitaori T, Suzumori N, Obayashi S, Suzuki S. Live birth rate according to maternal age and previous number of recurrent miscarriages. *Am J Reprod Immunol* 2009;**62**:314–319.
- Sugiura-Ogasawara M, Ozaki Y, Kitaori T, Kumagai K, Suzuki S. Midline uterine defect size is correlated with miscarriage of euploid embryos in recurrent cases. *Fertil Steril* 2010;**93**:1983–1988.
- Sugiura-Ogasawara M, Ozaki Y, Katano K, Suzumori N, Kitaori T, Mizutani E. Abnormal embryonic karyotype is the most frequent cause of recurrent miscarriage. *Hum Reprod* 2012;**27**:2297–2303.
- Teklenburg G, Salker M, Heijnen C, Macklon NS, Brosens JJ. The molecular basis of recurrent pregnancy loss: impaired natural embryo selection. *Mol Hum Reprod* 2010;**16**:886–895.
- Verpoest W, Staessen C, Bossuyt PM, Goossens V, Altarescu G, Bonduelle M, Devesa M, Eldar-Geva T, Gianaroli L, Griesinger G et al. Preimplantation genetic testing for aneuploidy by microarray analysis of polar bodies in advanced maternal age: a randomized clinical trial. *Hum Reprod* 2018;**33**:1767–1776.
- Yang Z, Liu J, Collins GS, Salem SA, Liu X, Lyle SS, Peck AC, Sills ES, Salem RD. Selection of single blastocysts for fresh transfer via standard morphology assessment alone and with array CGH for good prognosis IVF patients: results from a randomized pilot study. *Mol Cytogenet* 2012;**5**:24.

CASE REPORT

Open Access



A female patient with retinoblastoma and severe intellectual disability carrying an X;13 balanced translocation without rearrangement in the *RB1* gene: a case report

Makiko Tsutsumi¹, Hiroyoshi Hattori^{2,3}, Nobuhiro Akita³, Naoko Maeda³, Toshinobu Kubota⁴, Keizo Horibe³, Naoko Fujita^{1,5}, Miki Kawai¹, Yasuko Shinkai¹, Maki Kato¹, Takema Kato¹, Rie Kawamura¹, Fumihiko Suzuki⁶ and Hiroki Kurahashi^{1*} 

Abstract

Background: Female carriers of a balanced X; autosome translocation generally undergo selective inactivation of the normal X chromosome. This is because inactivation of critical genes within the autosomal region of the derivative translocation chromosome would compromise cellular function. We here report a female patient with bilateral retinoblastoma and a severe intellectual disability who carries a reciprocal X-autosomal translocation.

Case presentation: Cytogenetic and molecular analyses, a HUMARA (Human androgen receptor) assay, and methylation specific PCR (MSP) and bisulfite sequencing were performed using peripheral blood samples from the patient. The patient's karyotype was 46,X,t(X;13)(q28;q14.1) by G-banding analysis. Further cytogenetic analysis located the entire *RB1* gene and its regulatory region on der(X) with no translocation disruption. The X-inactivation pattern in the peripheral blood was highly skewed but not completely selected. MSP and deep sequencing of bisulfite-treated DNA revealed that an extensive 13q region, including the *RB1* promoter, was unusually methylated in a subset of cells.

Conclusions: The der(X) region harboring the *RB1* gene was inactivated in a subset of somatic cells, including the retinal cells, in the patient subject which acted as the first hit in the development of her retinoblastoma. In addition, the patient's intellectual disability may be attributable to the inactivation of the der(X), leading to a 13q deletion syndrome-like phenotype, or to an active X-linked gene on der (13) leading to Xq28 functional disomy.

Keywords: Retinoblastoma, Balanced X-A translocation, X-inactivation

Background

Balanced translocations generally have no impact on the clinical phenotype of the carrier unless the breakpoint disrupts a dosage sensitive gene. However, X; autosome (X-A) translocations in females are more complex because of the X-chromosome inactivation (XCI), which is a mechanism of dosage compensation of X-linked genes

between females and males [1, 2]. Since the derivative chromosome of an X-A translocation harboring the X-inactivation center may be subject to inactivation, its autosomal region is subject to unfavorable inactivation. This results in cellular dysfunction due to inactivation of critical genes leading to the pathological change or death of cells. In consequence, cells in females carrying an X-A translocation generally undergo selective inactivation of the normal X chromosome.

Retinoblastoma (RB, OMIM #180200) is a malignant intraocular tumor occurring in young children, which is caused by mutations in both alleles of the *RB1* gene [3].

* Correspondence: kura@fujita-hu.ac.jp

¹Division of Molecular Genetics, Institute for Comprehensive Medical Science, Fujita Health University, 1-98 Dengakugakubo, Kutsukake-cho, Toyoake, Aichi 470-1192, Japan

Full list of author information is available at the end of the article



Individuals with heterozygous germline pathogenic variations frequently develop bilateral retinoblastoma in infancy. Constitutional chromosomal abnormalities involving 13q14, where the *RB1* gene is located, are found in a subset of cases with a predisposition for RB. Large deletions that include the *RB1* gene lead to widely variable clinical phenotypes, including intellectual disability, referred to as 13q deletion syndrome [4, 5]. We here describe a female patient with bilateral retinoblastoma and severe intellectual disability who was found to carry an X;13 translocation. Cytogenetic and molecular analysis revealed inactivation of der(X) and the *RB1* gene in a subset of her cells, which explains the cause of her phenotype.

Case presentation

Cytogenetic analysis

Blood samples from the study subjects were obtained with informed consent in accordance with local institutional review board guidelines. An Epstein-Barr virus (EBV) transformed Lymphoblastoid cell line (LCL) was established from the peripheral blood derived from the patient as described previously [6]. Conventional G-banding and fluorescence in situ hybridization (FISH) analyses were performed using LCL. Cytogenetic analyses were performed using a standard method. The *ZytoLight* SPEC RB1/13q12 Dual Color Probe (*ZytoVision GmbH*, Bremerhaven, Germany) was used to detect the *RB1* gene. A bacterial artificial chromosome (BAC) DNA was labeled with SpectrumGreen or SpectrumOrange-labeled 2'-deoxyuridine-5'-triphosphate using the Nick-Translation Kit (*Abbott Japan*, Tokyo, Japan). To visualize late replicating regions, LCL was arrested with thymidine (300 µg/ml) for 18.5 h followed by a treatment with bromodeoxyuridine (BrdU; 25 µg/ml) for 6.5 h after release from the arrest. Metaphase cells were labeled with a FISH probe for the X chromosome centromere (*Cytocell*, Cambridge, UK), and BrdU was detected with Alexa Fluor 594-conjugated mouse anti-BrdU antibody (*ThermoFisher Scientific*, Tokyo, Japan).

HUMARA assay

For HUMARA assays, genomic DNA was extracted from peripheral blood or LCL using the QuickGene DNA whole blood DNA kit L (*Kurabo*, Osaka, Japan). Restriction enzyme treatment followed by PCR analysis was then conducted as described previously [7].

Methylation-specific PCR

Bisulfite conversion of genomic DNAs obtained from the peripheral bloods of the patient and healthy human volunteers was first performed with the *Epitect* Bisulfite kit (*QIAGEN*, Tokyo, Japan). PCR was then carried out using *EpiTaq HS* (*Takara*, Kusatsu, Japan). *EpiScope* Methylated HeLa gDNA (*Takara*) was used as a positive

control. The primers used in these analyses were designed with the *BiSearch* software [8] and are listed in Table 1.

Bisulfite sequencing

The *RB1* promoter region was amplified by PCR as described previously [9]. The PCR products were then used as the template for secondary PCR with primers containing sequencing adaptors. Amplicon sequencing was subsequently performed on an *Illumina MiSeq* in accordance with the manufacturer's protocol to obtain paired-end 150 bp reads. Sequencing data were analyzed with *Bismark* software [10].

Patient characteristics

The current study patient was a Japanese girl born at full term with a length of 50 cm and birth weight of 2894 g. G-banding analysis was performed because of her inadequate weight gain at 1 month of age and revealed a de novo balanced reciprocal translocation, t(X;13)(q28;q14.1) (Fig. 1a). She achieved head control at 6 months of age, began to sit up at 10 months, to pull up to a standing position at 12 months, and to walk at 30 months. At 18 months of age, her body length was 74.3 cm (−1.9 SD), and her weight was 8.3 kg (−1.6 SD). She was diagnosed with a unilateral retinoblastoma in the left eye (International Intraocular Retinoblastoma Classification, Group D) at 18 months of age. She was then treated with 4 cycles of systemic chemotherapy (vincristine, etoposide, and carboplatin). She suffered from chemotherapy-induced constipation during that period.

The parents refused consent for enucleation of the patient's left eye although her response to the chemotherapy was found to be inadequate, and side effects such as a tubular disorder were observed. We thus planned for an intra-arterial chemotherapy regimen due to the parents' wishes. New lesions were developed in the right eye four months later however while waiting for the intra-arterial chemotherapy. Three cycles of intra-arterial chemotherapy for the left eye and various cycles of laser transpupillary thermotherapy (4 cycles for left eye and 2 cycles for right eye) managed to control both eyes and maintain remission for 18 months. However, the retinoblastoma eventually relapsed in the left eye and this was followed by enucleation. The patient was still not talking at 6 years of age, and was thus manifesting severe speech, language and developmental disorders.

Breakpoint analysis of chromosome 13

To examine the underlying causes of the phenotype that manifested in our study patient, we analyzed the *RB1* gene by FISH because the chromosome 13 breakpoint was found to be located close to this gene locus at the

Table 1 Primers used for MSP in this study

Primer ^a	Forward (5'-3')	Reverse (5'-3')	Size (bp)
RB1-M	GGGAGTTTCGCGGACGTGAC	ACGTCGAAACACGCCCG	163
RB1-U	GGGAGTTTTGTGGATGTGAT	ACATCAAACACACCCCA	163
q13.1-M	AAAACCCGAACGCAACGAAC	TCGTCGTAGTTGTTATCGTC	120
q13.1-U	AAAACCCAAACACAACAAC	TTGTTGATGTTGTTATTGTT	120
q14.11-M	GCGCGATGGAGTTTTAGTAC	CGAAAAAAACCCGAACGAC	214
q14.11-U	GTGTGATGGAGTTTTAGTAT	CAAAAAAAACCCAAACAAC	214
q14.3-M	CCGCCTAACGTCAATAAAAC	GTGTTTAGAACGACGGGTGC	160
q14.3-U	CCACCTAACATCAATAAAAC	GTGTTTAGAATGATGGGTGT	160
q21.33-M	TAGGTTTCGTTTTTCGCGTTC	CTTTAACTCCCCGCTCCGC	226
q21.33-U	TAGGTTTTGTTTTTGTGTTT	CTTTAACTCCCCACTTCCAC	226
q31.1prox-M	AGATTCGCGGTTAGGTAGGGC	CGCGCTCTAAAAAATTAAC	368
q31.1prox-U	AGATTGGTGTAGGTAGGGT	CACACTCTAAAAAATTAAC	368
q31.1 dis-M	CGTACTACTACCCCGCTAC	GCGTTTTTAGCGTTTTTTA	194
q31.1 dis-U	CATACTACTACCCCACTAC	GTGTTTTTAGTGTTTTTA	194
q31.2-M	GCCGCTACGCTAAAAACGA	CGTATTTTCGGTTTGGGTCCG	283
q31.2-U	ACCACTACTACTAAAAACAA	TGTATTTTGGTTTGGGTTGT	283
q31.3-M	ACGAAATACCTACGCGCAAC	CGCGGGTAATAAAGTTTAC	149
q31.3-U	ACAAAATACCTACACCAAC	TGTGGGTAATAAAGTTTAT	149
q32.3-M	CGCGACTCCGAACAATAACC	AATGTAGTTATAATCGCGGC	243
q32.3-U	CACAACCTCAAACAATAACC	AATGTAGTTATAATTGTGGT	243
q34-M	AGGTTATAGGTTAGACGCGGC	CGAAACGAACGAAAACAAAC	252
q34-U	AGGTTATAGGTTAGATGTGGT	CAAAACAACAAAACAAAC	252

^aGiven as the corresponding chromosomal band of the long arm of chromosome 13

G-banding level (Fig. 1a). *RB1* signals were detected on the normal chromosome 13 and on der(X), indicating no breakpoint in the *RB1* gene (Fig. 1b). Further FISH analysis with BAC clones mapped the breakpoint to between RP11-179A7 (13q13.2) and RP11-91 K18 (13q13.3), which was 12 to 15 Mb upstream of the *RB1* locus (Fig. 1c). These results indicated that the translocation in our patient did not disrupt the *RB1* gene or its regulatory region. Whole genomic microarray analysis and sequencing of the coding regions of the *RB1* gene revealed no copy number changes or nucleotide variations (data not shown). Thus, we could not map the precise location of the translocation breakpoint using microarray.

XCI patterns

We next assessed whether the der(X) region had been subjected to XCI, which could inactivate *RB1* and nearby genes leading to the retinoblastoma and other symptoms observed in the patient. A HUMARA assay was performed using genomic DNA extracted from peripheral blood. The XCI of allele-1 and -2 was 90.2 and 9.8%, respectively (Fig. 2a). To determine which alleles of the *androgen receptor* gene were located on der(X), we

carried out BrdU labeling of the late-replicating heterochromatin in an EBV-transformed LCL (Fig. 2b). Thirty-eight percent of the cells were BrdU-positive at the normal X, whereas the der(X) was positive in 62% of the cells. The XCI of allele-1 and -2 was 29.3 and 70.7%, respectively, in a HUMARA assay of the LCL (Fig. 2a). From these results, we considered allele-1 to be linked to the normal X chromosome, indicating that the XCI was skewed to the normal X in the peripheral blood of our patient.

Methylation of the *RB1* gene and other regions of 13q

To examine whether the *RB1* gene itself was inactivated in our patient, MSP was performed for the *RB1* promoter using bisulfite-treated DNA as the template. PCR products were detected in the patient and in a positive control but not in a healthy control when a primer pair for amplifying methylated DNA was used (Fig. 3a). The methylation level of the 27 CpG sites in the *RB1* promoter was then investigated using a deep sequencing approach [11]. The patient had a higher methylation frequency than a healthy control (Fig. 3b), with the highest frequency found to be 5.6% at position #17 in her peripheral blood. Given our findings with the HUMARA

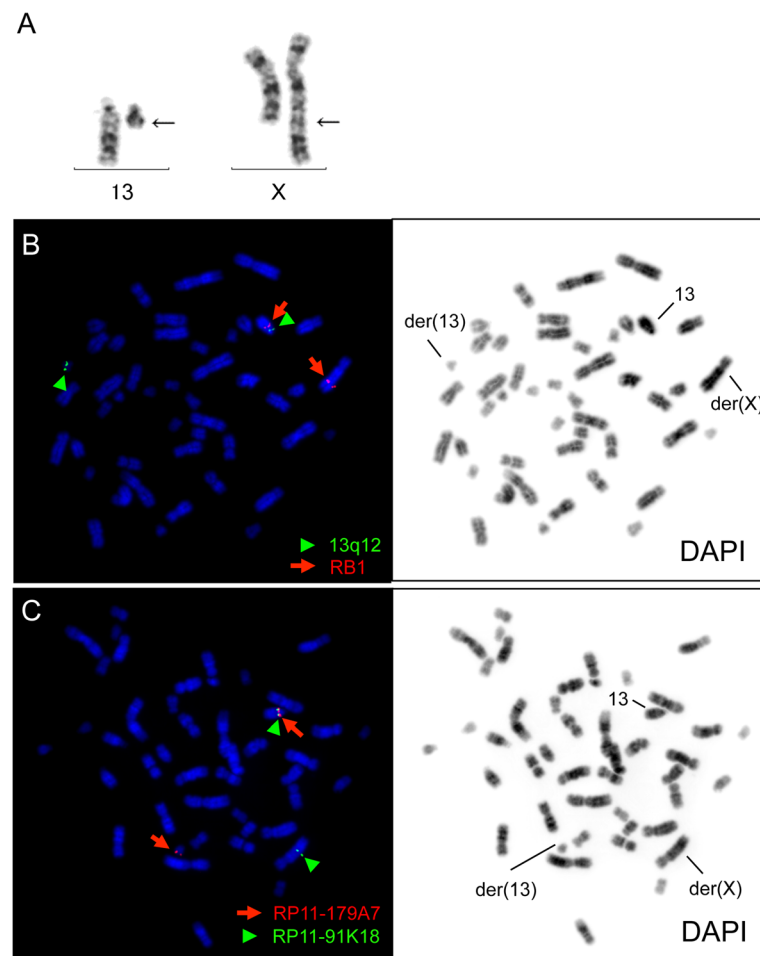


Fig. 1 G-banding and FISH analyses of the study patient. **(a)** A G-banded partial karyotype. The arrows indicate the breakpoints of the derivative chromosomes. **(b)** FISH analysis of the *RB1* gene. The arrows and arrowheads indicate *RB1* and 13q12 probes, respectively. **(c)** FISH analysis of the breakpoint on chromosome 13. The arrows and arrowheads indicate RP11-179A7 and RP11-91 K18 probes, respectively

assay in which ~10% of the cells showed the der(X) inactivation (Fig. 2a), we speculated that one *RB1* allele in each cell might be inactivated. Since position #17 is the activating transcription factor (ATF) binding site, methylation of this site might inhibit the binding of transcription factors [12].

We next demarcated the 13q region of inactivation on the der(X) using MSP (Table 2). The region proximal to the breakpoint was not found to be methylated, whereas those distal to it were extensively methylated in our study patient. Although methylation was also detected in regions distal to the *RB1* gene, those of 13q31 were not specific to the patient. Regions near to the 13q terminal were not methylated in the patient.

Discussion and conclusions

In a similar manner to our present patient, several prior cases of retinoblastoma carrying a constitutional X;13 translocation without disruption of the *RB1* gene had

been reported [13–17] and described an inactivation of the derivative chromosome harboring the *RB1* gene [18–23]. The breakpoints of most of these cases including our patient were located at 13q12-q14 regions. To our knowledge, our present case report is the first to demonstrate inactivation of the *RB1* gene at the molecular level i.e. by epigenetic mechanisms. Selective XCI in females with balanced X-A translocations is attributed to a haploinsufficiency of dosage sensitive genes near to the breakpoint in the autosomal region affecting cell viability. Our current case and similar prior retinoblastoma cases harboring X;13 translocations suggest that there are no such critical genes near to the breakpoint on 13q. This would mean that selective XCI of the normal X chromosome in X-A translocation carriers is dependent on the translocation partner chromosome. Moreover, such dosage-sensitive genes may be different between cell lineages, leading to different levels of inactivation among tissues. The HUMARA analysis of the peripheral

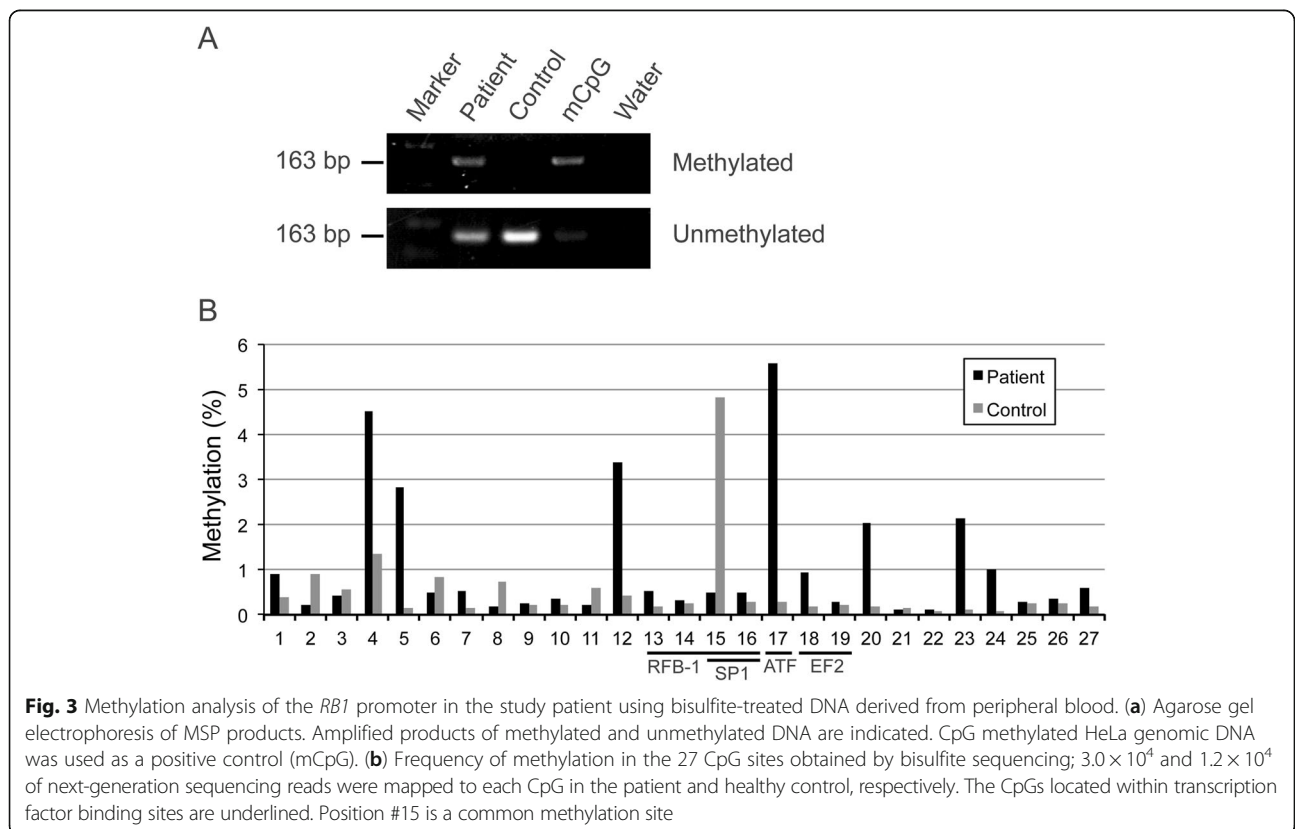
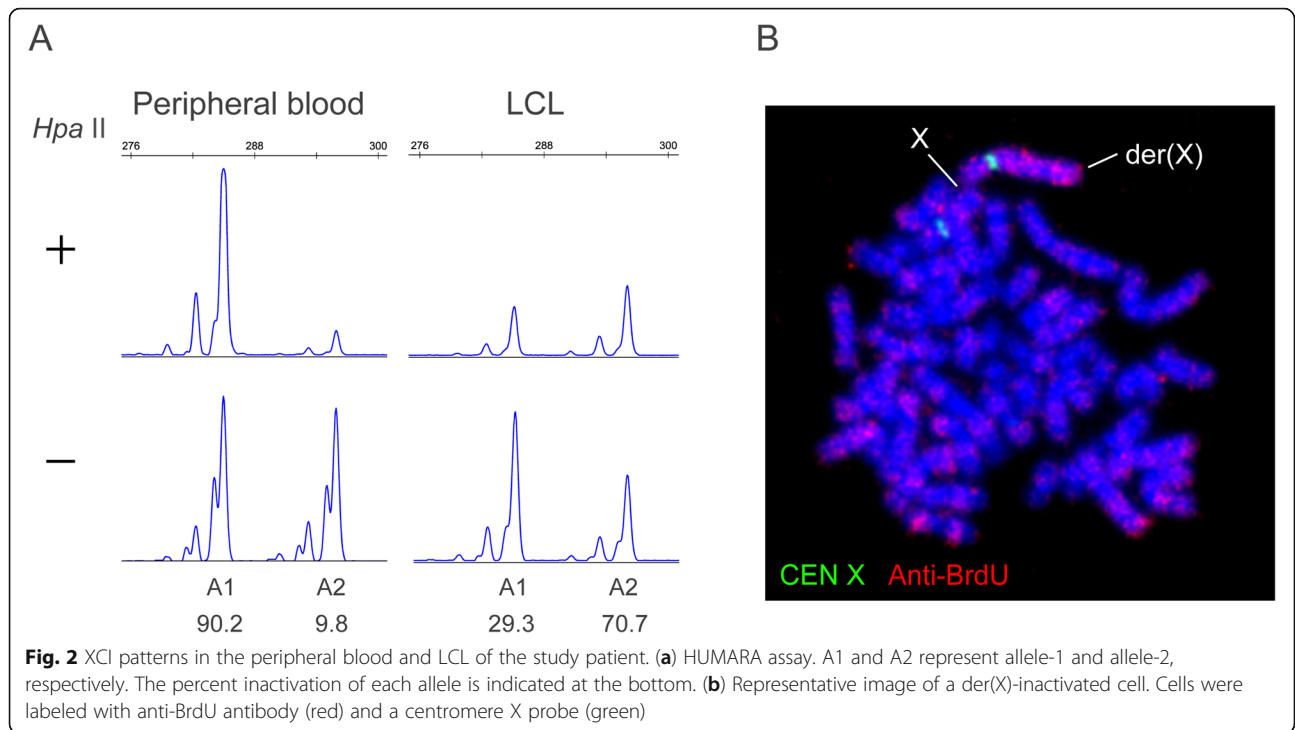


Table 2 MSP amplification of the 13q region in the study patient and healthy controls

	q13.1	q14.11	q14.2 (<i>RB1</i>)	q14.3	q21.33	q31.1prox	q31.1 dis	q31.2	q31.3	q32.3	q34
Patient	-	+	+	+	+	+	+	+	+	-	-
Control-1	-	-	-	-	-	+/-	+	+/-	+	-	-
Control-2	n.d.	n.d.	n.d.	n.d.	-	+	+	n.d.	-	+/-	n.d.
Control-3	n.d.	n.d.	n.d.	n.d.	-	-	+	n.d.	+/-	-	n.d.

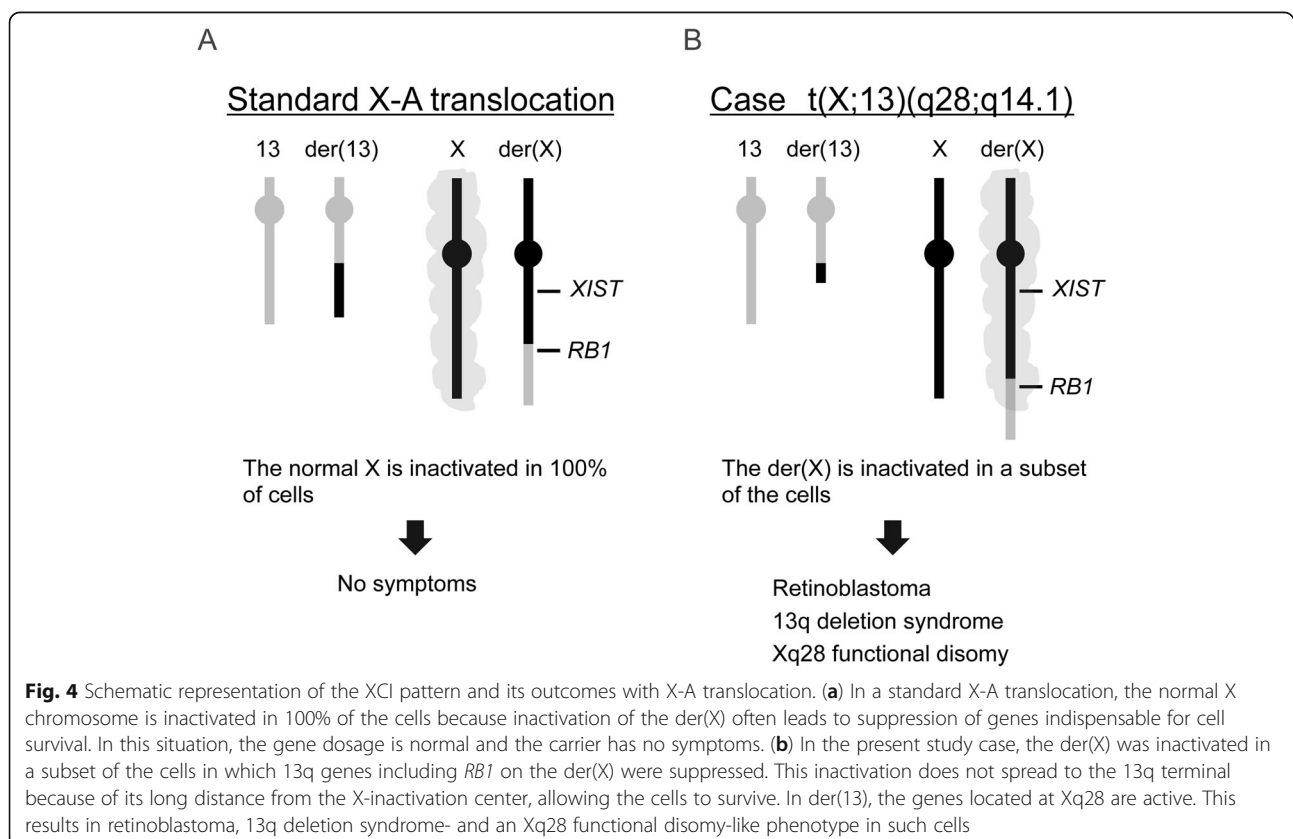
n.d.: not determined

blood from our current study patient revealed that the normal X was inactivated in 90% of the cells. Although specimens from other tissues in our subject were not available, we speculated that a high frequency of der(X) inactivation would be likely in the retinal cell lineage since our patient suffered from bilateral retinoblastoma. The retinal cell lineage has a relative tolerance to the inactivation of 13q and ironically develop RB. Furthermore, the systemic phenotype of our current study patient other than retinoblastoma implied the presence of a considerable number of cells with an inactivated der(X).

The 13q deletion syndrome is classified into three types depending on the deleted region [5, 24]. Group 1 comprises patients with deletions proximal to 13q32 who show mild or moderate intellectual disability, minor malformations, constipation, growth retardation and

inconstant retinoblastoma. Group 2 comprises cases of deletions encompassing 13q32 that show severe intellectual disability, growth retardation, one or more major malformations of the brain, genitourinary and gastrointestinal tract, and distal limb. Group 3 comprises patients with deletions distal to 13q32 who show severe intellectual disability without major malformations or growth retardation. The inactivated region of 13q in our current patient corresponded to group 1 (Table 2), and she had both growth retardation and constipation. However, her intellectual phenotype was more severe than was typically seen in patients categorized as group 1.

We speculated that the cause of the severe phenotype in our patient originated from a functional disomy of Xq28 which was translocated to der(13). Functional disomy is a situation in which X-linked genes, normally expressed monoallelically, are expressed biallelically in



individuals carrying chromosome X-involved structural variants with an unfavorable XCI pattern. As a result, X-linked genes are expressed at a 2-fold higher level than normal [25]. In this case, the der(X) was possibly inactivated in the brain of the patient derived from the common ancestral cell lineage with retina. Thus, Xq28 on the der(13) without the X-inactivation center likely escaped XCI resulting in a functional disomy. Severe developmental delays are common in patients with an Xq28 functional disomy, as was the case in our current patient [26]. The mechanism underlying the onset of retinoblastoma and 13q deletion syndrome- or an Xq28 functional disomy-like phenotype is illustrated in Fig. 4. Our patient was susceptible to the development of retinoblastoma because of the inactivation of the *RB1* gene on the der(X) in her retinal cell lineage. A somatic mutation in the other allele on the normal chromosome 13 became the second hit.

We describe a female patient with retinoblastoma and severe intellectual disability, carrying an X;13 translocation. Her *RB1* gene was not disrupted by this translocation but became inactivated by the XCI system. Our current data have important clinical implications. Females carrying an X;13 translocation should be followed-up closely for the early detection of retinoblastoma in infancy and other cancers throughout her life. This should be done even if the XCI is found to be 100% skewed in analysis of peripheral blood samples, because XCI patterns can vary in different tissues. Hence, a female retinoblastoma patient who is a suspected carrier of a germline mutation should be assessed using cytogenetic methods such as G-banding even when conventional analysis reveals no mutations of the *RB1* gene.

Abbreviations

ATF: Activating transcription factor; BAC: Bacterial artificial chromosome; BrdU: Bromodeoxyuridine; EBV: Epstein-Barr virus; FISH: Fluorescence in situ hybridization; HUMARA: Human androgen receptor assay; LCL: Lymphoblastoid cell line; MSP: Methylation specific PCR; RB: Retinoblastoma; X-A: X-autosome; XCI: X-chromosome inactivation

Acknowledgements

We thank to Narumi Kamiya for technical assistance.

Authors' contribution

MT, NF, RK and FS carried out the cytogenetic analysis; MT, MK, YS, MK and TK carried out molecular analysis; HH carried out the genetic counseling; HH, NA, NM, TK and KH carried out the clinical management of the patient; MT, HH and HK designed the study and drafted the manuscript. All authors read and approved the final manuscript.

Funding

This study was supported by grants-in-aid for Scientific Research from the Ministry of Education, Culture, Sports, Science, and Technology of Japan, that from Ministry of Health, Welfare and Labor, and that from Japan Agency for Medical Research and Development.

Availability of data and materials

The datasets used and/or analysed during the current study are available from the corresponding author on reasonable request.

Ethics approval and consent to participate

The genetic testing used in this study was approved by the ethics committee of Fujita Health University in accordance with the principles of the Declaration of Helsinki, and the Ethical Guidelines for Human Genome/ Gene Analysis Research by the Ministry of Education, Culture, Science, and Technology, the Ministry of Health, Labor, and Welfare, and the Ministry of Economy, Trade, and Industry of Japan. Written informed consent was obtained from all of the participants or their parents in accordance with local institutional review board guidelines.

Consent for publication

Written informed consent was obtained from a parent of the patient for publication of this study.

Competing interests

The authors declare that they have no competing interests.

Author details

¹Division of Molecular Genetics, Institute for Comprehensive Medical Science, Fujita Health University, 1-98 Dengakugakubo, Kutsukake-cho, Toyoake, Aichi 470-1192, Japan. ²Department of Clinical Genetics, National Hospital Organization, Nagoya Medical Center, Nagoya, Japan. ³Department of Pediatrics, National Hospital Organization, Nagoya Medical Center, Nagoya, Japan. ⁴Department of Ophthalmology, National Hospital Organization, Nagoya Medical Center, Nagoya, Japan. ⁵Genome and Transcriptome Analysis Center, Fujita Health University, Toyoake, Japan. ⁶Center for Collaboration in Research and Education, Fujita Health University, Toyoake, Japan.

Received: 27 September 2019 Accepted: 29 November 2019

Published online: 05 December 2019

References

- Lyon MF. Some milestones in the history of X-chromosome inactivation. *Annu Rev Genet.* 1992;26:16–28.
- Avner P, Heard E. X-chromosome inactivation: counting, choice and initiation. *Nat Rev Genet.* 2001;2(1):59–67.
- Lohmann DR, Gallie BL. Retinoblastoma. In: Adam MP, Ardinger HH, Pagon RA, Wallace SE, Bean LH, Stephens K, Amemiya A, editors. *GeneReviews*® [internet]. Seattle (WA): University of Washington, Seattle; 1993–2019. <https://www.ncbi.nlm.nih.gov/books/NBK1452/>.
- Allderdice PW, Davis JG, Miller OJ, Klinger HP, Warburton D, Miller DA, Allen FH Jr, Abrams CA, McGilvray E. The 13q-deletion syndrome. *Am J Hum Genet.* 1969;21(5):499–512.
- Mitter D, Ullmann R, Muradyan A, Klein-Hitpass L, Kanber D, Ounap K, Kaulisch M, Lohmann D. Genotype-phenotype correlations in patients with retinoblastoma and interstitial 13q deletions. *Eur J Hum Genet.* 2011;19(9):947–58.
- Tsutsumi M, Yokoi S, Miya F, Miyata M, Kato M, Okamoto N, Tsunoda T, Yamasaki M, Kanemura Y, Kosaki K, Saitoh S, Kurahashi H. Novel compound heterozygous variants in *PLK4* identified in a patient with autosomal recessive microcephaly and chorioretinopathy. *Eur J Hum Genet.* 2016;24(12):1702–6.
- Kawai M, Tsutsumi M, Suzuki F, Sameshima K, Dowa Y, Kyoya T, Inagaki H, Kurahashi H. Two siblings with 11qter deletion syndrome that had been rescued in their mother by uniparental disomy. *Eur J Med Genet.* 2019;62(3):224–8.
- Tusnády GE, Simon I, Váradi A, Arányi T. BiSearch: primer-design and search tool for PCR on bisulfite-treated genomes. *Nucleic Acids Res.* 2005;33(1):e9.
- Quiñonez-Silva G, Dávalos-Salas M, Recillas-Targa F, Ostrosky-Wegman P, Aranda DA, Benítez-Bribiesca L. Monoallelic germline methylation and sequence variant in the promoter of the *RB1* gene: a possible constitutive epimutation in hereditary retinoblastoma. *Clin Epigenetics.* 2016;8:1.
- Krueger F, Andrews SR. Bismark: a flexible aligner and methylation caller for bisulfite-Seq applications. *Bioinformatics.* 2011;27(11):1571–2.
- Stirzaker C, Millar DS, Paul CL, Warnecke PM, Harrison J, Vincent PC, Frommer M, Clark SJ. Extensive DNA Methylation spanning the *Rb* promoter in retinoblastoma tumors. *Cancer Res.* 1997;57(11):2229–37.
- Ohtani-Fujita N, Fujita T, Aoike A, Osifchin NE, Robbins PD, Sakai T. CpG methylation inactivates the promoter activity of the human retinoblastoma tumor-suppressor gene. *Oncogene.* 1993;8(4):1063–7.

13. Hida T, Kinoshita Y, Matsumoto R, Suzuki N, Tanaka H. Bilateral retinoblastoma with a 13qXp translocation. *J Pediatr Ophthalmol Strabismus*. 1980;17(3):144–6.
14. Ponzio G, Savin E, Cattaneo G, Ghiotti MP, Marra A, Zuffardi O, Danesino C. Translocation X;13 in a patient with retinoblastoma. *J Med Genet*. 1987; 24(7):431–4.
15. Stambolian D, Sellinger B, Derrington D, Sargent R, Emanuel BS. Cytogenetic and molecular investigation of a balanced Xq13q translocation in a patient with retinoblastoma. *Am J Med Genet*. 1992;42(6):771–6.
16. Laquis SJ, Rodriguez-Galindo C, Wilson MW, Fleming JC, Haik BG. Retinoblastoma in a patient with an X;13 translocation and facial abnormalities consistent with 13q-syndrome. *Am J Ophthalmol*. 2002;133(2): 285–7.
17. Dries D, Baca K, Truss L, Dobin S. Interstitial deletion of 13q and a 13;X chromosome translocation results in partial trisomy 13 and bilateral retinoblastoma. *Ophthalmic Genet*. 2003;24(3):175–80.
18. Cross HE, Hansen RC, Morrow G 3rd, Davis JR. Retinoblastoma in a patient with a 13qXp translocation. *Am J Ophthalmol*. 1977;84(4):548–54.
19. Nichols WW, Miller RC, Sobel M, Hoffman E, Sparkes RS, Mohandas T, Veomett I, Davis JR. Further observations on a 13qXp translocation associated with retinoblastoma. *Am J Ophthalmol*. 1980;89(5):621–7.
20. Ejima Y, Sasaki MS, Kaneko A, Tanooka H, Hara Y, Hida T, Kinoshita Y. Possible inactivation of part of chromosome 13 due to 13qXp translocation associated with retinoblastoma. *Clin Genet*. 1982;21(6):357–61.
21. Kajiji T, Tsukahara M, Fukushima Y, Hata A, Matsuo K, Kuroki Y. Translocation (X;13)(p11.21;q12.3) in a girl with incontinentia pigmenti and bilateral retinoblastoma. *Ann Genet*. 1985;28(4):219–23.
22. Gorski JL, Burreight EN, Harnden CE, Stein CK, Glover TW, Reyner EL. Localization of DNA sequences to a region within Xp11.21 between incontinentia pigmenti (IP1) X-chromosomal translocation breakpoints. *Am J Hum Genet*. 1991;48(1):53–64.
23. Jones C, Booth C, Rita D, Jazmines L, Brandt B, Newlan A, Horsthemke B. Bilateral retinoblastoma in a male patient with an X; 13 translocation: evidence for silencing of the RB1 gene by the spreading of X inactivation. *Am J Hum Genet*. 1997;60(6):1558–62.
24. Brown S, Russo J, Chitayat D, Warburton D. The 13q- syndrome: the molecular definition of a critical deletion region in band 13q32. *Am J Hum Genet*. 1995;57(4):859–66.
25. Sanlaville D, Schluth-Bolard C, Turleau C. Distal Xq duplication and functional Xq disomy. *Orphanet J Rare Dis*. 2009;4:4.
26. Sanlaville D, Prieur M, de Blois MC, Genevieve D, Lapiere JM, Ozilou C, Picq M, Gosset P, Morichon-Delvallez N, Munnich A, Cormier-Daire V, Baujat G, Romana S, Vekemans M, Turleau C. Functional disomy of the Xq28 chromosome region. *Eur J Hum Genet*. 2005;13(5):579–85.

Publisher's Note

Springer Nature remains neutral with regard to jurisdictional claims in published maps and institutional affiliations.

Ready to submit your research? Choose BMC and benefit from:

- fast, convenient online submission
- thorough peer review by experienced researchers in your field
- rapid publication on acceptance
- support for research data, including large and complex data types
- gold Open Access which fosters wider collaboration and increased citations
- maximum visibility for your research: over 100M website views per year

At BMC, research is always in progress.

Learn more biomedcentral.com/submissions





Two siblings with 11qter deletion syndrome that had been rescued in their mother by uniparental disomy

Miki Kawai^a, Makiko Tsutsumi^a, Fumihiko Suzuki^{a,b}, Kiyoko Sameshima^c, Yuri Dowa^d, Takuji Kyoya^e, Hidehito Inagaki^{a,f}, Hiroki Kurahashi^{a,b,f,*}

^a Division of Molecular Genetics, Institute for Comprehensive Medical Science, Fujita Health University, Toyoake, Japan

^b Center for Collaboration in Research and Education, Fujita Health University, Toyoake, Japan

^c Department of Pediatrics, Minamikyushu National Hospital, Aira, Japan

^d Department of Neurology, Gunma Children's Medical Center, Shibukawa, Japan

^e Department of Obstetrics, Gunma Children's Medical Center, Shibukawa, Japan

^f Genome and Transcriptome Analysis Center, Fujita Health University, Toyoake, Japan

ARTICLE INFO

Keywords:

11q23-qter deletion
Jacobsen syndrome
Deletion rescue
Uniparental disomy
Skewed X chromosome inactivation
Germline mosaicism

ABSTRACT

Jacobsen syndrome refers to a congenital anomaly caused by deletion at 11q23.3-qter. We here describe two siblings with the same 11q23.3-qter deletion. Both parents were healthy with a normal karyotype. Cytogenetic microarray analysis revealed no mosaicism in either parent but the mother showed uniparental disomy encompassing the deleted region found in the two siblings. The pattern of X chromosome inactivation was almost completely skewed in the mother. These data suggested that the mother was a carrier of the 11q23.3-qter deletion but that this had been rescued by disomy formation during early embryogenesis except for her germinal cells.

1. Introduction

Jacobsen syndrome (MIM#147791) is a contiguous gene deletion syndrome caused by deletion of the 11qter region. The typical clinical features of Jacobsen syndrome include pre- and postnatal physical growth and psychomotor retardation, facial dysmorphic features, and thrombocytopenia. Some patients with this syndrome also have malformations of the heart, kidney, gastrointestinal tract, and central nervous system. Ocular and hearing problems can be also present. The estimated occurrence of Jacobsen syndrome is about 1/100,000 births (Mattina et al., 2009).

About 85% of Jacobsen syndrome cases are caused by a simple *de novo* terminal deletion. Other cases result from a variety of chromosomal abnormalities including segregation of a familial reciprocal balanced translocation, *de novo* unbalanced translocations, recombination of a parental pericentric inversion, or other rearrangements such as ring chromosomes. An 11q deletion has also been reported in the mosaic form of this condition. The breakpoints in these deletions occur within or distal to 11q23.3, and the deletions usually extend to the telomere (Grossfeld et al., 2004). The deletion size ranges from 7 to 20 Mb. The chromosomal region conferring specificity for the Jacobsen syndrome

phenotype is the 11q24.2 band, but the gene responsible for this phenotype is still unknown.

We here report on two siblings with the same 11q23.3-qter deletion, one with Jacobsen syndrome and the other detected by amniocentesis and terminated. The parents however showed a normal karyotype. Cytogenetic microarray analyses revealed that the healthy mother had uniparental disomy (UPD) encompassing the 11q22.3-ter region deleted in the siblings. A possible mechanism for the recurrence of this deletion is discussed.

2. Clinical report

A 4-year old Japanese male subject was the first child of a non-consanguineous healthy 36-year old father and 28-year old mother after having three miscarriages with no notable family history of disease (Fig. 1A). At 22 weeks of pregnancy, a congenital heart defect, mitral valve stenosis and aortic valve stenosis were suspected. He had been born after a 41 week gestation by an induced labor with a birth weight of 2644 g (−0.9SD), height of 47.5 cm (−0.7SD), head circumference of 34.5 cm (+0.8SD), and chest circumference of 30 cm. He showed a hypoplastic left heart, conductive auditory impairment in the left ear,

* Corresponding author. Division of Molecular Genetics, Institute for Comprehensive Medical Science, Fujita Health University, 1-98 Dengakugakubo, Kutsukakecho, Toyoake, Aichi, 470-1192, Japan.

E-mail address: kura@fujita-hu.ac.jp (H. Kurahashi).

<https://doi.org/10.1016/j.ejmg.2018.07.018>

Received 1 March 2018; Received in revised form 12 June 2018; Accepted 17 July 2018

Available online 18 July 2018

1769-7212/ © 2018 Elsevier Masson SAS. All rights reserved.

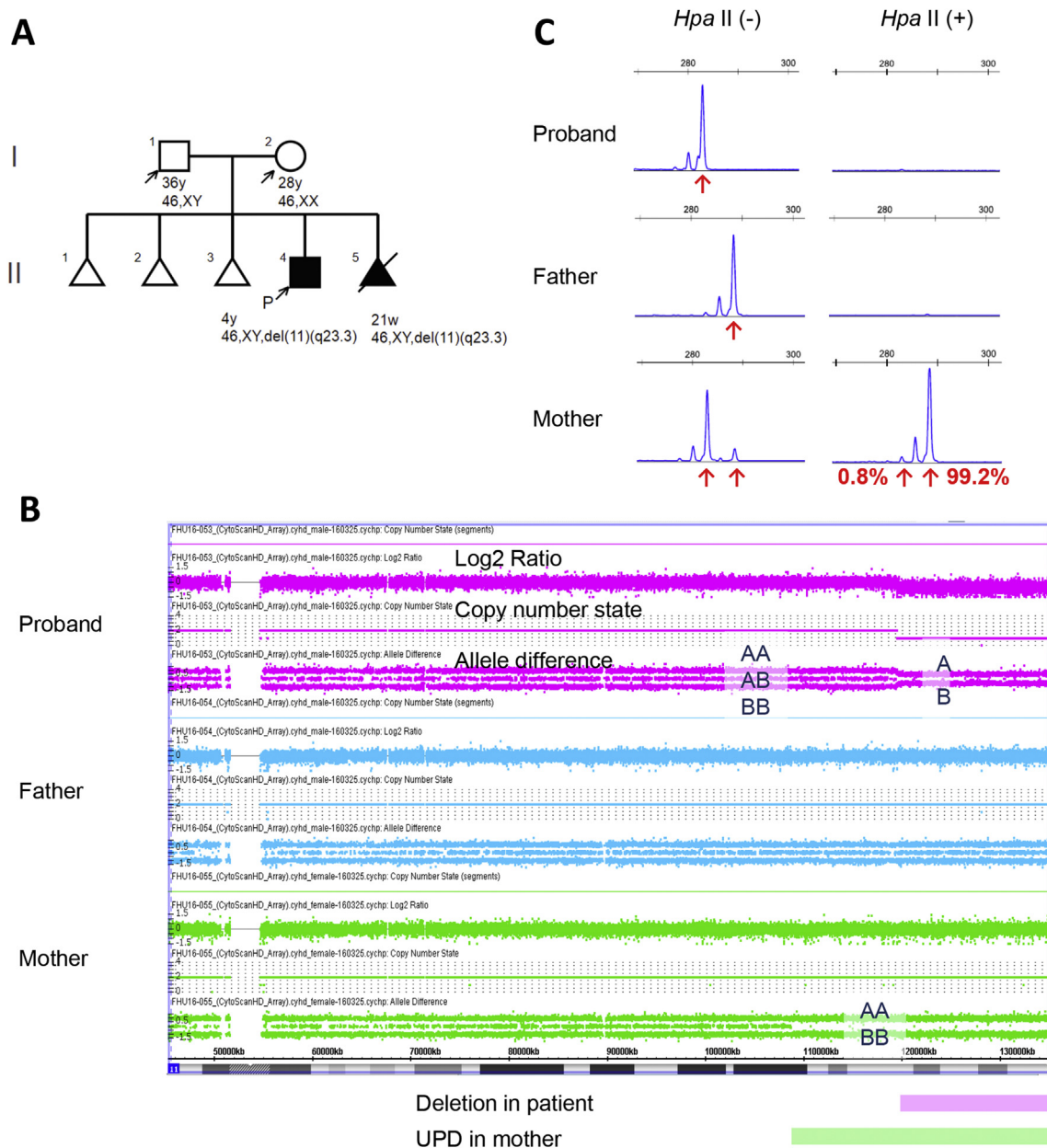


Fig. 1. Deletion rescue on 11qter. **(A)** Pedigree of the study family. **(B)** Cytogenetic microarray results for the 11q region for the proband (pink), father (blue), and mother (green). The copy number log2 ratio (top), copy number state (middle), and allele difference (bottom) are shown for each sample. The pink bar at the bottom indicates the deleted region in the proband. The green bar indicates the UPD region in the mother. **(C)** HUMARA assay results. The electropherogram shows the fragment analysis of the amplicons from undigested (left) and digested (right) genomic DNA from the proband (top), father (middle), and mother (bottom). The major peaks depicted by the red arrows indicate the sizes of the PCR products with different numbers of short tandem repeats at the HUMARA locus. The two major peaks found in the mother represent two X chromosome alleles (282bp, 288bp). Digestion of the DNA from the proband (son)'s and father's sample showed complete loss of one allele, whereas a preferential loss of the short alleles was evident in the mother (282bp). (For interpretation of the references to colour in this figure legend, the reader is referred to the Web version of this article.)

widely spaced eyes, a short nose, a small ear lobe, thin vermilion of upper lip and lower lip, shortness in both fifth fingers, and a bifid scrotum. He also had an old cerebral hemorrhage in the nucleus basalis.

The subject also showed severely retarded psychomotor development. The ability to hold up his head, roll over, and speak, were recognized at 2 years and 7 months, 2 years and 7 months, and 3 years and 3 months. Serial complete blood counts revealed transient thrombocytopenia. At the age of 4 years and 2 months, he showed a height of $-3.5SD$, weight of $-2.2SD$, and head circumference of $-1.2SD$. His karyotype revealed 46,XY,del(11)(q23.3), which is known as Jacobsen syndrome.

At 2 years after the birth of this first child, the mother again became

pregnant with a boy. The fetus was diagnosed with the same karyotype as the brother by amniocentesis at 15 weeks and 4 days of gestation. At 20 weeks and 4 days, a hypoplastic left heart with severe atrioventricular regulation was evident on ultrasound examination. At 21 weeks, the pregnancy was terminated and the fetus was found to weigh 344 g. Karyotype analysis of the parental peripheral blood lymphocytes revealed 46, XY [20] and 46, XX [20].

3. Materials and methods

3.1. Subjects

Peripheral blood samples were obtained from the study subject and the parents. The research protocol for this study was approved by the local ethics committee of Fujita Health University, Japan. Written informed consent to participate in the study was obtained from the parents.

3.2. DNA extraction

Genomic DNA was extracted from whole blood using QuickGene 610 L (Fuji film, Tokyo, Japan). The concentration of the DNA was measured using an ND-1000 spectrophotometer (NanoDrop, Wilmington, DE) and the quality was determined by gel electrophoresis.

3.3. Cytogenetic microarray

High-resolution chromosomal microarray analysis using the CytoScan HD array (Affymetrix, Santa Clara, CA) was performed. DNA samples of 50 ng were used in this analysis in accordance with the manufacturer's instructions. The genomic coordinates were based upon genome build 37/hg19 (2009). Hybridization, data extraction and analysis were performed as per the manufacturer's protocols. Chromosome Analysis Suite software 3.0 (ChAS, Affymetrix Santa Clara, CA) was used for raw data analysis, review and reporting. Regions of copy-number changes were extracted with 20 probes of 50 kb. All of the extracted regions containing a copy-number change were confirmed by visual comparisons with the normal control data from Database of Genomic Variants (<http://dgv.tcag.ca>). UPD regions were extracted with 5 Mb. Regions with a sparse SNP density were carefully evaluated to exclude false calls.

3.4. FISH analysis

Peripheral blood lymphocytes and buccal samples were obtained by standard methods. FISH analysis was performed using standard techniques. The probes used for the FISH analysis were TelVysion 11p SpectrumGreen (D11S2071), TelVysion 11q SpectrumOrange (D11S1037) (Abbott Molecular, IL, USA). A hundred interphases nuclei were analyzed for pter/qter of chromosome 11.

3.5. HUMARA assay

To assess skewing of the X chromosome inactivation, we performed HUMARA assay according to the protocol described elsewhere (Beever et al., 2003). Briefly, we digested the genomic DNA with methylation-sensitive restriction enzyme *HpaII*. PCR primers, one of which was labeled with FAM, were designed across the polymorphic CAG repeat as well as two *HpaII* sites in the androgen receptor gene on the X chromosome. PCR amplification would be achieved only from the inactivated allele having the *HpaII* sites methylated. PCR products were analyzed by capillary electrophoresis (ABI3730 Genetic Analyzer) and quantified the area under the curve using GeneMapper software.

4. Results

We performed cytogenetic microarray analysis to demarcate the deleted region in our current case subject. A 15.4-Mb region was found to have been deleted at 11q23.3q25-qter in this patient (arr [hg19] 11q23.3q25 (119, 484, 933_134, 938, 470)×1), which is consistent with the typically deleted region in Jacobsen syndrome (Fig. 1B). The deleted region was found to contain 128 Refseq genes, and 70 OMIM genes. Single nucleotide polymorphism (SNP) genotyping indicated that the deleted chromosome was derived from the mother (data not

shown).

A possible explanation for the abnormal 46,XY,del (11) (q23.3) karyotype in two siblings from parents with a normal karyotype was that one of the parents harbored FRA11B, a (CCG)_n repeat expansion in the 5′ untranslated region of the *CBL2* gene. In more than 70% of normal individuals, this repeat is present in 11 copies but can be expanded to several hundred copies and lead to genomic instability and a susceptibility for terminal deletion (Mattina et al., 2009). However, the deletion breakpoint of our current patient was at chr11:119, 484, 933 (hg19), which is approximately 400 kb distal from FRA11B.

Neither of the parents showed deletion mosaicism at the 11q23.3-qter region. Interphase FISH on 100 peripheral blood lymphocytes and 100 buccal cells revealed no deletion for the 11q subtelomere-specific probe (data not shown). It was notable however that SNP array analysis of the patient's mother detected a 26.2-Mb region with a loss of heterozygosity at 11q22.3-qter consistent with uniparental disomy (UPD) (arr [hg19]11q22.3q25 (108, 657, 506_134, 942, 626)×2 hmz) (Fig. 1B). The deletion breakpoint in the son was 10-Mb distal from the UPD boundary in the mother.

A HUMARA assay was performed to determine when the UPD was generated in the mother. The patterns of X chromosome inactivation (XCI) showed 99.2% skewing in the mother (Fig. 1C), suggesting that she originally had the same deletion as her son and the chromosome copy number loss was corrected by UPD after XCI occurred in the early embryogenesis.

5. Discussion

Our analysis by cytogenetic microarray of our current case subject with 11qter deletion syndrome and his family suggests that segmental UPD corrected the chromosomal copy number of the deleted region and thereby rescued the phenotype in his healthy mother. To our knowledge, there have only been two previous reports of siblings showing a deletion of 11q23.3-qter despite a normal parental karyotype (Affifi et al., 2008; Johnson et al., 2014). One of those reports also provided detailed molecular analyses showing a maternal UPD at the 11qter region (Johnson et al., 2014). A 22q13 deletion rescued by paternal UPD has also been reported (Bonaglia et al., 2009). Such deletion rescue event has not been reported for other terminal deletions. Our current case is therefore the third report to describe a deletion rescued by post-zygotic UPD generation.

It is likely that the mother of our current case subject originally carried the 11q23.3-qter deletion that had been transmitted from a gamete of a maternal grandfather or grandmother. After fertilization, this deletion was likely rescued during the post-zygotic stage via a DNA repair pathway for coincidental double-strand-breaks (DSBs) at the proximal region of the deletion breakpoint, thereby generating the segmental UPD. The UPD boundary in the mother is located 10 Mb more proximal than the breakpoint of deleted region of the patient, which is a strong evidence that the UPD developed after the deletion. The principal molecular mechanisms that have been postulated to explain segmental UPD are mitotic recombination or break-induced replication (BIR) (Costantino et al., 2014; Carvalho et al., 2015).

We observed an almost completely skewed XCI in the mother's DNA. Generally, an XCI pattern increases the extent of skewing with age as a consequence of hematopoietic stem cell senescence. At 20–39 years old, mean skewing level is reported to be 70.6% (Hatakeyama et al., 2004). Our current patient's mother was 30 years old at the time of genetic testing and showed very high skewing at 99.2%. This indicated that her blood cells were derived from a single clone after XCI (Kurahashi et al., 1991). We speculated that the mother originally harbored the 11q23.3-qter deletion as a zygote which was subsequently repaired in one of the somatic cells by mitotic recombination or BIR after XCI has been completed. The repaired cell likely obtained selective advantage during embryonic development and unrepaired cells were eliminated (Fig. 2). This resulted in a normal phenotype at birth and no evidence of

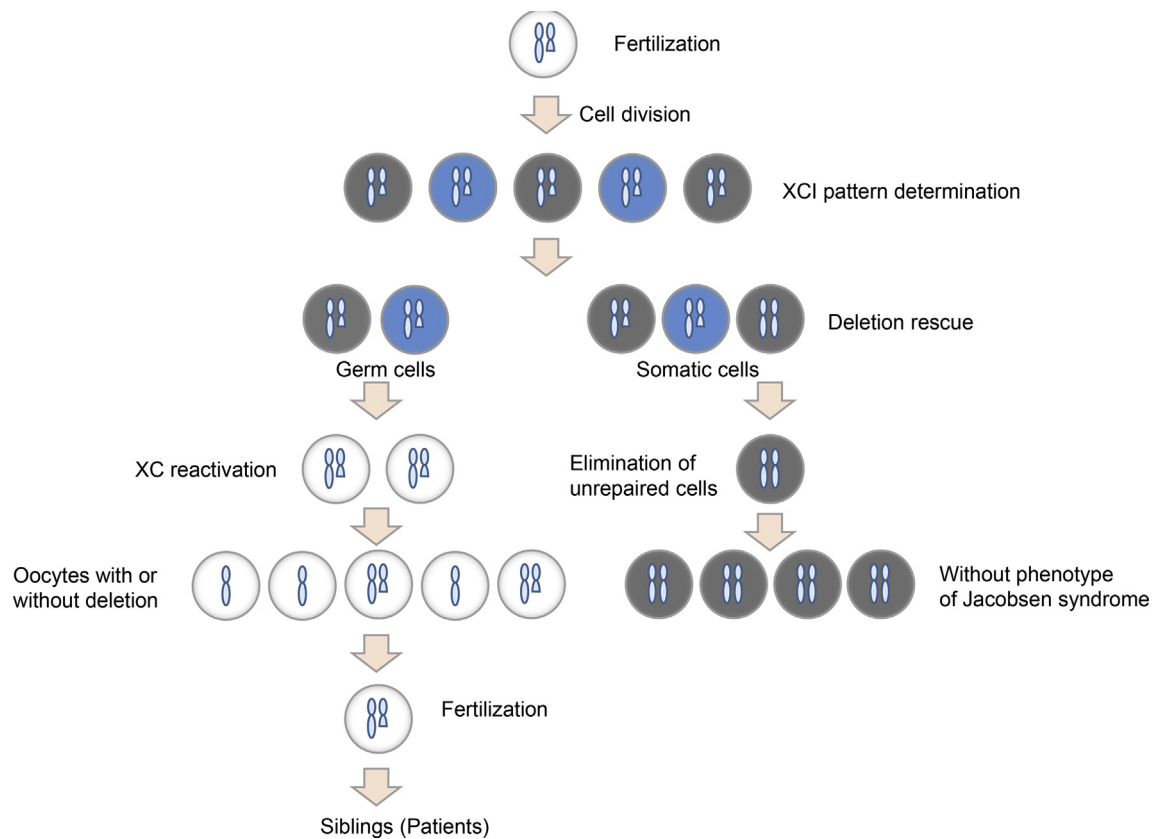


Fig. 2. An illustration for the status of the mother and the two siblings.

Jacobsen syndrome. It appears however that although her somatic cells had all been rescued by UPD her germ cells retained the 11q23-qter deletion. Such monoclonality has been described previously in trisomy rescue of chromosome 15 (Butler et al., 2007). Thus, this mother had no Jacobsen syndrome phenotype but transmitted the causative deletion to her two sons.

As far as we are aware, there have been only two other case reports of ‘deletion rescue’ (Bonaglia et al., 2009; Johnson et al., 2014). It would be intriguing if 11q23.3-qter was found to be a hotspot for deletion rescue. One possible explanation for this phenomenon is a strong negative selection process as a result of gene loss. An alternative possibility is that there might be a DSB hotspot that induces mitotic recombination or BIR at the region proximal to the 11q23.3 breakpoint. If this is indeed the case, the recurrence risk in the affected siblings would be slightly higher than in the general population. SNP array analysis of the parents might be advisable even in an apparent *de novo* case of Jacobsen syndrome.

In conclusion, we speculate that the maternal 11q23.3-qter deletion was repaired in our current study family via mitotic recombination or BIR leading to UPD generation. As a consequence of this DNA repair, the chromosomal copy number was corrected in the mother resulting in a normal phenotype. On the other hand, some of maternal germline cells retained 11q23-ter deletion, leading to a recurrence of Jacobsen syndrome in her offspring. Careful genetic counseling is therefore warranted regarding the recurrence of Jacobsen syndrome.

Acknowledgements

We thank the parents of our patient subject for agreeing to participate in this study. We also thank Naoko Fujita and Asami Kuno for technical assistance. This study was supported by grants-in-aid for Scientific Research from the Ministry of Education, Culture, Sports, Science and Technology of Japan (15H04710), from the Ministry of

Health, Welfare and Labor (H27-Nanchitou-Ippan(nan)-024), and from the Japan Agency for Medical Research and Development (17ek0109151h0003).

References

- Afifi, H.H., Zaki, M.S., El-Gerzawy, A.M., Kayed, H.F., 2008. Distal 11q monosomy syndrome: a report of two Egyptian sibs with normal parental karyotypes confirmed by molecular cytogenetics. *Genet. Counsel.* 19, 47–58.
- Beever, C.L., Stephenson, M.D., Peñaherrera, M.S., Jiang, R.H., Kalousek, D.K., Hayden, M., Field, L., Brown, C.J., Robinson, W.P., 2003. Skewed x-chromosome inactivation is associated with trisomy in women ascertained on the basis of recurrent spontaneous abortion or chromosomally abnormal pregnancies. *Am. J. Hum. Genet.* 72, 399–407. <https://doi.org/10.1086/346119>.
- Bonaglia, M.C., Giorda, R., Beri, S., Bigoni, S., Sensi, A., Baroncini, A., Capucci, A., De Agostini, C., Gwilliam, R., Deloukas, P., Dunham, L., Zuffardi, O., 2009. Mosaic 22q13 deletions: evidence for concurrent mosaic segmental isodisomy and gene conversion. *Eur. J. Hum. Genet.* 17, 426–433. <https://doi.org/10.1038/ejhg.2008.195>.
- Butler, M.G., Theodoro, M.F., Bittel, D.C., Kuipers, P.J., Driscoll, D.J., Talebizadeh, Z., 2007. X-chromosome inactivation patterns in females with Prader–Willi syndrome. *Am. J. Med. Genet.* 143A, 469–475.
- Carvalho, C.M.B., Pfundt, R., King, D.A., Lindsay, S.J., Zuccherato, L.W., Macville, M.V.E., Liu, P., Johnson, D., Stankiewicz, P., Brown, C.W., Shaw, C.A., Hurles, M.E., Ira, G., Hastings, P.J., Brunner, H.G., Lupski, J.R., 2015. Absence of heterozygosity due to template switching during replicative rearrangements. *Am. J. Hum. Genet.* 96, 555–564. <https://doi.org/10.1016/j.ajhg.2015.01.021>.
- Costantino, L., Sotiriou, S.K., Rantala, J.K., Magin, S., Mladenov, E., Helleday, T., Haber, J.E., Iliakis, G., Kallioniemi, O.P., Halazonetis, T.D., 2014. Break-induced replication repair of damaged forks induces genomic duplications in human cells. *Science* 343 (80), 88–91. <https://doi.org/10.1126/science.1243211>.
- Grossfeld, P.D., Mattina, T., Lai, Z., Favier, R., Jones, K.L., Cotter, F., Jones, C., 2004. The 11q terminal deletion disorder: a prospective study of 110 cases. *Am. J. Med. Genet.* 129A, 51–61. <https://doi.org/10.1002/ajmg.a.30090>.
- Hatakeyama, C., Anderson, C.L., Beever, C.L., Peñaherrera, M.S., Brown, C.J., Robinson, W.P., 2004. The dynamics of X-inactivation skewing as women age. *Clin. Genet.* 66, 327–332. <https://doi.org/10.1111/j.1399-0004.2004.00310.x>.
- Johnson, J.P., Haag, M., Beischel, L., Mccann, C., Phillips, S., Tunby, M., Hansen, J., Schwanke, C., Reynolds, J.F., 2014. “Deletion rescue” by mitotic 11q uniparental disomy in a family with recurrence of 11q deletion Jacobsen syndrome. *Clin. Genet.* 85, 376–380. <https://doi.org/10.1111/cge.12164>.
- Kurahashi, H., Hara, J., Yumura-Yagi, K., Murayama, N., Inoue, M., Ishihara, S., Tawa, A.,

- Okada, S., Kawa-Ha, K., 1991. Monoclonal nature of transient abnormal myelopoiesis in Down's syndrome. *Blood* 77, 1161–1163.
- Mattina, T., Perrotta, C.S., Grossfeld, P., 2009. Jacobsen syndrome. *Orphanet J. Rare Dis.* 4, 1–10. <https://doi.org/10.1186/1750-1172-4-9>.



Obstetric complication-associated *ANXA5* promoter polymorphisms may affect gene expression via DNA secondary structures

Hidehito Inagaki¹ · Sayuri Ota¹ · Haruki Nishizawa² · Hironori Miyamura² · Kumiko Nakahira³ · Machiko Suzuki¹ · Sachie Nishiyama² · Takema Kato¹ · Itaru Yanagihara³ · Hiroki Kurahashi¹

Received: 25 October 2018 / Revised: 1 February 2019 / Accepted: 4 February 2019 / Published online: 22 February 2019
© The Author(s) under exclusive licence to The Japan Society of Human Genetics 2019

Abstract

Recent findings have highlighted the possibility that polymorphisms within the annexin A5 gene (*ANXA5*) promoter contribute to the etiology of various obstetric complications. However, the underlying mechanisms are unknown. The M2 haplotype of the *ANXA5* shows lower activity and less expression of *ANXA5* mRNA. This gene promoter region has a motif that potentially forms a G-quadruplex structure. In vitro G-quadruplex propensity estimated by circular dichroism indicated that the M2 haplotype oligonucleotide manifested a decreased potential for G-quadruplex formation. In addition, in vivo G-quadruplex formation of the promoter region was evidenced by the presence of single-stranded DNA shown by sodium bisulfite treatment of placental genomic DNA. Comparative analysis indicated less potential in the M2 allele than the major allele. Promoter activity of the two haplotypes determined by luciferase reporter analysis correlated with the estimated G-quadruplex propensity. Our data lend support to the developing paradigm that genomic variation affects gene expression levels via DNA secondary structures leading to the disease susceptibility.

Introduction

Many common human diseases are believed to be polygenic disorders associated with several genetic and environmental factors [1]. Based on the “common disease-common variant” hypothesis, genome-wide association studies (GWAS) using common single nucleotide polymorphisms (SNPs) have identified hundreds of genetic variants that are statistically associated with different target diseases. However, most of the polymorphisms that have been identified by

GWAS to date are not deleterious variants and confer relatively small increases in disease risk. In addition, the functional impact of the majority of these SNPs on gene expression has not yet been validated since these sequence variations are mostly located at non-coding or intergenic regions [2]. The processes by which these SNPs confer a higher risk of disease thus remain an enigma.

Previously published results suggest that polymorphisms within the annexin A5 gene (*ANXA5*) are associated with common obstetric complications, such as recurrent pregnancy loss (RPL), pre-eclampsia, and pregnancy-related thrombophilic disorder [3–8]. The *ANXA5* gene upstream region contains four common variations, i.e., SNP1 (g. –467G>A, rs112782763) and SNP2 (g. –448A>C, rs28717001) in the untranscribed promoter region, and SNP3 (g. –422T>C, rs28651243) and SNP4 (g. –373G>A, rs113588187) near and downstream of the transcription start points, respectively. These four SNPs manifest strong linkage disequilibrium, generating two major haplotypes: the N haplotype with all major alleles and an M2 haplotype with all minor alleles. The frequency of the M2 allele in the general Japanese population was reported to be 5.4%, lower than that in the western countries (~16%) [6].

The M2 haplotype has been associated with various disorders. Annexin A5 is known as a placental

Supplementary information The online version of this article (<https://doi.org/10.1038/s10038-019-0578-4>) contains supplementary material, which is available to authorized users.

✉ Hiroki Kurahashi
kura@fujita-hu.ac.jp

- ¹ Division of Molecular Genetics, Institute for Comprehensive Medical Science, Fujita Health University, Toyoake, Japan
- ² Department of Obstetrics and Gynecology, Fujita Health University School of Medicine, Toyoake, Aichi 470-1192, Japan
- ³ Department of Developmental Medicine, Osaka Medical Center and Research Institute for Maternal and Child Health, Izumi, Osaka 594-1101, Japan

anticoagulation factor that shields the apical surface of the syncytiotrophoblasts covering the placental villi [9]. Hence, the low expression of the *ANXA5* gene might reasonably account for a higher susceptibility to obstetric complications. Indeed, lower expression of the *ANXA5* gene from the M2 allele has been reported [10, 11]. However, it remains unclear how these polymorphisms affect the *ANXA5* gene expression levels and thereby lead to disease. For example, there was no association found between the M2 haplotype and RPL risk in a previous northern European study [12]. It is therefore critically important to elucidate the biological impact of the different *ANXA5* haplotypes.

With regard to the effects of gene polymorphisms on gene expression, the contribution of DNA secondary structures has been highlighted previously [13, 14]. A considerable body of evidence now indicates that certain SNPs located within the transcribed region of a gene can affect mRNA stability or translation efficiency via the propensity for stem-loop formation. Guanine-rich DNA can fold into a non-canonical DNA structure known as a G-quadruplex [15]. This structure comprises intrastrand interactions of G-tetrads paired by Hoogsteen bonds. G-quadruplexes are often identified in and around the untranslated region of genes and are potentially associated with gene regulation [16, 17]. The association between the G-quadruplex structure and transcriptional regulation has been extensively characterized for oncogenes such as *MYC*, *KIT*, or *KRAS* [18–20]. Recently, it has also been reported that some polymorphisms disrupt the formation of G-quadruplex structures, leading to alterations in the expression of nearby genes [21]. In our present study, we examined the *ANXA5* gene promoter variants in terms of the association between the potential for G-quadruplex formation and the *ANXA5* gene expression levels.

Methods

Samples and ethical approval

Four placental samples were obtained from women with an uncomplicated pregnancy at the Department of Obstetrics and Gynecology, Fujita Health University Hospital. Informed consent was obtained from each patient and the study protocol was approved by the Ethical Review Board for Human Genome Studies at the Fujita Health University. The genotypes of the SNPs at the *ANXA5* promoter region were determined by sequencing as previously described [6]. All methods were performed in accordance with the relevant guidelines and regulations including a biosafety regulation in Japan, the Act on the Conservation and Sustainable Use of Biological Diversity through Regulations on the Use of Living Modified Organisms.

Circular dichroism

Circular dichroism (CD) experiments were performed using a J-720 spectropolarimeter (JASCO). Oligonucleotides were synthesized and diluted to 50 ng/μl with a buffer containing 100 mM potassium chloride and 10 mM Tris-HCl (pH 7.4). Where indicated, the potassium chloride concentration was decreased, and lithium chloride was added to adjust the salt concentration to 100 mM. The samples were next heat-denatured at 95 °C for 5 min and then cooled slowly for 6 h to 25 °C. Scans were performed at 25 °C using a 1 cm cuvette over a 200–360 nm range. CD spectra were recorded from the average of five scans at 50 nm/min, with a 2 s response time, 1 nm bandwidth, and 0.1 nm resolution. The molar ellipticity was then plotted. The 56 oligonucleotides used in this CD analysis are described in Fig. 1c.

Methylation analysis

Bisulfite sequencing was performed to determine the methylation status of the *ANXA5* promoter region. One N/N homozygous and three N/M2 heterozygous samples were analyzed. Bisulfite conversion was performed using an EpiTect Bisulfite Kit (Qiagen, Tokyo, Japan) in accordance with the manufacturer's protocol. Bisulfite-treated DNA was amplified using an uracil stalling-free polymerase, EpiTaq HS (Takara bio, Kusatsu, Japan) and the primers: 5'-GGTTATA-GAGGGTAGGGAGGTTTAA-3' and 5'-CACCCAACTA-TAAAACCCAAATAC-3'. The ~300 bp resulting products were then cloned into the pT7Blue T-vector (Merck, Darmstadt, Germany). Colonies were subsequently selected, and the plasmids were isolated for sequencing.

Bisulfite sequencing for detection of DNA secondary structure

Bisulfite treatment was applied to genomic DNAs of N/M2 heterozygous samples purifying under mild conditions. Briefly, placental tissues were powdered under liquid nitrogen and treated with proteinase K at 37 °C. Genomic DNAs were then column-purified using DNeasy Blood & Tissue Kit (Qiagen, Tokyo, Japan) in accordance with the manufacturer's instructions. Approximately 500 ng of DNA was used for sodium bisulfite treatment using an EpiTect Bisulfite Kit (Qiagen) in general accordance with the manufacturer's protocol except that the conditions for the sodium bisulfite reaction involved a constant temperature at 37 °C for 16 h. The resulting converted DNAs were used as PCR templates. Primers were designed for the regions containing few T nucleotides to normalize the annealing efficiency between the converted and unconverted DNAs. The 5' end of each primer was designed for use with the Nextera system (Illumina). The primers are listed in Supplementary Table S1.

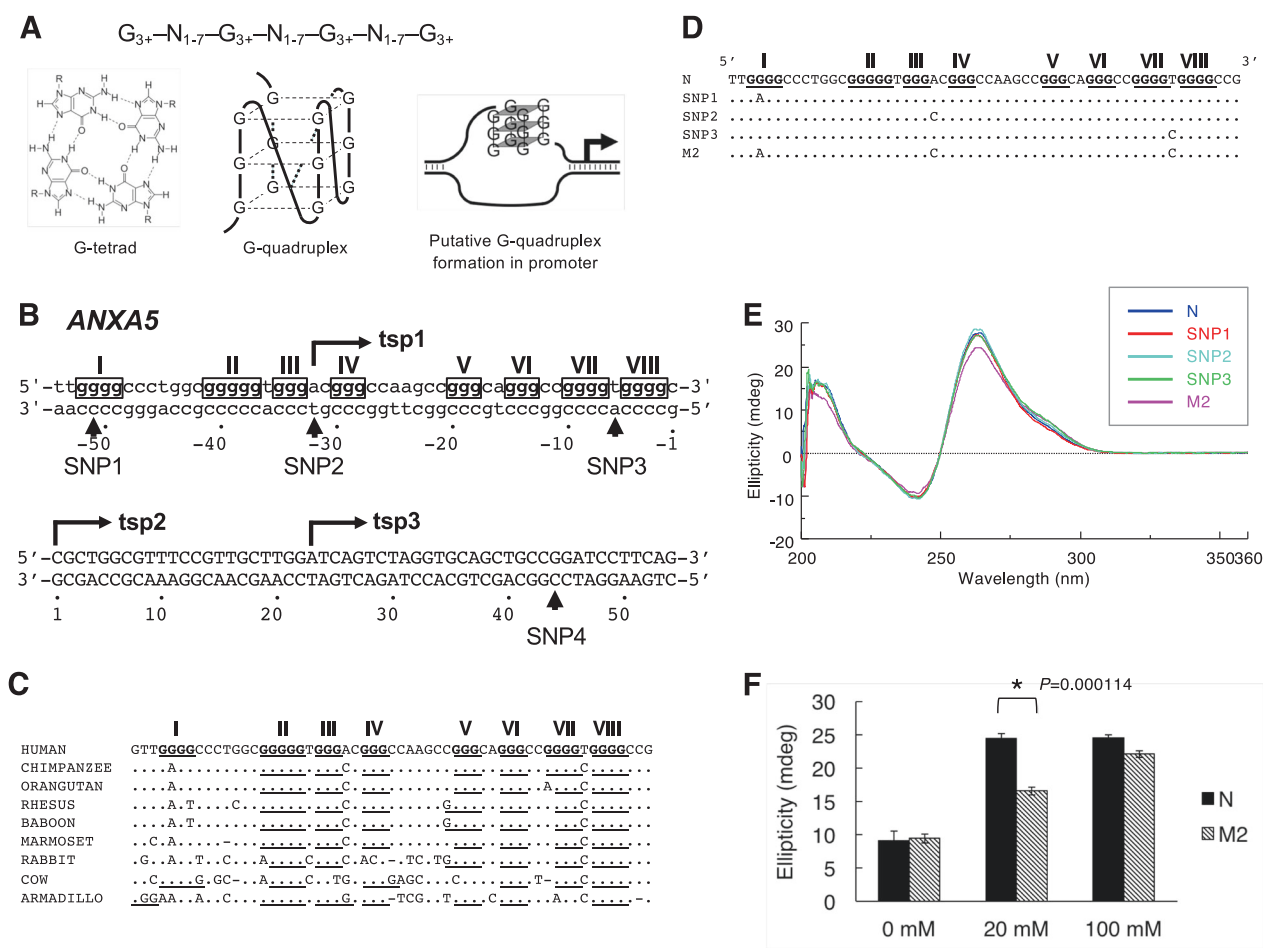


Fig. 1 G-quadruplex structure formation at the ANXA5 promoter region in vitro. **a** A square planar structure of a G-quartet (left), possible form of an intramolecular G-quadruplex structure (middle), and possible G-quadruplex formation at a gene promoter. **b** Genomic structure of the ANXA5 gene promoter region in terms of its G-quadruplex structure. Eight runs of three or four guanines are indicated by the boxed regions. Transcription start points (tsp) are indicated by arrows. The nucleotide at tsp2 is numbered + 1, and the nucleotides within the transcript are capitalized. Polymorphisms are indicated by arrowheads. **c** Conservation of the ANXA5 gene promoter region among mammalian species. Dots indicate conserved nucleotides, and

conserved guanine runs are underlined. Dashes indicate the absence of nucleotides. **d** Oligonucleotides used for CD spectra analysis. **e** The propensity for G-quadruplex structure formation at the ANXA5 gene promoter region in vitro evaluated by CD spectra. Each polymorphic allele was analyzed. The vertical bars indicate the levels of ellipticity estimated by CD spectra. The ellipticity was measured four times and the curves indicate the mean data values. **f** Propensity for G-quadruplex structure formation at various concentrations of potassium chloride evaluated by CD spectra. The ellipticity was measured at 260 nm, and the error bars represent the S.D. (n = 3)

PCR amplifications were carried out using EpiTaq HS (Takara bio, Kusatsu, Japan). The reaction conditions were 94 °C for 2 min, followed by 35 cycles of 98 °C for 10 s, 55 °C for 30 s, and 72 °C for 1 min. There was a final incubation step at 72 °C for 10 min. The resulting products were ligated into pBluescriptII (Agilent, Tokyo, Japan) and plasmids were grown in *E. coli*, purified and sequenced. These sequences were designated as the upper or lower strand in accordance with the conversion of the nucleotides (C>T or G>A) and as N or M2 alleles according to the haplotype. The PCR products were also analyzed by massive parallel sequencing using Nextera index primers (Illumina) following a second round of PCR. After purification and quantification, the products were applied to a Miseq

sequencer (Illumina) at a 250 bp single-end read. The sequence data were quality filtered using FASTX-Toolkit 0.0.14 (http://hannonlab.cshl.edu/fastx_toolkit/) trimming with a cut-off of 20 (phred score) and a minimum length of 12 and filtering with a cut-off of 20 and minimum percentage of 80. The resulting data was further processed by filtering-out PCR duplicates and sequences with indels. After conversion of the fastq to fasta format, clustering analysis of the sequences was carried out using MAFFT [22].

qRT-PCR

Quantitative real-time RT-PCR (qRT-PCR) analysis was performed using the TaqMan System. The Superscript First-

strand Synthesis System for RT-PCR (Invitrogen) with random primers was used to produce single-stranded cDNA templates. TaqMan probes and primers for the *ANXA5* gene (Hs00134054_m1) were obtained commercially (Applied Biosystems). A housekeeping gene, *18S RNA* (Hs99999901_s1), was used to normalize the mRNA levels because the expression levels among the samples were stable. All qRT-PCR reactions were performed in triplicate in a final volume of 25 μ l. The cycling conditions used were 2 min at 50 °C, 30 min at 60 °C, and 1 min at 95 °C for RT, followed by 40 cycles of 15 s at 95 °C and 1 min at 60 °C for PCR amplification.

Allele-specific qRT-PCR was carried out as previously described [11]. The transcript from N allele was amplified with the primers 5'-CAGTCTAGGTGCAGCTGCCG-3' and 5'-GGTGAAGCAGGACCAGACTGT-3', and that from the M2 allele was amplified with 5'-CAGTC-TAGGTGCAGCTGCCA-3' and 5'-GGTGAAGCAG-GACCAGACTGT-3'. The product levels were quantified using SYBR Premix Ex Taq II (Takara BIO) and the 7300 real-time PCR system (Applied Biosystems). The *TBP* gene was used as an internal control.

Promoter assay

Luciferase reporter constructs were kindly provided by Dr. Arseni Markoff (University of Muenster, Germany), and the assay was performed as previously described [3]. Briefly, the promoter region and exon 1 encompassing SNP1 to 4 was amplified by PCR and the ~450 bp products were cloned immediately upstream of luciferase initiation codon in the pGL3-Basic Vector (Promega) using the *Mlu*I and *Xho*I sites. Each polymorphic nucleotide change was introduced to the vector by means of site-directed mutagenesis. The resulting constructs were co-transfected with pRL-TK into the HeLa cell line using Lipofectamine 2000 (Invitrogen). Luciferase activity was measured at 48 h after transfection using a Dual-Luciferase Reporter Assay System (Promega).

Statistical analysis

Statistical significance was determined using the Student *t*-test and one-way analysis of variance (ANOVA). *P*-values of <0.05 were considered statistically significant. Data are reported as the mean \pm SD for each group.

Results

We identified eight runs of three or four guanines with 1–7 nucleotide intervals upstream of the *ANXA5* gene that corresponded to a consensus sequence of a potential

G-quadruplex forming motif, $G_{3+}-N_{1-7}-G_{3+}-N_{1-7}-G_{3+}-N_{1-7}-G_{3+}$ (Fig. 1a, b) [15]. The *ANXA5* gene has multiple transcription start points (tsp) [23], and although transcripts from tsp1 include 5 runs of guanines at the 5' region, all eight runs of guanines are located 5' upstream of the non-transcribed region in cases of transcription starting from tsp2 and tsp3. The first run of guanines is unique to humans, but all of other seven runs are highly conserved among primates. Other mammalian species also carry at least six runs of guanines, suggesting that this G-rich region plays an important role in gene regulation (Fig. 1c).

To evaluate the G-quadruplex structure forming propensity of this region in vitro, we performed a CD spectroscopy experiment using synthesized oligonucleotides that included the consensus sequence of the potential G-quadruplex forming motif. Typically, parallel form G-quadruplexes display a characteristic positive peak at 260 nm and a negative peak at 240 nm, whereas the anti-parallel form of these structures displays a positive peak at 295 nm and a negative peak at 265 nm on the CD spectra [24]. The oligonucleotide with the N allele sequence produced a positive peak at 260 nm and a trough at 240 nm with a small additional positive peak at 290 nm. This indicates that the N allele DNA forms a G-quadruplex structure in vitro, adopting a mixture of parallel and anti-parallel forms. When SNP1, SNP2, and SNP3 were separately introduced into the N allele, no remarkable change was observed in the CD spectra. However, when these variations were combined to form the M2 allele, the CD spectra showed a reduction in the positive peak at 260 nm, suggesting that the potential for G-quadruplex formation had been decreased (*t*-test, $P < 0.01$) (Fig. 1d, e). To evaluate the propensity for G-quadruplex structure formation in vitro, we analyzed the CD spectra for the oligonucleotides under various potassium ion concentrations (Fig. 1e). The M2 allele showed lower positive peaks at 260 nm in 100 mM, and especially in 20 mM, of potassium chloride ($P < 0.01$), again suggesting that the potential for G-quadruplex formation had been decreased.

It was of interest to us to determine how the M2 haplotype, which appears to possess less potential for G-quadruplex structure formation than the N haplotype, impacted on the promoter activity of the *ANXA5* gene. The restricted methylation of a G-quadruplex structured DNA region was reported previously [25]. On the assumption that *ANXA5* polymorphisms would affect the methylation status of the gene promoter via G-quadruplex structures, and thereby alter gene expression, we performed bisulfite sequencing to locate methylated cytosines in this region. We found that the CpG islands of the *ANXA5* gene upstream region were hypomethylated in placental DNA. However, we did not observe any allele-specific alteration of the *ANXA5* promoter methylation status (Supplementary Fig. S1).

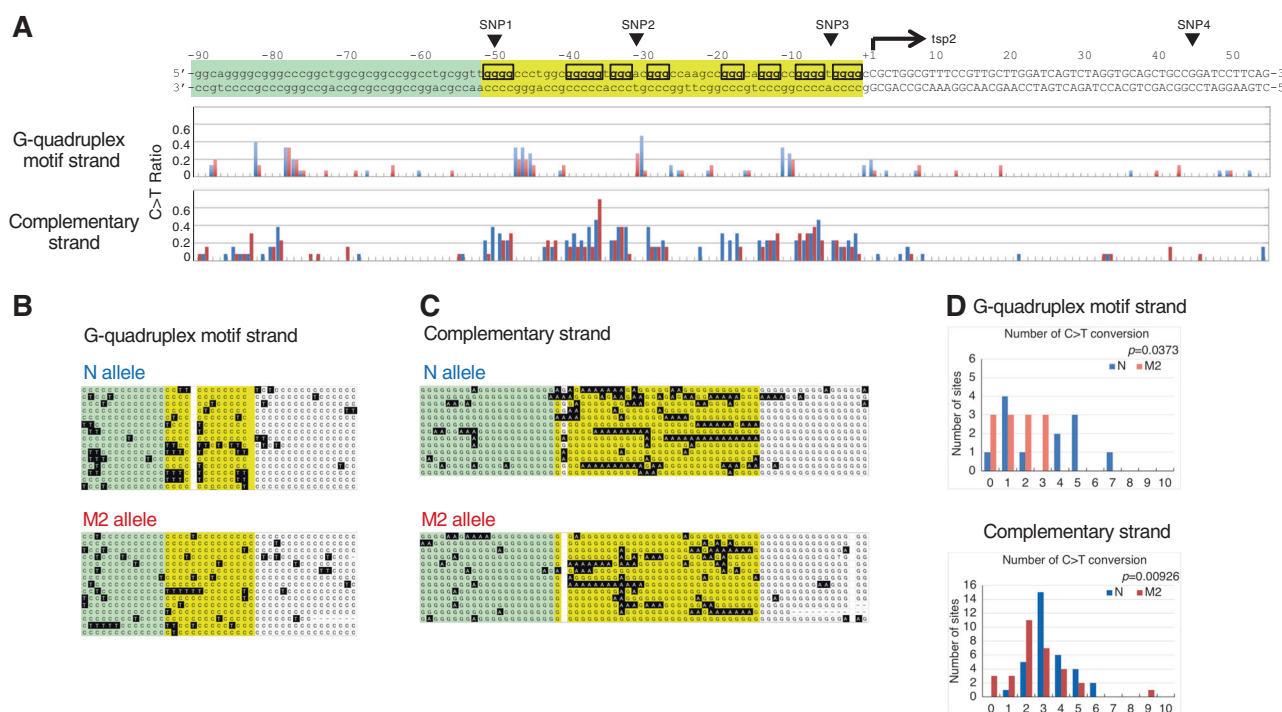


Fig. 2 Bisulfite modification analysis that could reflect the DNA secondary structure status within the *ANXA5* gene promoter region. The presented data were obtained by gentle bisulfite treatment of placental DNA harboring various *ANXA5* promoter genotypes containing different polymorphisms. Cytosines on each strand of the double helix were evaluated for C-to-T bisulfite modification by cloning and sequencing of the PCR products. **a** The upper panel shows the *ANXA5* promoter sequence. The upstream promoter region, G-quadruplex motif region and transcribed region are depicted in green, yellow and white, respectively. The nucleotide at *tsp2* is numbered +1, and the

transcribed nucleotides are capitalized. Polymorphisms are indicated by arrowheads. Lower panels show the ratios of modified cytosines in the G-quadruplex motif strand and its complementary strand. Blue indicates N allele data and red indicates those for the M2 allele. **b** Sanger sequencing results for each clone derived from the products of N or M2 alleles of the G-quadruplex motif strand, or **c** the complementary strand. **d** Histograms showing the number distribution of modified cytosines at the G-quadruplex motif region (G-quadruplex motif strand, $n = 13$; complementary strand, $n = 15$

The question that therefore arose from our current findings was the actual cause of the differential gene expression between the M2 and N haplotype alleles. Prior experimental findings had suggested the existence of a G-quadruplex structure at the *ANXA5* promoter in vivo, which could be detected by an antibody specific for this structure [26]. In addition, this G-quadruplex remained in the genomic DNA after purification from cells [27]. We therefore next tested these G-quadruplex structures in genomic DNA using sodium bisulfite modification assays. In the bisulfite modification reaction, cytosines in a single-stranded DNA are converted to uracils but not those in a double-stranded DNA. It is expected therefore that most of the cytosines in a double-strand helix would not change, whereas those that form secondary structure, e.g., the dissociated strand, would be converted (Fig. 1a). Hence, the secondary structure status of a DNA region could be reflected by the bisulfite conversion rate of the cytosines.

Genomic DNAs from N and M2 heterozygous placentas were treated with sodium bisulfite under mild conditions that would not dissociate the strands during the treatment. This DNA was then used as a PCR template to amplify the

ANXA5 promoter region using specific primers. Sanger sequencing of the resulting cloned PCR products demonstrated a C-to-T conversion by the sodium bisulfite treatment that was specific to the G-quadruplex motif region (Fig. 2a, yellow). The results indicated that a small subset (5–10%) of the molecules had indeed formed the single-stranded DNA as evidenced by successive converted nucleotides that extended across a region of around 30 bp (Fig. 2b, c). Similar results were obtained by massive parallel sequencing of the PCR products (Supplementary Fig. S2). The observed clusters at the complementary strand of the G-quadruplex motif region suggested that G-quadruplex formation occurs in vivo since the formation of the G-quadruplex structure on its own strand may inhibit the C-to-T conversion whilst the single-strandedness of the complementary strand may manifest a higher conversion rate. Notably, the proportion of converted Cs was found to be higher in N allele than in the M2 allele on the complementary strand ($P = 0.00926$) and the G-quadruplex motif strand ($P = 0.0373$), indicating that G-quadruplex formation in vivo might be affected by SNPs, and might contribute to the upregulation of *ANXA5* gene expression (Fig. 2d).

Hence, we examined the expression levels of the *ANXA5* gene against the various SNP genotypes in its promoter. As the *ANXA5* gene is abundantly expressed in the human placenta, we examined the expression effects of its promoter SNPs in this tissue. As homozygotes for high-risk M2 alleles are rare, we compared the *ANXA5* expression levels in M2/N-heterozygous and N-homozygous placentas. The *ANXA5* transcripts were detected at significantly lower levels in the M2/N heterozygote (Supplemental Fig. S3A). To exclude the possible effects of various confounders, we examined allele-specific expression in each M2/N-heterozygous placenta and compared the levels of expression from M2 and N alleles. As was expected, this was lower from the M2 allele (Supplemental Fig. S3B, C). In addition, we examined the effects of the SNPs to the *ANXA5* gene promoter activity using the luciferase reporter system. We amplified the ~450 bp region upstream of the *ANXA5* gene incorporating SNP1 to 4, which was cloned into upstream of the luciferase reporter vector. The M2 haplotype was found to have lower promoter activity (Supplemental Fig. S3D). Thus, at least one of the four SNPs within the M2 haplotype appears to affect *ANXA5* promoter activity leading to its low levels of expression in placental tissues. These results suggest that the M2 haplotype is associated with obstetric complications that arise via altered expression of the *ANXA5* gene, and the expression of the gene might be regulated via G-quadruplex formation in vivo.

Discussion

In our current study, we show from both in silico and in vitro experiments that the *ANXA5* promoter has the potential for G-quadruplex formation. CD analyses further indicated that the G-rich region of this promoter forms a mixture of parallel and anti-parallel G-quadruplexes in vitro. On the other hand, G-quadruplex formation at this gene promoter in vivo is still somewhat controversial. The formation of these structures requires a long single-stranded DNA at the G-rich region, but this is unlikely to occur upstream of a transcription start point (tsp). However, it is possible that G-quadruplex formation upstream of a tsp might be facilitated by the negative supercoiling induced by transcription [28]. Our current data demonstrated that clustering of the bisulfite modification on the complementary strand of the G-quadruplex motif region, and differences were observed between the N and M2 allele, suggesting that G-quadruplex structures form in vivo at the *ANXA5* promoter and impact its transcription regulation.

The question arises as to the underlying mechanism that drives transcriptional activation when the *ANXA5* upstream region forms a G-quadruplex. Several lines of evidence have suggested that G-quadruplex formation in transcribed

RNA molecules likely contributes to gene regulation at the translational level [29, 30]. It has emerged also that RNA polymerase pausing may contribute to transcription down-regulation of *ANXA5* [31]. These could not apply to the G-quadruplex at the *ANXA5* untranscribed promoter region. Another intriguing hypothesis is that methylation restriction in regions with the potential for G-quadruplex formation affects gene expression [25]. However, we did not observe any methylation differences between the N and M2 alleles in our present analysis. On the other hand, the placenta is a hypomethylated organ, suggesting that G-quadruplex formation might be facilitated in the context of a hypomethylation phenomenon. To shed further light on the relationship between G-quadruplex formation and placental environment, additional analyses will be necessary such as an evaluation of G-quadruplex formation at the *ANXA5* promoter in blood cells. These investigations will provide new insights into the connection between pregnancy success and maternal or placental *ANXA5* haplotypes.

A relatively recent genome-wide surveillance of G-quadruplex structures unveiled high G-quadruplex density in functional regions such as 5' untranslated regions and splicing sites [32]. Enrichment of the promoter regions of highly transcribed genes was observed in another study using an antibody-based G-quadruplex chromatin immunoprecipitation technique [33]. G-quadruplex helicases, XPB and XPD, are enriched near the transcription start site, especially highly transcribed genes [34]. These observations raise the possibility of a regulatory role of G-quadruplex formation on transcriptional regulation. In addition, small molecules or oligonucleotides that target possible G-quadruplex motifs in the promoters of genes responsible for embryonic development have been shown to decrease their expressions in zebrafish [35]. This suggests a role for G-quadruplex formation in the regulation of the gene expression at specific developmental stages.

It is possible that polymorphisms affect the affinity of transcriptional regulatory proteins for a G-quadruplex and thereby lead to the change in transcriptional efficiency [36]. On the other hand, this G-rich region of the *ANXA5* gene includes consensus motifs for transcription factors such as MTF-1, HNF-3, and Sp1 [3], and polymorphisms in the *ANXA5* gene region may possibly alter the binding affinity for these molecules. Recently, a differential impact of the SNPs on *ANXA5* promoter activity was shown using a luciferase promoter assay and electrophoretic mobility shift assay (EMSA) [8]. These findings indicate an effect on gene regulation through the combination of the SNPs, irrespective of whether it is through an alteration of the primary sequence or secondary structure. Theoretically, a conventional method such as EMSA using short DNA duplexes does not necessarily reflect the G-quadruplex formation in long double-strand DNAs. Other genome-wide profiling

such as ChIP-seq technology described above can be used to quantify the propensity for the G-quadruplex formation of each *ANXA5* allele in vivo.

The M2 haplotype is common to mammals other than humans, indicating an ancestral lineage. In this regard, the genomic data of Denisova hominin was recently made available on the UCSC genome browser (<http://genome.ucsc.edu/>). The haplotype of the sequenced Denisovan was shown to be the same as the M1 allele, which is another haplotype of the *ANXA5* promoter in the modern human population that shares SNP2 and SNP3 with the M2 allele. The promoter activity of M1 is weaker than that of the N allele but stronger than the M2 allele [3]. An evolutionary advantage of the N allele over the ancestral M2 or M1 alleles could explain majority of the N allele in the modern humans, which express more anticoagulation factor on placental villi, reducing the risk of pre-eclampsia or other obstetric complications. Investigation of the relationship between the evolution of the human phenotype and that from the M2 to N haplotype may provide new insights into the functional propensities of these polymorphisms.

Many common human diseases are believed to be polygenic disorders associated with several genetic and environmental factors [1]. However, most of the disease-susceptible SNPs that have been identified to date confer relatively small increments only in disease risk. Mechanisms by which these SNPs affect gene expression and confer a higher risk of disease thus remains somewhat of an enigma. Our current findings however highlight the contribution of the DNA secondary structure to the fine tuning of the gene expression regulation. A more thorough analysis of G-quadruplexes combined with genome-wide association analyses would likely reinforce the hypothesis that the DNA secondary structure has a fine tuning role in controlling gene expression and thereby has an effect on the susceptibility to common diseases.

Acknowledgements We thank Ms. Y. Nakura (Osaka Women's and Children's Hospital, Japan) for technical assistance, and Drs. H. Kogo, M. Tsutsumi, T. Ohye, M. Shimada (Fujita Health University, Japan), A. Markoff (University of Muenster, Germany), K. Hata (National Research Institute for Child Health and Development, Japan), and K. Shiraki (University of Tsukuba) for helpful discussions. This study was supported by grants-in-aid for Scientific Research from the Ministry of Education, Culture, Sports, Science, and Technology of Japan (HK and IY), grants-in-aid for Scientific Research from the Ministry of Health, Labor, and Welfare of Japan (HK and IY), and AMED under Grant Number JP17gk0110018 (HK).

Compliance with ethical standards

Conflict of interest The authors that they have no conflict of interest.

Publisher's note Springer Nature remains neutral with regard to jurisdictional claims in published maps and institutional affiliations.


References

- Manolio TA, Collins FS, Cox NJ, Goldstein DB, Hindorf LA, Hunter DJ, et al. Finding the missing heritability of complex diseases. *Nature*. 2009;461:747–53.
- Gibson G. Rare and common variants: twenty arguments. *Nat Rev Genet*. 2012;13:135–45.
- Bogdanova N, Horst J, Chlystun M, Croucher PJ, Nebel A, Bohring A, et al. A common haplotype of the annexin A5 (*ANXA5*) gene promoter is associated with recurrent pregnancy loss. *Hum Mol Genet*. 2007;16:573–8.
- Tiscia G, Colaizzo D, Chinni E, Pisanelli D, Sciannamè N, Favuzzi G, et al. Haplotype M2 in the annexin A5 (*ANXA5*) gene and the occurrence of obstetric complications. *Thromb Haemost*. 2009;102:309–13.
- Grandone E, Tiscia G, Colaizzo D, Chinni E, Pisanelli D, Bafunno V, et al. Role of the M2 haplotype within the annexin A5 gene in the occurrence of pregnancy-related venous thromboembolism. *Am J Obstet Gynecol*. 2010;203:461.e1–5.
- Miyamura H, Nishizawa H, Ota S, Suzuki M, Inagaki A, Egusa H, et al. Polymorphisms in the annexin A5 gene promoter in Japanese women with recurrent pregnancy loss. *Mol Hum Reprod*. 2011;17:447–52.
- Ota S, Miyamura H, Nishizawa H, Inagaki H, Inagaki A, et al. Contribution of fetal *ANXA5* gene promoter polymorphisms to the onset of pre-eclampsia. *Placenta*. 2013;34:1202–10.
- Tiscia GL, Dørum E, Myklebust CF, Grandone E, Sandset PM, Stretting G. Functional characterization of annexin A5 gene promoter allelic variants. *Thromb Res*. 2016;144:93–9.
- Rand JH. The annexinopathies: a new category of diseases. *Biochim Biophys Acta*. 2000;1498:169–73.
- Chinni E, Tiscia GL, Colaizzo D, Vergura P, Margaglione M, Grandone E. Annexin V expression in human placenta is influenced by the carriership of the common haplotype M2. *Fertil Steril*. 2009;91:940–2.
- Markoff A, Gerdes S, Feldner S, Bogdanova N, Gerke V, Grandone E. Reduced allele specific annexin A5 mRNA levels in placentas carrying the M2/*ANXA5* allele. *Placenta*. 2010;31:937–40.
- Nagiraj L, Nömmemees D, Rull K, Christiansen OB, Nielsen HS, Laan M. Annexin A5 promoter haplotype M2 is not a risk factor for recurrent pregnancy loss in northern Europe. *PLoS ONE*. 2015;10:e0131606.
- Plotkin JB, Kudla G. Synonymous but not the same: the causes and consequences of codon bias. *Nat Rev Genet*. 2011;12:32–42.
- Sauna ZE, Kimchi-Sarfaty C. Understanding the contribution of synonymous mutations to human disease. *Nat Rev Genet*. 2011;12:683–91.
- Burge S, Parkinson GN, Hazel P, Todd AK, Neidle S. Quadruplex DNA: sequence, topology and structure. *Nucleic Acids Res*. 2006;34:5402–15.
- Eddy J, Maizels N. Conserved elements with potential to form polymorphic G-quadruplex structures in the first intron of human genes. *Nucleic Acids Res*. 2008;36:1321–33.
- Huppert JL, Bugaut A, Kumari S, Balasubramanian S. G-quadruplexes: the beginning and end of UTRs. *Nucleic Acids Res*. 2008;36:6260–8.
- Siddiqui-Jain A, Grand CL, Bearss DJ, Hurley LH. Direct evidence for a G-quadruplex in a promoter region and its targeting with a small molecule to repress c-MYC transcription. *Proc Natl Acad Sci USA*. 2002;99:11593–8.
- Fernando H, Reszka AP, Huppert J, Ladame S, Rankin S, Venkitaraman AR, et al. A conserved quadruplex motif located in a transcription activation site of the human c-kit oncogene. *Biochemistry*. 2006;45:7854–60.

20. Cogoi S, Xodo LE. G-quadruplex formation within the promoter of the KRAS proto-oncogene and its effect on transcription. *Nucleic Acids Res.* 2006;34:2536–49.
21. Baral A, Kumar P, Halder R, Mani P, Yadav VK, Singh A, et al. Quadruplex-single nucleotide polymorphisms (Quad-SNP) influence gene expression difference among individuals. *Nucleic Acids Res.* 2012;40:3800–11.
22. Katoh K, Misawa K, Kuma K, Miyata T. MAFFT: a novel method for rapid multiple sequence alignment based on fast Fourier transform. *Nucleic Acids Res.* 2002;30:3059–66.
23. Carcedo MT, Iglesias JM, Bances P, Morgan RO, Fernandez MP. Functional analysis of the human annexin A5 gene promoter: a downstream DNA element and an upstream long terminal repeat regulate transcription. *Biochem J.* 2001;356:571–9.
24. Balagurumoorthy P, Brahmachari SK, Mohanty D, Bansal M, Sasisekharan V. Hairpin and parallel quartet structures for telomeric sequences. *Nucleic Acids Res.* 1992;20:4061–7.
25. Halder R, Halder K, Sharma P, Garg G, Sengupta S, Chowdhury S. Guanine quadruplex DNA structure restricts methylation of CpG dinucleotides genome-wide. *Mol Biosyst.* 2010;6:2439–47.
26. Biffi G, Tannahill D, McCafferty J, Balasubramanian S. Quantitative visualization of DNA G-quadruplex structures in human cells. *Nat Chem.* 2013;5:182–6.
27. Lam EY, Beraldi D, Tannahill D, Balasubramanian S. G-quadruplex structures are stable and detectable in human genomic DNA. *Nat Commun.* 2013;4:1796.
28. Kouzine F, Sanford S, Elisha-Feil Z, Levens D. The functional response of upstream DNA to dynamic supercoiling in vivo. *Nat Struct Mol Biol.* 2008;15:146–54.
29. Kumari S, Bugaut A, Huppert JL, Balasubramanian S. An RNA G-quadruplex in the 5' UTR of the NRAS proto-oncogene modulates translation. *Nat Chem Biol.* 2007;3:218–21.
30. Beaudoin JD, Perreault JP. 5'-UTR G-quadruplex structures acting as translational repressors. *Nucleic Acids Res.* 2010;38:7022–36.
31. Eddy J, Vallur AC, Varma S, Liu H, Reinhold WC, Pommier Y, et al. G4 motifs correlate with promoter-proximal transcriptional pausing in human genes. *Nucleic Acids Res.* 2011;39:4975–83.
32. Chambers VS, Marsico G, Boutell JM, Di Antonio M, Smith GP, Balasubramanian S. High-throughput sequencing of DNA G-quadruplex structures in the human genome. *Nat Biotechnol.* 2015;33:877–81.
33. Hänsel-Hertsch R, Beraldi D, Lensing SV, Marsico G, Zyner K, Parry A, et al. G-quadruplex structures mark human regulatory chromatin. *Nat Genet.* 2016;48:1267–72.
34. Gray LT, Vallur AC, Eddy J, Maizels N. G quadruplexes are genomewide targets of transcriptional helicases XPB and XPD. *Nat Chem Biol.* 2014;10:313–8.
35. David AP, Margarit E, Domizi P, Banchio C, Armas P, Calcaterra NB. G-quadruplexes as novel cis-elements controlling transcription during embryonic development. *Nucleic Acids Res.* 2016;44:4163–73.
36. Simonsson T. G-quadruplex DNA structures--variations on a theme. *Biol Chem.* 2001;382:621–8.

ORIGINAL ARTICLE

Multiplex PCR in noninvasive prenatal diagnosis for *FGFR3*-related disorders

Sumire Terasawa^{1,2*}, Asuka Kato^{1*}, Haruki Nishizawa¹ , Takema Kato², Hikari Yoshizawa^{1,2}, Yoshiteru Noda^{1,2}, Jun Miyazaki^{1,2}, Mayuko Ito^{1,2}, Takao Sekiya¹, Takuma Fujii¹, and Hiroki Kurahashi²

¹Department of Obstetrics and Gynecology, Fujita Health University, School of Medicine and ²Division of Molecular Genetics, Institute for Comprehensive Medical Science, Fujita Health University, Toyoake, Japan

ABSTRACT Thanatophoric dysplasia and achondroplasia are allelic disorders caused by a constitutively active mutation in the *FGFR3* gene. Because thanatophoric dysplasia is a lethal disorder and achondroplasia is non-lethal, they need to be distinguished after ultrasound identification of fetal growth retardation with short limbs. Accordingly, we have developed a noninvasive prenatal test using cell-free fetal DNA in the maternal circulation to distinguish thanatophoric dysplasia and achondroplasia. A multiplex PCR system encompassing five mutation hotspots in the *FGFR3* gene allowed us to efficiently identify the responsible mutation in cell-free DNA in all examined pregnancies with a suspected thanatophoric dysplasia or achondroplasia fetus. This system will be helpful in the differential diagnosis of thanatophoric dysplasia and achondroplasia in early gestation and in couples concerned about the recurrence of thanatophoric dysplasia due to germinal mosaicism.

Key Words: achondroplasia, *FGFR3*, noninvasive prenatal testing, thanatophoric dysplasia

INTRODUCTION

Thanatophoric dysplasia (TD) is the most common skeletal dysplasia, affecting 1 in 20,000 births (Karczeski and Cutting 2004). TD is classified into two types: TD type 1 (TD1) involves short-limb dwarfism with bowed femurs, and TD type 2 (TD2) has similar symptoms with straight femurs and a prominent skull deformity called cloverleaf skull. Most affected infants die of respiratory failure shortly after birth. Both types of TD are caused by a constitutively active mutation in the *FGFR3* gene. Whereas p.Arg248Cys, p.Ser249Cys, p.Gly370Cys, p.Ser371Cys, p.Tyr373Cys, p.Lys650Met, p.stop807Gly, p.stop807Arg, p.stop807Cys, p.stop807Trp, and p.stop807Leu mutations are found in TD1, p.Lys650Glu is consistently found in TD2.

Achondroplasia (ACH) is another disorder of disproportionate small stature that shows a similar live-birth frequency to TD (Pauli 1998). Intelligence and life span are usually normal. Because TD is a lethal disorder and ACH is non-lethal, they need to be distinguished after ultrasound identification of fetal growth retardation with short limbs. Although TD and ACH are both

allelic disorders caused by the same *FGFR3* gene, we can clearly distinguish them through the causative mutation.

Noninvasive prenatal testing (NIPT) was made possible by the identification of fetal cell-free DNA (cfDNA) in the maternal circulation (Lo and Chiu 2007). To detect fetal trisomy in maternal peripheral blood, older strategies required the distinction of fetal DNA from maternal DNA, which was the main hurdle. However, the development of next-generation sequencing (NGS) enabled us to perform massive parallel sequencing of cfDNA to detect subtle differences in sequence reads between trisomy and normal pregnancy without distinguishing fetal DNA from maternal DNA (Chiu et al. 2008; Fan et al. 2008). NGS technology also allowed us to use a SNP-based approach to examine the copy number of fetal chromosomes (Kitzman et al. 2012). Nowadays, NIPT for fetal trisomy detection has become a standard screening method in pregnancy of aged women and even in low-risk pregnancy (Bianchi et al. 2014; Norton et al. 2015).

Genetic material absent from the maternal genome has long been a target for NIPT. Fetal sex determination by identification of the fetal Y chromosome in the maternal circulation is considered straightforward because women do not have the Y chromosome (Lo et al. 1989). Screening for Rhesus D-positive fetus in Rhesus D-negative pregnant women is vital and is not difficult because most mutations involve homozygous deletion of the Rhesus D locus (Lo 2001). Similarly, detection of *de novo* mutations for rare Mendelian diseases might be feasible by means of deep sequencing of cfDNA using NGS. In the present study, we attempted to detect *de novo FGFR3* gene mutations responsible for TD or ACH in cfDNA in pregnancies with fetal growth retardation with short limbs in order to set up NIPT for TD or ACH in next pregnancy.

MATERIALS AND METHODS

Samples

All clinical samples were collected at the Department of Obstetrics and Gynecology, Fujita Health University Hospital, Japan. Seven cases were enrolled in this study: three with TD, two with ACH, one with osteogenesis imperfecta type 1, and one with non-specific fetal growth retardation (Table 1). All cases were found by ultrasound examination at consultation in 17–35 weeks of gestation and clinically diagnosed by 3D computed tomography. Maternal blood samples were collected from pregnant women at 18–37 weeks of gestation. Paternal saliva samples were also obtained. Cord blood samples were obtained after delivery to identify the mutation in the newborn. Informed consent was obtained from each participant. This study was approved by the Ethical Review Board for Clinical Studies at Fujita Health University.

Correspondence: Haruki Nishizawa, Department of Obstetrics and Gynecology, Fujita Health University, 1-98 Dengakugakubo, Kutsukake, Toyoake, Aichi, 470-1192 Japan. Email: nharuki@fujita-hu.ac.jp

*These authors contributed equally to this work.

Received November 19, 2017; revised and accepted March 9, 2018.

Table 1 Characteristics of the study subjects and clinical findings

Sample ID	Maternal age	Sonographic findings	3D-CT findings	Clinical diagnosis	Gestational weeks of blood sampling	Mutations detected
FHU15-005	27	(26 + 6 weeks) BPD80.7 mm (+3.9SD) FL20.2 (-9.2SD) HL14.8 mm (-11.8SD) EFW852g (-1.5SD)	(24 + 6 weeks) Short limb and bowed femurs Epiphysis cupping Spinal hypoplasia Narrow chest	Thanatophoric dysplasia susp.	30 + 3 weeks	<i>FGFR3</i> exon9 c.1118A>G (p.Tyr373Cys)
FHU16-249	37	(24 + 3 weeks) BPD70.9 mm (+3.5SD) FL17.7 mm (-8.1SD) HL19.2 mm (-8.3SD) EFW601g (-1.0SD)	(30 + 0 weeks) Short limb and bowed femurs Narrow chest Spinal hypoplasia Epiphysis cupping	Thanatophoric dysplasia susp.	26 + 3 weeks	<i>FGFR3</i> exon7 c.742C>T (p.Arg248Cys)
FHU16-306	28	(18 + 3 weeks) BPD45.3 mm (+1.5SD) FL15.7 mm (-3.9SD) HL13.3 mm (-5.4SD) EFW172g (-1.2SD)	Not done	Thanatophoric dysplasia susp.	18 + 3 weeks	<i>FGFR3</i> exon9 c.1118A>G (p.Tyr373Cys)
FHU15-276	22	(35 + 1 weeks) BPDnormal FL49.9 mm (-4.1SD) HL42.9 mm (-4.9SD) EFW1933g (-1.6SD)	(37 + 4 weeks) Short limb Epiphysis cupping Spinal hypoplasia	Achondroplasia susp.	37 + 0 weeks	<i>FGFR3</i> exon9 c.1138G>A or C (p.Gly380Arg)
FHU17-081	31	(35 + 5 weeks) BPD90.2 mm (+1.0SD) FL48.4 mm (-4.7SD) HL47.2 mm (-3.6SD) EFW1888g (-2.0SD)	(35 + 5 weeks) Short limb Epiphysis cupping Angular ossification of femoral trochanter Short and square ilium	Achondroplasia susp.	35 + 5 weeks	<i>FGFR3</i> exon9 c.1138G>A or C, p.Gly380Arg
FHU16-325	32	(25 + 5 weeks) BPD66.2 mm (+0.8SD) FL33.2 mm (-3.7SD) HL32.7 mm (-3.7SD) EFW682g (-1.4SD)	(30 + 5 weeks) Short limb and bowed femurs Cranium expanding Epiphysis cupping Short ilium	Achondroplasia or Osteogenesis imperfecta susp.	29 + 5 weeks	<i>COL1A1</i> exon32 c.2155G>A (p.Gly719Ser)
FHU16-353	40	(17 + 0 weeks) BPD32.8 mm (-1.3SD) FL14.2 (-3.2SD) HL15.0 mm (-3.0SD)	(31 + 0 weeks) Short limb and bowed femurs Epiphysis cupping Square ilium Forehead bulging	Achondroplasia susp.	29 + 0 weeks	No mutant allele detected

Isolation of cell-free DNA

Maternal plasma was collected by standard methods. Three milliliters of the plasma was used for isolation of cfDNA using a QIAamp Circulating Nucleic Acid kit (Qiagen, Frankfurt, Germany) according to the manufacturer’s protocol. The cfDNA was eluted by 20 µL of elution buffer.

Screening of mutations

We performed Sanger sequencing of the mutation hotspots in the *FGFR3* gene (Fig. 1). The PCR primers used in this study are listed in Table 2. These PCRs cover all of the mutation hotspots observed in TD/ACH/HCH except for two rare HCH mutations

(p.Tyr278Cys and p.Gly342Cys). For case FHU16–325, mutation of the *COL1A1* gene was screened using a TruSight One Sequencing Panel on the MiSeq platform according to the manufacturer’s instructions (Illumina, San Diego, CA, USA).

Multiplex PCR and NGS

To establish an efficient method, we performed multiplex PCR for five regions that were reported to be hotspots for mutations in the *FGFR3* gene (Fig. 1). The PCR reactions were performed in multiplex under the following conditions: initial denaturation of 95°C for 15 min followed by 35 cycles of 94°C for 30 s, 60°C for

FGFR3 gene: NM_000142.4

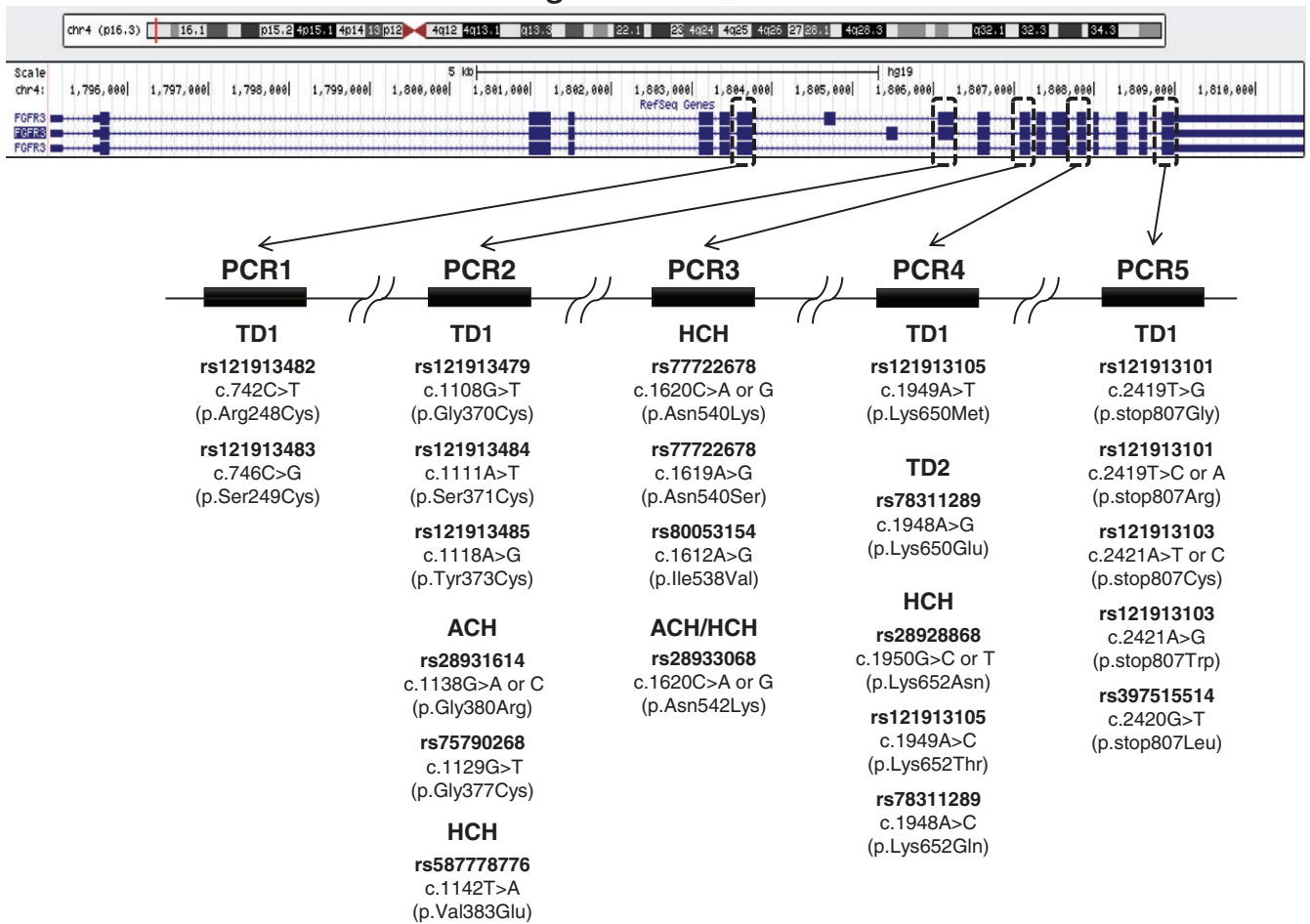


Fig. 1 Location of the mutation hotspots for TD and ACH in the *FGFR3* gene. Five PCR primer sets were designed to cover all of these regions.

Table 2 PCR primers used for genomic sequencing

	Positions	Target mutations	Size (bp)	Forward primer	Backward primer
PCR1	chr4: 1803540–1803598	R248C, S249C (TD1)	59	TGAGCGTCATC TGCCCCCACA	AGCCCCGCCTGCAGGATGG
PCR2	chr4: 1806068–1806147	G370C, S371C, Y373C (TD1) G380R, G377C (ACH) V383G (HCH)	80	CTGGTGGAGG CTGACGAGG	ACCAGGATGAAC AGGAAGAAGCC
PCR3	chr4: 1807329–1807408	N540K, N540S, I538V (HCH) N542L(ACH/HCH)	80	GGAGATGATGAA GATGATCGGGA	TACCGCACCTACCGCCCTGC
PCR4	chr4: 1807859–1807912	K650M (TD1) K650E (TD2) L652N, L652T, L652Z (HCH)	54	CGGGACGTGCAC AACCTCGACTAC	GGCCGGGCTCACGTTGGTC
PCR5	chr4: 1808931–1809010	X807G, X807R, X807C, L652T, L652Z (TD1)	80	TGTTTGCCAC GACCTGCTG	TTGTTGGGACCAGTGGCC

ACH, achondroplasia; HCH, hypochondroplasia; TD1, thanatophoric dysplasia type I; TD2: thanatophoric dysplasia type II.

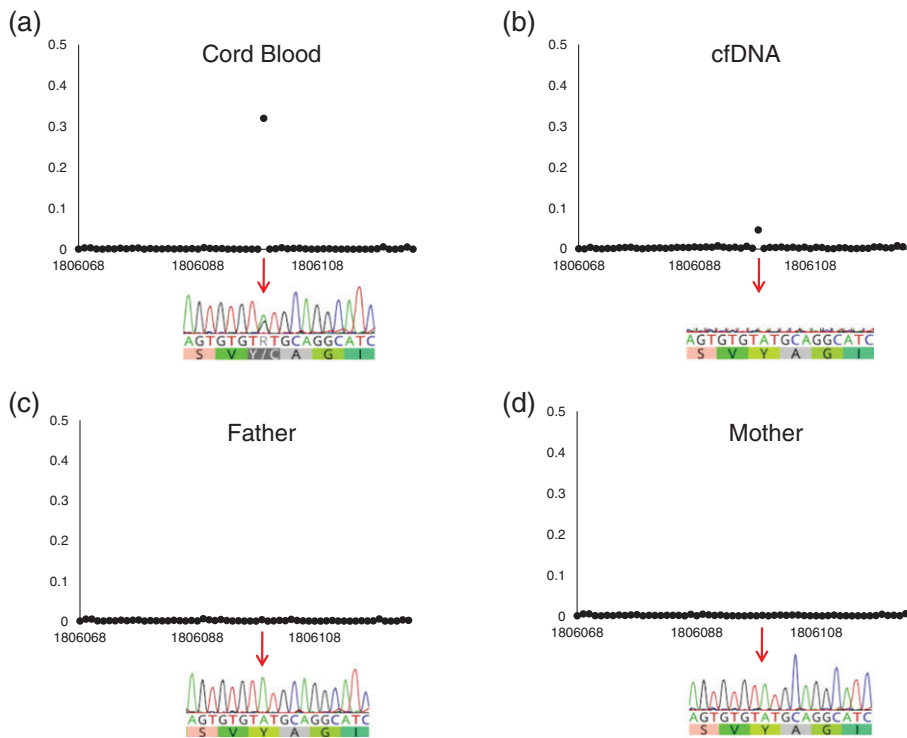


Fig. 2 Analysis of the deep sequence of the product of PCR2 from FHU15-005. A heterozygous c.1118A>G (p.Tyr373Cys) mutation was identified in the cord blood, whereas an identical mutation was found in a small fraction of cfDNA. Sanger sequencing results are also displayed below. Arrows indicate the location of the mutation. (a) cord blood. (b) cfDNA. (c) paternal DNA. (d) maternal DNA.

90 s, and 72°C for 30 s. Successful amplification of the five PCR products was confirmed by agarose gel electrophoresis. Pooled DNA libraries were prepared using a Nextera XT DNA Sample Preparation Kit according to the manufacturer's protocol (Illumina). Single ends were sequenced for 100 bp using a MiSeq Reagent Kit v2 (Illumina). Sequence reads were mapped to a human reference sequence (RefSeq: NM_030916.2). Approximately 50,000 reads from cfDNA and 5000 reads for parental samples were obtained and analyzed for genotyping.

RESULTS

We first established the system for the detection of fetal *de novo* mutations in cfDNA using one case with TD1 (FHU15-005). The heterozygous c.1118A>G (p.Tyr373Cys) mutation in the *FGFR3* gene was determined by cord blood DNA after delivery. We did not detect this mutation in parental samples. Although standard Sanger sequencing did not detect the c.1118A>G mutation in cfDNA from maternal plasma obtained at 30 weeks of gestation, deep sequencing by means of NGS allowed us to successfully do so (Fig. 2). While the mutation rate in the cord blood was 44.7%, the mutation rate in the cfDNA was 4.2%, suggesting that the fetal fraction of cfDNA was 8.4%. We did not detect any mutations in cfDNA from normal pregnancies (data not shown).

To establish a diagnostic protocol, we developed a multiplex PCR system encompassing all of the mutation hotspots for TD1/TD2 and ACH in the *FGFR3* gene. The combined PCR products were subjected to deep sequencing using a next-generation sequencer. We applied this technique to another six cases showing fetal growth retardation with short limbs by ultrasound examination. Four cases showed a small amount of mutation in the *FGFR3* gene (Fig. 3). Two cases, FHU16-249 and FHU16-306, showed mutations in the *FGFR3* gene that were characteristic for TD1. In FHU16-249, a c.742C>T (p.

Arg248Cys) mutation was identified within PCR1 and c.1118A>G (p.Tyr373Cys) mutation was identified within PCR2 of FHU16-306, both of which were designed to cover the hotspots for TD1 mutations. Neither parent had these mutations. These were clinically typical TD cases by ultrasound examination. Another two cases, FHU15-276 and FHU17-081, also showed mutations in the *FGFR3* gene but these were characteristic of ACH. A c.1138G>A mutation was identified in FHU15-276 and c.1138 G>C mutation was identified in FHU17-081. Both cases showed the same p.Gly380Arg missense mutation in the PCR2 protocol, which was designed to cover codon 380, a hotspot for ACH mutations. Neither parent had these mutations in either case. These cases were clinically typical of ACH in the ultrasound examination.

The remaining two cases did not show any mutations following deep sequencing of the *FGFR3* mutation hotspots (Fig. 3). Because the FHU16-325 case showed a clinical phenotype similar to that of osteogenesis imperfecta type 1, the genomic DNA from the cord blood of this subject was screened for a mutation in the *COL1A1* gene. We identified a c.2155G>A (p.Gly719Ser) substitution in the *COL1A1* gene which has been reported as an osteogenesis imperfecta type 1-responsible mutation (Steiner et al. 2005). A parental study revealed that this mutation was of *de novo* origin. We designed a PCR protocol to amplify this mutation and performed deep sequencing of resulting amplicon from cfDNA (Fig. 4). Similar to the *FGFR3* gene, we successfully identified the *COL1A1* mutation in the cfDNA. Because the FHU16-353 case was a proportional small-for-gestational-week baby, we did not perform further mutational studies on this subject.

DISCUSSION

We performed NIPT using cfDNA to enable an accurate diagnosis in pregnancies with a possible fetal bone disease. In the case of

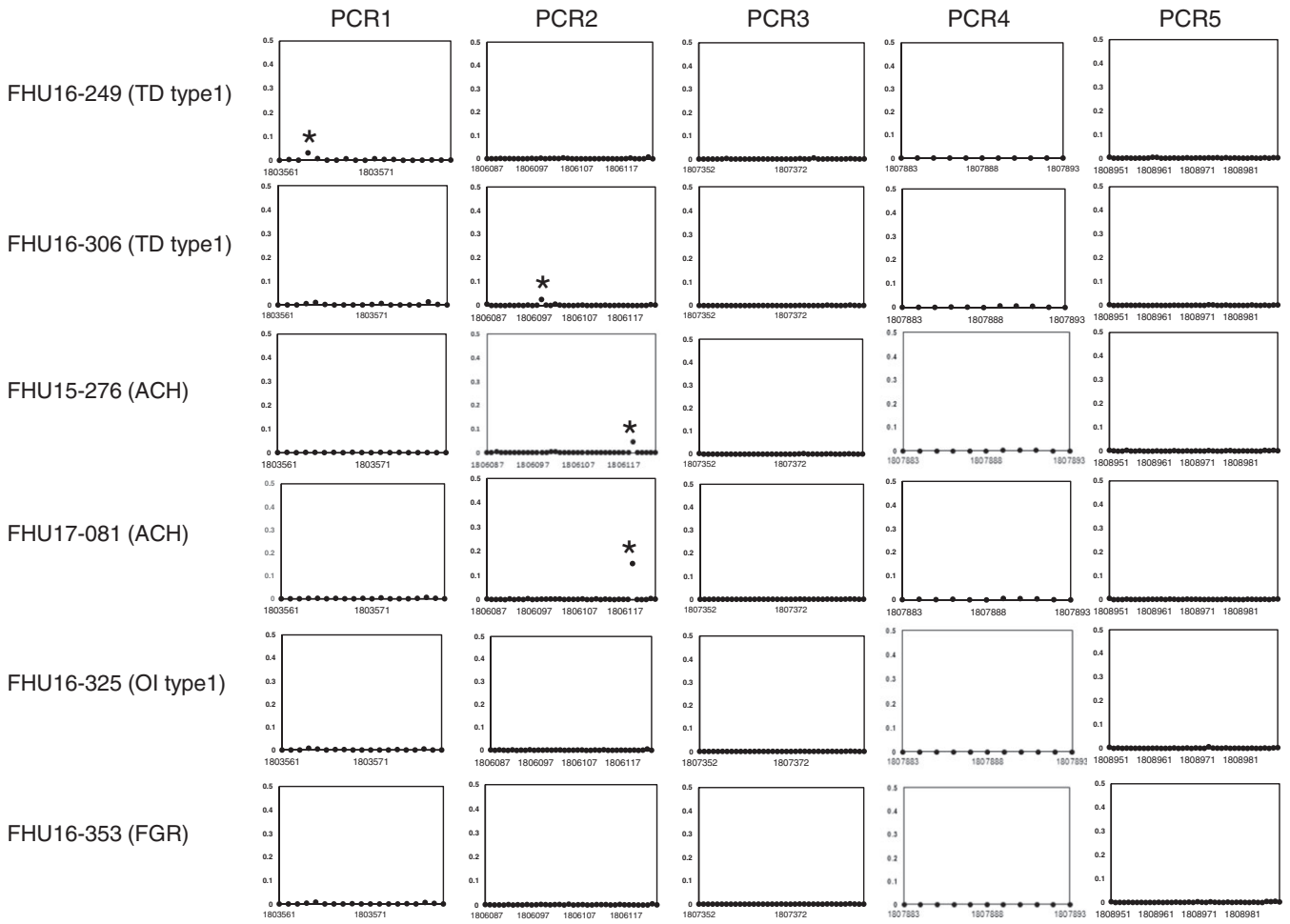


Fig. 3 Results of six samples from pregnant women showing fetal growth retardation with short limbs. Five products were obtained by multiplex PCR using cfDNA as a template. Deep sequencing was performed by NGS. Asterisks indicate the identified mutations.

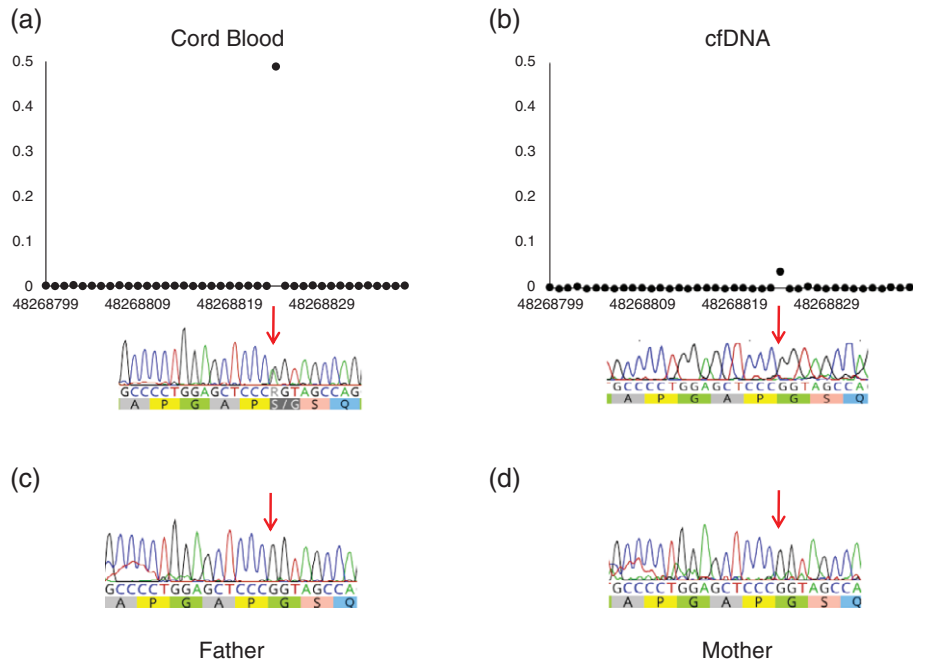


Fig. 4 Analysis of the deep sequence of the PCR product of exon 32 of the *COL1A1* gene from FHU16-325. A heterozygous c.2155G>A (p. Gly719Ser) mutation was identified in the cord blood, whereas an identical mutation was found in a small fraction of cfDNA. Sanger sequencing results are also displayed below. Arrows indicate the location of the mutation. (a) cord blood. (b) cfDNA. (c) paternal DNA. (d) maternal DNA.

fetal growth retardation with short limbs detected by ultrasound, several possible disorders need to be differentially diagnosed. TS and ACH are the most common of these. Previously, Chitty et al. (2013) reported that the combination of ultrasound and NIPT by restriction analysis of the PCR products of mutation hotspots in the *FGFR3* gene could accurately diagnose TD. For the differential diagnosis of TD and ACH, the same authors reported a panel of multiple PCRs using cfDNA as a template followed by deep sequencing with NGS (Chitty et al. 2015). In our present study, we performed multiplex PCR for these mutational hotspots in the *FGFR3* gene using cfDNA. We found two TD mutations in cases of clinically suspected TD pregnancy, whereas two ACH mutations were identified in clinically suspected ACH pregnancy. Our multiplex PCR approach thus appears useful for the accurate differential diagnosis of TD and ACH.

TD is a *de novo* dominant disorder, and most ACH cases arise as *de novo* mutations that mostly originate from the paternal germline. This is because *de novo* mutations generally arise as an error in DNA replication, and the number of cell divisions and DNA replications is much higher in male germ cells than in female. Similarly, the proportion of mutant sperm in the testis increases in an age-dependent manner (Crow 2000). Furthermore, *FGFR2* mutations in Crouzon disease or *FGFR3* mutations of TD or ACH are constitutively active and have a dominant effect on the cell growth rates of spermatogonia, leading to clonal expansion of the mutant ahead of the surrounding normal cells (Tiemann-Boege et al. 2002; Goriely et al. 2003). This means that when a mutation occurs in the *FGFR3* gene, it often leads to germinal mosaicism. In the general case of *de novo* mutations, the recurrence risk for the sibling is not high and similar to that of the background level. However, there may be a small increase in recurrence risk for siblings via germinal mosaicism in TD or ACH. In fact, several reports have described affected siblings of TD or ACH (Mettler and Fraser 2000; Osoba et al. 2000).

Hence, some of the parents of patients with TD or ACH might worry about the recurrence of the same disorder in the next pregnancy. Chorionic villus sampling or amniocentesis might be a possible option in such cases, but these approaches are invasive and occasionally lead to fatal complications such as miscarriage or stillbirth. This strategy is unjustifiable if the risk of the complication is higher than that of recurrence by germinal mosaicism. In such a situation, NIPT is a good option to avoid complications and our current strategy would be useful for NIPT in pregnant couples who had a previous pregnancy with TD or ACH.

The limitation of our present strategy is the possibility for false-negative results due to a low fetal fraction of cfDNA. To estimate the fetal fraction, the detection of the Y chromosome in pregnancy with a male fetus is feasible. Differences between the paternal and maternal genotype in a single nucleotide polymorphism might also be useful for estimating the fetal fraction concentration (Lo et al. 2010). The level of the paternal allele in the cfDNA sample might reflect the fetal fraction concentration. Addition of the PCR products including such polymorphisms to the DNA library followed by deep sequencing could ensure the detection of *de novo* mutation by detecting the paternal allele. A combination of our PCR method with these techniques to estimate the fetal fraction could help to determine the presence or absence of TD or ACH mutations in cfDNA and thereby assist couples with a previous TD or ACH pregnancy. To exclude the possibility for false-positive caused by the maternal low-level somatic mosaicism, we always examine parental samples as a negative control (Fig. 2c,d). Maternal DNA sample is obtained by the buffy coat DNA that do not contain fetal DNA. Further, since most of the *de novo* FGFR3

mutations arise during paternal spermatogenesis, the possibility of the somatic mosaicism in maternal blood is considerably low. However, in case that the mutation is positive in cfDNA, confirmative test with invasive sampling would be required.

ACKNOWLEDGMENTS

This study was supported by the Ogyaa Donation Foundation from the Japan Association of Obstetricians and Gynecologists, and by grants-in-aid for Scientific Research from the Ministry of Education, Culture, Sports, Science, and Technology, Japan (16K11117, 15H04710) and from the Ministry of Health, Labour and Welfare, Japan (H27-nanchitou (nan)-ippan-024).

DISCLOSURES

Authors have nothing to disclose and no conflict of interest.

REFERENCES

- Bianchi DW, Parker RL, Wentworth J et al. 2014. DNA sequencing versus standard prenatal aneuploidy screening. *N Engl J Med* 370(9):799–808.
- Chitty LS, Khalil A, Barrett AN, Pajkrt E, Griffin DR, Cole TJ. 2013. Safe, accurate, prenatal diagnosis of thanatophoric dysplasia using ultrasound and free fetal DNA. *Prenat Diagn* 33(5):416–423.
- Chitty LS, Mason S, Barrett AN et al. 2015. Non-invasive prenatal diagnosis of achondroplasia and thanatophoric dysplasia: next-generation sequencing allows for a safer, more accurate, and comprehensive approach. *Prenat Diagn* 35(7):656–662.
- Chiu RW, Chan KC, Gao Y et al. 2008. Noninvasive prenatal diagnosis of fetal chromosomal aneuploidy by massively parallel genomic sequencing of DNA in maternal plasma. *Proc Natl Acad Sci USA* 105(51):20458–20463.
- Crow JF. 2000. The origins, patterns and implications of human spontaneous mutation. *Nat Rev Genet* 1(1):40–47.
- Fan HC, Blumenfeld YJ, Chitkara U, Hudgins L, Quake SR. 2008. Noninvasive diagnosis of fetal aneuploidy by shotgun sequencing DNA from maternal blood. *Proc Natl Acad Sci USA* 105(42):16266–16271.
- Goriely A, McVean GA, Røjmyr M, Ingemarsson B, Wilkie AO. 2003. Evidence for selective advantage of pathogenic FGFR2 mutations in the male germ line. *Science* 301(5633):643–646.
- Karczeski B, Cutting GR. 2004. Thanatophoric dysplasia. In: Pagon RA, Adam MP, Ardinger HH, Wallace SE, Amemiya A, Bean LJH, Bird TD, Ledbetter N, Mefford HC, Smith RJH, Stephens K *GeneReviews*® [Internet]. Seattle: University of Washington.
- Kitzman JO, Snyder MW, Ventura M et al. 2012. Noninvasive whole-genome sequencing of a human fetus. *Sci Transl Med* 4(137):137ra76.
- Lo YM. 2001. Fetal DNA in maternal plasma: application to non-invasive blood group genotyping of the fetus. *Transfus Clin Biol* 8(3):306–310.
- Lo YM, Chiu RW. 2007. Prenatal diagnosis: progress through plasma nucleic acids. *Nat Rev Genet* 8(1):71–77.
- Lo YM, Patel P, Wainscoat JS, Sampietro M, Gillmer MD, Fleming KA. 1989. Prenatal sex determination by DNA amplification from maternal peripheral blood. *Lancet* 2(8676):1363–1365.
- Lo YM, Chan KC, Sun H et al. 2010. Maternal plasma DNA sequencing reveals the genome-wide genetic and mutational profile of the fetus. *Sci Transl Med* 2(61):61ra91.
- Mettler G, Fraser FC. 2000. Recurrence risk for sibs of children with "sporadic" achondroplasia. *Am J Med Genet* 90(3):250–251.
- Norton ME, Jacobsson B, Swamy GK et al. 2015. Cell-free DNA analysis for noninvasive examination of trisomy. *N Engl J Med* 372(17):1589–1597.

- Osoba O, Aziz NL, Krishnamoorthy U. 2000. Review of the diagnosis and transmission of thanatophoric dysplasia and report of a familial case with three affected siblings. *J Obstet Gynaecol* 20(5):540–541.
- Pauli RM. 1998. Achondroplasia. In: Pagon RA, Adam MP, Ardinger HH, Wallace SE, Amemiya A, LJH B, Bird TD, Ledbetter N, Mefford HC, RJH S, Stephens K, editors. *GeneReviews*[®] [Internet]. Seattle: University of Washington.
- Steiner RD, Adsit J, Basel D. 2005. COL1A1/2-related osteogenesis imperfecta. In: Pagon RA, Adam MP, Ardinger HH, Wallace SE, Amemiya A, LJH B, Bird TD, Ledbetter N, Mefford HC, RJH S, Stephens K, editors. *GeneReviews*[®] [Internet]. Seattle: University of Washington.
- Tiemann-Boege I, Navidi W, Grewal R et al. 2002. The observed human sperm mutation frequency cannot explain the achondroplasia paternal age effect. *Proc Natl Acad Sci USA* 99(23):14952–14957.



Clinical and genetic aspects of mild hypophosphatasia in Japanese patients

Katsuyuki Yokoi^{a,b}, Yoko Nakajima^{a,*}, Yasuko Shinkai^b, Yoshimi Sano^c, Mototaka Imamura^c, Tomoyuki Akiyama^d, Tetsushi Yoshikawa^a, Tetsuya Ito^a, Hiroki Kurahashi^b

^a Department of Pediatrics, Fujita Health University School of Medicine, Toyoake 470-1192, Japan

^b Division of Molecular Genetics, Institute for Comprehensive Medical Science, Fujita Health University, Toyoake 470-1192, Japan

^c Department of Plastic Surgery, Division of Pediatric Dentistry & Orthodontics, Fujita Health University of Medicine, Toyoake 470-1192, Japan

^d Department of Child Neurology, Okayama University Hospital, Okayama 700-8558, Japan



ARTICLE INFO

Keywords:

Hypophosphatasia
ALPL
Premature loss of deciduous teeth
Dominant-negative mutations

ABSTRACT

Background: Hypophosphatasia (HPP) is a rare inborn error of metabolism that results from a dysfunctional tissue non-specific alkaline phosphatase enzyme (TNSALP). Although genotype-phenotype correlations have been described in HPP patients, only sparse information is currently available on the genetics of mild type HPP. **Methods:** We investigated 5 Japanese patients from 3 families with mild HPP (patients 1 and 2 are siblings; patient 4 is a daughter of patient 5) who were referred to Fujita Health University due to the premature loss of deciduous teeth. Physical and dental examinations, and blood, urine and bone density tests were conducted. Genetic analysis of the *ALPL* gene was performed in all patients with their informed consent.

Results: After a detailed interview and examination, we found characteristic symptoms of HPP in some of the study cases. Mobile teeth or the loss of permanent teeth were observed in 2 patients, and 3 out of 5 patients had a history of asthma. The serum ALP levels of all patients were 30% below the lower limit of the age equivalent normal range. *ALPL* gene analysis revealed compound heterozygous mutations, including Ile395Val and Leu520Argfs in family 1, Val95Met and Gly491Arg in family 2, and a dominant missense mutation (Gly456Arg) in family 3. The 3D-modeling of human TNSALP revealed three mutations (Val95Met, Ile395Val and Gly456Arg) at the homodimer interface. Severe collisions between the side chains were predicted for the Gly456Arg variant. **Discussion:** One of the characteristic findings of this present study was a high prevalence of coexisting asthma and a high level serum IgE level. These characteristics may account for the fragility of tracheal tissues and a predisposition to asthma in patients with mild HPP. The genotypes of the five mild HPP patients in our present study series included 1) compound heterozygous for severe and hypomorphic mutations, and 2) dominant-negative mutations. All of these mutations were at the homodimer interface, but only the dominant-negative mutation was predicted to cause a severe collision effect between the side chains. This may account for varying mechanisms leading to different effects on TNSALP function.

1. Objective

Hypophosphatasia (HPP) is an inherited disorder characterized by defective bone and tooth mineralization, and a deficiency in tissue-non-specific alkaline phosphatase isoenzyme (TNSALP) activity [1]. The incidence of this disorder is not accurately known, but the birth prevalence of the most severe forms of HPP, i.e. perinatal and infantile, is estimated at 1:100,000 [2]. An estimate of 1:6370 has been suggested previously for less severe forms of HPP using molecular data [3].

TNSALP is a phosphomonoesterase of 507 residues that is anchored at its carboxyl terminus to the plasma membrane by a

phosphatidylinositol-glycan moiety. This enzyme is physiologically active in its dimeric form and cleaves the extracellular substrates pyridoxal-5'-phosphate (PLP), phosphoethanolamine (PEA) and inorganic pyrophosphates (PPi) [1]. Low TNSALP activity has impacts on multiple systems, including the respiratory, central nervous, renal, musculoskeletal, and immune systems, and on dental structures [4].

HPP is caused by mutations in the liver/bone/kidney alkaline phosphatase (*ALPL*) gene encoding TNSALP [5,6]. To date, 390 mutations have been identified in *ALPL* that show an association with HPP. (http://www.sesep.uvsq.fr/03_hypo_mutations.php). HPP symptoms are highly variable in terms of their clinical expression, and six clinical

* Corresponding author at: Department of Pediatrics, Fujita Health University School of Medicine, 1-98 Dengakugakubo, Kutsukake-cho, Toyoake, Aichi 470-1192, Japan.

E-mail address: yonaka@fujita-hu.ac.jp (Y. Nakajima).

<https://doi.org/10.1016/j.ymgmr.2019.100515>

Received 3 July 2019; Received in revised form 5 August 2019; Accepted 2 September 2019

Available online 11 October 2019

2214-4269/ © 2019 The Authors. Published by Elsevier Inc. This is an open access article under the CC BY-NC-ND license (<http://creativecommons.org/licenses/by-nc-nd/4.0/>).

forms are currently recognized. These are based on the age at diagnosis and the severity of disease features including lethal perinatal, benign perinatal, infantile, childhood, adult, and odontohypophosphatasia (odonto-HPP) [6]. Enzyme replacement therapy (ERT) has recently been reported to be efficient and improve patient outcomes even in cases of life-threatening forms of HPP [7]. Although some genotype/phenotype correlations have been described for a portion of the *ALPL* mutations, the mechanisms underlying HPP remain incompletely understood, particularly in the mild forms of this disorder.

In our present study, we analyzed the clinical and genetic aspects of a small series of Japanese patients with mild HPP.

2. Material and methods

2.1. Informed consent and ethical approval

Informed consent was obtained from each patient and/or their family. The study protocol was approved by the Ethical Review Board for Human Genome Studies at Fujita Health University.

2.2. Clinical survey of mild HPP patients

In our present study, mild HPP refers to childhood and adult HPP, odontohypophosphatasia, and perinatal benign HPP. Severe HPP denotes the perinatal and infantile forms. We reviewed the medical charts of 5 patients from 3 families who presented with mild HPP and had sufficient follow-up data. Patients 1 and 2 are siblings, and patient 4 is the daughter of patient 5. All of these cases had been referred to Fujita Health University Hospital for a detailed medical examination due to the premature loss of deciduous teeth. Our review of these cases included all available data from the physical examinations and medical care provided at the Fujita Health University Hospital.

All patients had a diagnosis of HPP clinically, biochemically, and genetically. The diagnosis of HPP required that all of the following criteria be met at the first admission: 1) a medical history or physical examination consistent with one or more dento-osseous complication(s) of HPP; 2) no evidence of any other condition that could cause the early loss of primary teeth; and 3) a serum ALP activity level below the age-matched reference ranges [8]. Physical and dental histories were recorded through a diagnostic interview process. Dental examinations were carried out at Department of Plastic Surgery, Division of Pediatric Dentistry & Orthodontics, Fujita Health University of Medicine. Clinical signs and symptoms were evaluated based upon a physical and oral examination, and the available medical or dental records. Biochemical and radiographic tests were performed at diagnosis. The serum ALP, PLP, Ca, phosphorus, parathyroid hormone (PTH), total serum IgE and 1,25-OH vitamin D levels, and the urine PEA levels on a spot urine test, were evaluated in all patients. The reference values for serum ALP, serum PLP/PL and urine PEA were obtained from Tanaka et al. [9], Akiyama et al. [10] and SRL Inc., respectively. A high total serum IgE was defined as a level higher than the adult standard value (> 250 IU/mL). Short stature was defined as a height below -2SD. Non atopy was

defined as no evidence of pruritic skin, including no reporting by a parent of any rubbing or scratching by the child [11].

Bone mineral density (BMD) was measured at the level of the lumbar spine (L2-L4) using dual-energy X-ray absorptiometry. BMD Z-scores were calculated using data from a general population of Japanese children and adolescents (BMD of the lumbar spine and total body mass) after adjusting for age. However, because these prior data do not include children under 6 years of age, the Z-scores were calculated for our current study patients 1 and 2 only.

2.3. *ALPL* gene analysis

ALPL gene analysis was performed with informed consent. DNA was extracted from peripheral blood samples and sequenced using the Sanger method to screen for genetic variations at the nucleotide level throughout all coding exons of the *ALPL* gene. We used the UCSC genome browser (<http://genome-asia.ucsc.edu/human> GRCh38/hg38) as the human genome assembly. PCR was carried out in a 10 µL volume containing 5.7 µL of distilled water, 2 µL of 5×PrimeSTAR GXL buffer (TaKaRa, Japan), 0.2 µL of each primer (10 µM), 0.1 µL of PrimeSTAR GXL DNA polymerase (TaKaRa, Japan), and 1 µL of template DNA (20 ng/µL). The primer sequences are listed in the Online Supplementary Table. PCR amplifications were performed using a DNA thermal cycler (Applied Biosystems) under the following cycling conditions: initial denaturation at 94 °C for 2.5 min followed by 35 cycles at 98 °C for 10s, 60 °C for 15 s and 68 °C for 45 s. The PCR products were sequenced using a standard Sanger method. The *ALPL* sequence from the HPP patients was compared to control subjects and the reference *ALPL* sequence (Ref Seq NM_000478.5). Allele frequencies were investigated via gnomAD browser beta (<http://gnomad.broadinstitute.org/>). In silico analysis was performed using PolyPhen and SIFT.

2.4. 3D-modeling

A 3D model of the TNSALP molecule was previously constructed using the homology between TNAP and human placental alkaline phosphatase, which has a determined crystal structure. The locations of the mutations were determined using the UCSF Chimera (www.cgl.ucsf.edu/chimera).

3. Results

3.1. Clinical evaluations

The chief complaints at diagnosis were premature loss of deciduous teeth in patients 1 to 4 and permanent teeth loss in patient 5. The dental features of these cases are summarized in Table 1. All of the study patients had premature loss of their anterior deciduous teeth and atrophy of the alveolar bone. Permanent tooth loss was found in patient 5 only, but the mobility of permanent teeth was also evident in patient 1. Elongation of teeth and enamel hypoplasia were observed in 2 and 3 of the 5 patients, respectively. The results of biochemical of

Table 1
Dental features of the study patients.

Dental features	Patient 1	Patient 2	Patient 3	Patient 4	Patient 5
Age at diagnosis	9 y	7 y	1 y	4 y	39 y
Premature loss of anterior deciduous teeth	+	+	+	+	+
Premature loss of posterior deciduous teeth	+	Mobility	–	–	+
Loss of permanent teeth	Mobility	–	– ^a	– ^a	+, Mobility
Delay of eruption	–	–	–	–	–
Atrophy of alveolar bone	+	+	+	+	+
Elongation of teeth	–	+	–	–	+
Enamel hypoplasia	+	–	+	+	–

^a Deciduous dentition.

Table 2

Clinical, biochemical and radiographic data for the study patients. N/A, not available. Reference values: Serum ALP from Tanaka et al. [9]; Serum PLP and PL from Akiyama et al. [8]; urine PEA from SRL Inc. For serum ALP, reference values are shown for patients over 20 years of age. For serum PLP and PL, reference values for 7–17 year-old patients are shown.

Patient ID	Patient 1	Patient 2	Patient 3	Patient 4	Patient 5
Age	10	8	1	4	39
Gender	Female	Male	Female	Female	Female
Biochemical test					
Ca (mg/dl)	9.7 (Reference: 8.7–10.3)	9.8 (8.7–10.3)	11.1 (8.7–10.3)	10.4 (8.7–10.3)	9.7 (8.7–10.3)
Phosphorus (mg/dl)	5.3 (2.5–4.7)	5.9 (2.5–4.7)	7.5 (2.5–4.7)	4.9 (2.5–4.7)	4.3 (2.5–4.7)
ALP (U/L)	228 (470–1450)	245 (450–1300)	155 (395–1289)	286 (430–1150)	50 (120–340)
PTH (pg/ml)	31 (15–65)	27 (15–65)	8 (15–65)	21 (15–65)	32 (15–65)
1,25-OH vitD (pg/ml)	62.2 (20–70)	58.1 (20–70)	88.3 (20–70)	61.2 (20–70)	57.2 (20–60)
PLP (pyridoxal-5'-phosphate)(nmol/L)	469.9 (14.5–57.3)	322.5 (14.5–57.3)	375.2 (16.2–57.4)	325.9 (16.2–57.4)	89.9 (14.5–57.3)
PL (pyridoxal)(nmol/L)	39.9 (7.4–17.7)	28.8 (7.4–17.7)	27.2 (8.8–28.0)	43.8 (8.8–28.0)	6.7 (7.4–17.7)
PLP/PL	11.8	11.2	13.8	7.4	13.3
Total IgE (IU/ml)	638.4	349.5	267.5	1099	17.1
Urine PEA (μ mol/g Cr)	480.1 (39.4–93.5)	720.6 (29.1–75.6)	662.7 (39.4–93.5)	507.7 (39.4–93.5)	274.7 (39.4–93.5)
Clinical findings without dental features					
Shortening or deformity of the extremities	–	–	–	–	–
Bone fractures (NO.)	1	0	0	0	1
Part of fractures	Forearm	–	–	–	Right shoulder
Seizure	–	–	–	–	–
Enlargement of the anterior fontanelle	–	–	–	–	–
Renal calcification	–	–	–	–	–
Stature (cm)	130 (–1.4SD)	123 (–0.2SD)	71.5 (–1.9SD)	100.4 (–0.85SD)	148.1 (–1.96SD)
Body weight (kg)	28.8 (–0.7SD)	23.9 (–0.1SD)	8.29 (–1.9SD)	15.5 (–0.9SD)	35.9
Deafness	–	–	–	–	–
Asthma	+	+	+	–	–
Atopy	–	–	–	–	–
Muscle ache	–	+	–	–	–
Dysphagia	–	–	+	–	–
Other symptom	–	–	–	–	Headache
Radiographic findings					
Hypomineralisation	–	–	–	–	–
Deformity of long bones	–	–	–	–	–
Flared metaphyses	–	–	+	–	–
Narrow thorax	–	–	–	–	–
Bone mineral density (g/cm^2)	0.644 (Z-score – 1.2)	0.551 (Z-score – 1.8)	0.298	0.395	N/A
Birth					
Gestational age	39w5d	38w0d	38w2d	39w6d	N/A
Birth weight (g)	2786 (–0.5SD)	2770 (–0.4SD)	2405 (–1.1SD)	2538 (–1.4SD)	N/A
Birth stature (cm)	47 (–1.2SD)	48.5 (0.2SD)	48 cm (–0.2SD)	49 (–0.2SD)	N/A
Birth head circumference (cm)	30 (–2.5SD)	33 (0.0SD)	N/A	31.4 (–1.5SD)	N/A
Birth chest circumference (cm)	31	31	N/A	30	N/A

radiographic testing, and the clinical findings other than the dental features at diagnosis, for all 5 study patients are presented in Table 2. Our present cases had been referred to our hospital in the first instance due to a single symptom i.e. the premature loss of deciduous teeth. After a detailed interview and examination however, other characteristic symptoms, and biochemical and radiographic findings, became evident as follows: dysphagia (1/5), headache (1/5), muscle ache (1/5), bone fractures (2/5), asthma (3/5), low serum ALP levels (5/5), high serum PLP/PL (5/5), high urine PEA levels (5/5), high serum IgE (4/5), flared metaphyses (1/5), and low Z-score BMD (2/2). All of our study patients showed serum ALP levels at > 30% below the lower limit of the age equivalent normal range. The serum PLP/PL and urine PEA levels were higher in all of our HPP patients compared to the control subjects. The BMD was measured in four patients, of whom two patients showed a low Z-score but this could not be calculated in the remaining two cases because their age were under 6.

3.2. Gene analysis

The results of our *ALPL* mutation sequencing analyses are presented in Table 3. The clinical forms of the genotypes were described previously [12–15]. The three families in our current series all harbored different mutations that are rare within the general population, and had

a minor allele frequency ranging from completely unreported to 0.00003716 (gnomAD browser beta). Family 1 (patients 1 and 2) members carried the compound heterozygous *ALPL* variants c.1183A > G (p.Ile395Val) and c.1559delT (p.Leu520Argfs). The c.1183A > G (p.Ile395Val) mutation was reported previously to result in a prenatal benign phenotype as the gene product still possessed residual ALP activity of 19.1% [16]. The c.1559delT (p.Leu520Argfs) variant is a null mutation that was previously reported to be common in Japanese severe HPP patients [17].

Family 2 (patient 3) was found to harbor compound heterozygous variants including c.283G > A (p.Val95Met) and c.1471G > A (p.Gly491Arg). Mutation c.283G > A (p.Val95Met) was registered previously in a public database (Institute of Human Genetics, University Of Wurzburg), and classified as “with likely pathogenic” in ClinVar, but no clinical information has been reported to date for this variation. Analysis of the Val95Met substitution using SIFT and PolyPhen prediction software indicated that this mutation was ‘tolerable’ and ‘possibly damaging’, with scores of 0.12 and 0.897, respectively. In contrast, c.1471G > A (p.Gly491Arg) is reported to be a severe perinatal phenotype mutation [14]. These data suggest that the c.1471G > A (p.Gly491Arg) mutation may be null whereas the gene product harboring the c.283G > A (p.Val95Met) variation may still possess residual enzymatic activity.

Table 3
Genotype-phenotype correlations within the HPP families examined in this study.

Mode of inheritance	Family 1 (patients 1 and 2)		Family 2 (patient 3)		Family 3 (patients 4 and 5)
	AR	AR	AR	AR	AD
Genotype	c.1183A > G(p.Ile395Val)	c.1559delT(p.Leu520Argfs)	c.283G > A(p.Val95Met)	c.1471G > A(p.Gly491Arg)	c.1366G > A(p.Gly456Arg)
In silico function (PolyPhen)	0.535	0.535	0.897	1	0.945
In silico function (SIFT)	0.08	0.08	0.12	0	0
Clinical form of the genotype	Prenatal benign	Infantile	Unknown	Perinatal	Infantile
Previous report	Wenkert et al. 2011	Orimo et al. 1994	Novel	Mornet et al. 1998	Ozono et al. 1996
Prevalence (% east Asia/total)	0.002031/ 0	0.0008803/ 0.01187	0.003716/ 0	0/0	0/0
ACMG evaluation	Likely pathogenic	Pathogenic	Likely pathogenic	Likely pathogenic	Pathogenic
Position in the 3D structure	Interface of homodimer	Unclear lesion	Interface of homodimer	Surface of protein	Interface of homodimer

Family 3 (patients 4 and 5) had only one heterozygous mutation, c.1366G > A (p.Gly456Arg), which had been initially reported as one of the compound heterozygous mutations in the infantile form of HPP [15]. Furthermore, a recent study using transfection experiments has indicated that this mutation has a dominant-negative effect [18].

3.3. 3D-modeling

The locations of the identified mutated residues in the 3D structures of human TNSALP are presented in Fig. 1. In contrast to the severe Gly491Arg mutation located at the surface of this protein, the three mutations that characterized the mild HPP cases in our present study (Val95Met, Ile395Val and Gly456Arg) were all localized at the homodimer interface. Severe collisions between the side chains were predicted in the Gly456Arg variant (Fig. 2a), whereas a mild only and no effect were predicted for the Val95Met and Ile395Val mutations, respectively (Fig. 2b, c).

4. Discussion

One of the characteristic findings in our present study series of 5 patients was the high percentage of coexisting asthma (3/5) as well as high level serum IgE (4/5). In addition, 3 out of the 4 patients with a high serum IgE had asthma. Tracheomalacia is a known symptom of perinatal lethal HPP [5] but the frequency of other clinical conditions associated with wheezing in these cases, such as asthma and the serum

IgE level, have remained unknown. Although we examined only a very small cohort of patients in our present study, more than half of these cases showed a past or current medical history of asthma and a high serum IgE. These characteristics may account for the fragility of tracheal tissues and a predisposition to asthma in mild HPP patients. Although the treatment approaches for HPP have historically been supportive in nature, enzyme replacement therapy (ERT) has recently become available for these patients using asfotase alfa (Strensiq™), a bone-targeting recombinant alkaline phosphatase [19]. This enzyme has produced beneficial effects in terms of survival and function in HPP patients [20,21]. However the selection of appropriate candidates for this ERT has remained challenging when the condition is not life-threatening [19]. The loss of permanent teeth has a detrimental impact on quality of life but no study has demonstrated the effectiveness of an early ERT in preventing this outcome in mild HPP. Further studies are needed to assess the efficacy of these therapies.

Our present mutational analysis identified compound heterozygous mutations in family 1, i.e. one obvious loss-of-function mutation (1559delT) and one variant that still possessed some residual enzymatic activity (Ile395Val). In family 2, one identified mutation (Gly491Arg) was previously described as severe, and another (Val95Met) to have only weak effects, by in silico functional data. Since the phenotype of patient 3 in this family was mild, it is possible that Val95Met may possess some residual ALP activity in this case. Family 3 harbored only one mutation (Gly456Arg) with an autosomal dominant transmission. This variant was reported previously to have a dominant-negative effect

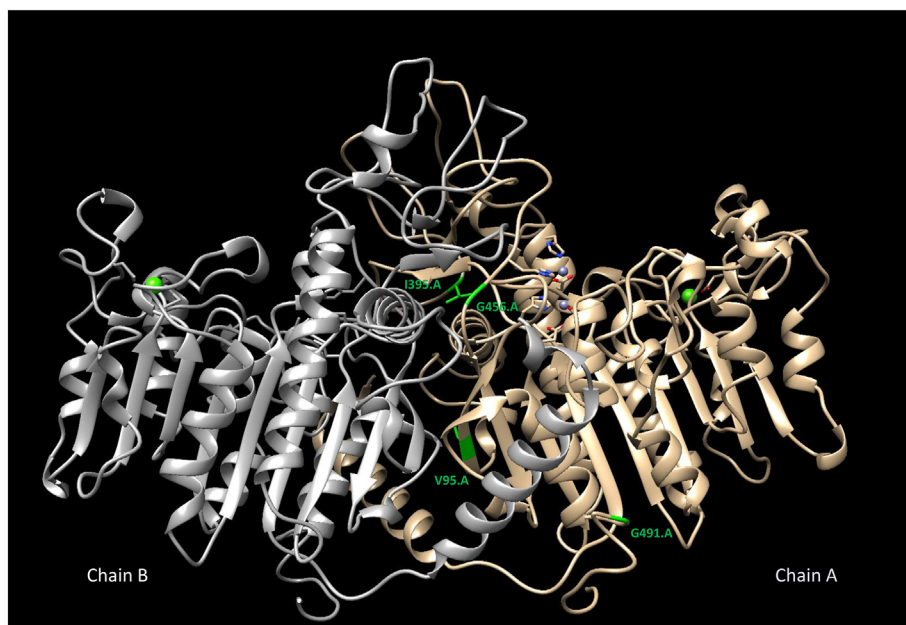


Fig. 1. 3D strand view of the human TNSALP protein. The two monomers are denoted by Chain A and Chain B. The three amino-acid residues that were found to be mutated in our mild HPP cases (G456R, V95M, I395V) are localized on the homodimer interface. Gly491Arg is located on the surface of the protein. Leu520Argfs is located within the region where the 3D structure has not yet been clearly determined.

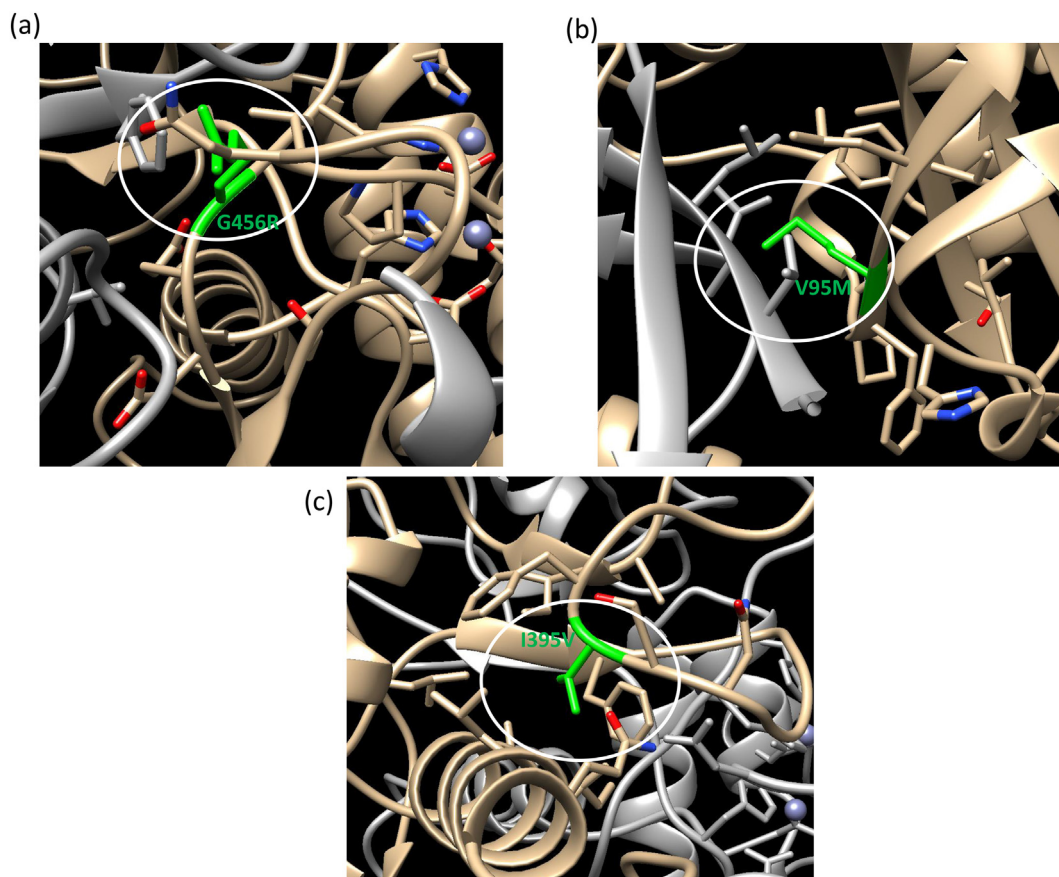


Fig. 2. Structural models of the human TNSALP protein. (a) Gly456 is located at the homodimer interface. Severe collisions between the side chains occur in the case of Gly456Arg (green).

(b) Val95 is located at the homodimer interface. Mild collisions occur in the case of Val95Met (green).

(c) Ile395 is located at the homodimer interface. No significant changes occur in the case of Ile395Val (green). (For interpretation of the references to colour in this figure legend, the reader is referred to the web version of this article.)

in vitro, although our present study is the first to clinically demonstrate Gly456Arg as autosomal dominant. Hence, the genotype of mild HPP can be classified as either 1) compound heterozygous for a severe and hypomorphic mutation; or 2) dominant-negative mutations. In family 1, two patients harboring the same mutations seemed to manifest a similar degree of disease severity. In family 3, patient 5 is the mother of patient 4 harboring the same mutation and had similar symptoms in her own childhood. Hence, a genotype-phenotype correlation was present in our current cases. Genetic testing for these genotypes will assist with genetic counseling.

The mechanisms underlying the effects of the mutations in our current study series, i.e. the reasons for a dominant or recessive effect, are still unclear. However, interactions between the monomers of the dimeric TNSALP protein structure are likely to be involved [22]. TNSALP has five regions (the active site and its vicinity, the active site valley, the homodimer interface, the crown domain, and the calcium-binding domain), which are crucial for enzyme function and bone mineralization [23]. It was previously reported that the TNSALP mutations identified to date with a dominant effect are restricted to three regions of the protein: the active site, homodimer and crown domain. However the difference between the standard recessive mutation and these dominant mutations is still unknown. A prevailing hypothesis is that the dominant-negative effect may be due to the inhibition of the wild-type monomer by a mutated monomer in the heterodimer, or the sequestration of the wild-type protein by a mutant product in the Golgi apparatus that prevents it from being transported to the membrane [24]. In our current analysis, three of the identified mutations were located at the homodimer interface, but the Gly456Arg mutation

showing a dominant-negative effect produced the most severe change in 3-D modeling. TNSALP Gly456Arg variants may maintain monomer interactions and might directly affect the enzymatic activity of dimers, including those harboring mutations, whilst the dimers from normal monomers would maintain small amounts of enzymatic activity. In contrast, the dimers of the proteins containing the hypomorphic mutations identified in families 1 and 2 (Ile395Val, Val95Met) could maintain low levels of enzymatic activity because of the lesser impact of these variations compared to Gly456Arg. Future investigations of the differences in the 3D structures of TNSALP variants may reveal the precise mechanisms underlying dominant-negative and recessive but weak mutation effects.

Ethics approval and consent to participate

All procedures in this study were conducted in accordance with the ethical standards of the responsible committee on human experimentation (institutional and national) and with the Helsinki Declaration of 1975, as revised in 2005(5).

Consent for publication

Written informed consent to publish medical information and images was obtained from all patients and/or their family reported in this publication.

Declaration of Competing Interests

The authors declare no conflicts of interest in relation to this study.

Funding

This research did not receive any specific grant from funding agencies in the public, commercial, or not-for-profit sectors.

Contributions of individual authors

Katsuyuki Yokoi: Sanger sequencing, data retrieval, drafting and revision of the manuscript.

Yoko Nakajima: conception and design, analysis and interpretation, drafting of the manuscript.

Yasuko Shinkai: 3-D modeling.

Yoshimi Sano: dental examinations.

Mototaka Imamura: dental examinations.

Tomoyuki Akiyama: analysis of the serum PLP, PL and urine PEA levels.

Tetsushi Yoshikawa: experimental analysis and interpretation of data.

Tetsuya Ito: experimental analysis and interpretation of data.

Hiroki Kurahashi: conception and design, analysis and interpretation, critical revision of the manuscript for important intellectual content.

Acknowledgements

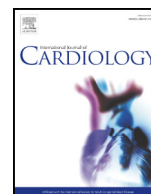
We thank the patients and their families for their participation. We also thank past and present members of our laboratory.

Appendix A. Supplementary data

Supplementary data to this article can be found online at <https://doi.org/10.1016/j.ymgmr.2019.100515>.

References

- [1] E. Mornet, Hypophosphatasia, *Orphanet. J. Rare. Dis.* 2 (2007) 40, <https://doi.org/10.1186/1750-1172-2-40>.
- [2] D. Fraser, Hypophosphatasia, *Am. J. Med.* 22 (1957) 730–746.
- [3] E. Mornet, A. Yvard, A. Taillandier, D. Fauvert, B. Simon-Bouy, A molecular-based estimation of the prevalence of hypophosphatasia in the European population, *Ann. Hum. Genet.* 75 (3) (2011) 439–445.
- [4] A.B. Daniel, V. Saraff, N.J. Shaw, R. Yates, M.Z. Mughal, R. Padidela, Healthcare resource utilization in the management of hypophosphatasia in three patients displaying a spectrum of manifestations, *Orphanet. J. Rare. Dis.* 13 (2018) 142, <https://doi.org/10.1186/s13023-018-0869-4>.
- [5] T. Taketani, K. Onigata, H. Kobayashi, Y. Mushimoto, S. Fukuda, S. Yamaguchi, Clinical and genetic aspects of hypophosphatasia in Japanese patients, *Arch. Dis. Child.* 99 (2014) 211–215, <https://doi.org/10.1136/archdischild-2013-305037>.
- [6] L. Martins, T.L. Rodrigues, M.M. Ribeiro, M.T. Saito, A.P. Giorgetti, M.Z. Casati, et al., Novel ALPL genetic alteration associated with an odontohypophosphatasia phenotype, *Bone* 56 (2) (2013) 390–397, <https://doi.org/10.1016/j.bone.2013.06.010>.
- [7] M.P. Whyte, C.R. Greenberg, N.J. Salman, M.B. Bober, W.H. McAlister, D. Wenkert, et al., Enzyme-replacement therapy in life-threatening hypophosphatasia, *N. Engl. J. Med.* 366 (10) (2012) 904–913, <https://doi.org/10.1056/NEJMoa1106173>.
- [8] M.P. Whyte, F. Zhang, D. Wenkert, W.H. McAlister, K.E. Mack, M.C. Benigno, et al., Hypophosphatasia: validation and expansion of the clinical nosology for children from 25 years experience with 173 pediatric patients, *Bone* 75 (2015) 229–239, <https://doi.org/10.1016/j.bone.2015.02.022>.
- [9] T. Tanaka, A. Yamashita, K. Ichihara, Reference intervals of clinical tests in children determined by a latent reference value extraction method (in Japanese), *J. Jpn. Pediatr. Soc.* 112 (2008) 1117–1132.
- [10] T. Akiyama, Y. Hayashi, Y. Hanaoka, T. Shibata, M. Akiyama, H. Tsuchiya, et al., Pyridoxal 5'-phosphate, pyridoxal, and 4-pyridoxic acid in the paired serum and cerebrospinal fluid of children, *Clin. Chim. Acta* 472 (2017) 118–122, <https://doi.org/10.1016/j.cca.2017.07.032>.
- [11] H.C. Williams, *Clinical practice. Atopic dermatitis*, *N. Engl. J. Med.* 352 (22) (2005) 2314–2324.
- [12] D. Wenkert, W.H. McAlister, S.P. Coburn, J.A. Zerega, L.M. Ryan, K.L. Ericson, et al., Hypophosphatasia: nonlethal disease despite skeletal presentation in utero (17 new cases and literature review), *J. Bone Miner. Res.* 26 (10) (2011) 2389–2398, <https://doi.org/10.1002/jbmr.454>.
- [13] H. Orimo, Z. Hayashi, A. Watanabe, T. Hirayama, T. Shimada, Novel missense and frameshift mutations in the tissue-nonspecific alkaline phosphatase gene in a Japanese patient with hypophosphatasia, *Hum. Mol. Genet.* 3 (9) (1994) 1683–1684.
- [14] E. Mornet, A. Taillandier, S. Peyramaure, F. Kaper, F. Muller, R. Brenner, et al., Identification of fifteen novel mutations in the tissue-nonspecific alkaline phosphatase (TNSALP) gene in European patients with severe hypophosphatasia, *Eur. J. Hum. Genet.* 6 (4) (1998) 308–314.
- [15] K. Ozono, M. Yamagata, T. Michigami, S. Nakajima, N. Sakai, G. Cai, et al., Identification of novel missense mutations (Phe310Leu and Gly439Arg) in a neonatal case of hypophosphatasia, *J. Clin. Endocrinol. Metab.* 81 (12) (1996) 4458–4461.
- [16] B. Chen, L. Li, W. Ren, L. Yi, Y. Wang, F. Yan, A novel missense mutation in the ALPL gene causes dysfunction of the protein, *Mol. Med. Rep.* 16 (1) (2017) 710–718, <https://doi.org/10.3892/mmr.2017.6668>.
- [17] T. Michigami, T. Uchihashi, A. Suzuki, K. Tachikawa, S. Nakajima, K. Ozono, Common mutations F310L and T1559del in the tissue-nonspecific alkaline phosphatase gene are related to distinct phenotypes in Japanese patients with hypophosphatasia, *Eur. J. Pediatr.* 164 (5) (2005) 277–282.
- [18] G. Del Angel, E. Mornet, J. Reynders, Combining large-scale in vitro functional testing with protein stability simulations to develop new insights into hypophosphatasia genotype/phenotype correlation, *Abstract ASHG*, 2018.
- [19] E.T. Rush, Childhood hypophosphatasia: to treat or not to treat, *Orphanet. J. Rare. Dis.* 13 (2018) 116, <https://doi.org/10.1186/s13023-018-0866-7>.
- [20] M.P. Whyte, J.H. Simmons, S. Moseley, K.P. Fujita, N. Bishop, N.J. Salman, et al., Asfotase alfa for infants and young children with hypophosphatasia: 7 year outcomes of a single-arm, open-label, phase 2 extension trial, *Lancet Diabetes Endocrinol.* 7 (2) (2019) 93–105, [https://doi.org/10.1016/S2213-8587\(18\)30307-3](https://doi.org/10.1016/S2213-8587(18)30307-3).
- [21] P.S. Kishnani, C. Rockman-Greenberg, F. Rauch, M.T. Bhatti, S. Moseley, A.E. Denker, et al., Five-year efficacy and safety of asfotase alfa therapy for adults and adolescents with hypophosphatasia, *Bone* 121 (2019) 149–162, <https://doi.org/10.1016/j.bone.2018.12.011>.
- [22] A.S. Lia-Baldini, F. Muller, A. Taillandier, J.F. Gibrat, M. Mouchard, B. Robin, et al., A molecular approach to dominance in hypophosphatasia, *Hum. Genet.* 109 (1) (2001) 99–108.
- [23] E. Mornet, E. Stura, A.S. Lia-Baldini, T. Stigbrand, A. Menez, M.H. Le Du, Structural evidence for a functional role of human tissue nonspecific alkaline phosphatase in bone mineralization, *J. Biol. Chem.* 276 (33) (2001) 31171–31178.
- [24] D. Fauvert, I. Brun-Heath, A.S. Lia-Baldini, L. Bellazi, A. Taillandier, J.L. Serre, et al., Mild forms of hypophosphatasia mostly result from dominant negative effect of severe alleles or from compound heterozygosity for severe and moderate alleles, *BMC Med. Genet.* 10 (2009) 51, <https://doi.org/10.1186/1471-2350-10-51>.



Frequent intragenic microdeletions of elastin in familial supravalvular aortic stenosis



Satoshi Hayano ^{a,1}, Yusuke Okuno ^{b,1}, Makiko Tsutsumi ^{c,1}, Hidehito Inagaki ^{c,1}, Yoshie Fukasawa ^{a,1}, Hiroki Kurahashi ^{c,1}, Seiji Kojima ^{a,1}, Yoshiyuki Takahashi ^{a,1}, Taichi Kato ^{a,*,1}

^a Department of Pediatrics, Nagoya University Graduate School of Medicine, 65 Tsurumai-cho, Showa-ku, Nagoya, Japan

^b Center for Advanced Medicine and Clinical Research, Nagoya University Hospital, 65 Tsurumai-cho, Showa-ku, Nagoya, Japan

^c Division of Molecular Genetics, Institute for Comprehensive Medical Science, Fujita Health University, 1-98 Dengakugakubo, Kutsukake-cho, Toyoake, Japan

ARTICLE INFO

Article history:

Received 10 April 2018

Received in revised form 1 September 2018

Accepted 7 September 2018

Available online 13 September 2018

Keywords:

Supravalvular aortic stenosis

Elastin

Congenital heart defects

Whole exome sequencing

ABSTRACT

Background: Supravalvular aortic stenosis (SVAS) is a congenital heart disease affecting approximately 1:25,000 live births. SVAS may occur sporadically, be inherited in an autosomal dominant manner, or be associated with Williams-Beuren syndrome, a complex developmental disorder caused by a microdeletion of chromosome 7q11.23. *ELN* on 7q11.23, which encodes elastin, is the only known gene to be recurrently mutated in less than half of SVAS patients.

Methods: Whole-exome sequencing (WES) was performed for seven familial SVAS families to identify other causative gene mutations of SVAS.

Results: Three truncating mutations and three intragenic deletions affecting *ELN* were identified, yielding a diagnostic efficiency of 6/7 (85%). The deletions, which explained 3/7 of the present cohort, spanned 1–29 exons, which might be missed in the course of mutational analysis targeting point mutations. The presence of such deletions was validated by both WES-based copy number estimation and multiplex ligation-dependent probe amplification analyses, and their pathogenicity was reinforced by co-segregation with clinical presentations.

Conclusions: The majority of familial SVAS patients appear to carry *ELN* mutations, which strongly indicates that elastin is the most important causative gene for SVAS. The frequency of intragenic deletions highlights the need for quantitative tests to analyze *ELN* for efficient genetic diagnosis of SVAS.

© 2018 Elsevier B.V. All rights reserved.

1. Introduction

Supravalvular aortic stenosis (SVAS; MIM #185500) is a congenital heart disease affecting approximately 1:25,000 live births [1]. Congenital narrowing of the lumen of the ascending aorta or peripheral pulmonary arteries provokes increased resistance to blood flow and causes elevated ventricular pressure and hypertrophy resulting in heart failure. Peripheral pulmonary stenosis (PPS) is known to occasionally coexist with SVAS [2]. Approximately 30% to 50% of patients with SVAS have Williams-Beuren Syndrome (WBS; MIM #194050) [2–4], which is a complex genetic disorder caused by 7q11.23 microdeletion and

characterized by growth failure, a characteristic facial appearance (so-called “Elfin face”), mental retardation, and SVAS [5].

On the other hand, Eisenberg et al. first reported non-syndromic “familial SVAS” with autosomal dominant inheritance in 1964 [3], accounting for 20% of SVAS cases (approximately 1:125,000 live births) [6]. These patients showed normal intelligence and lacked the dysmorphic features of WBS. Genetic analysis including linkage analysis identified *ELN*, which encodes elastin, as a causative gene of non-syndromic familial SVAS [1,7–17]. In harmony with the genetic findings, luminal obstruction of the aorta was shown in a transgenic mouse model carrying homozygous or heterozygous elastin gene deletion [18,19].

Metcalfe et al. sequenced *ELN* exons of patients with non-syndromic SVAS, which showed truncating mutations in 35 cases, but no causative variants were found in the remaining 64 patients (of which 8 were familial cases) [20]. Micale et al. also investigated *ELN* gene mutations in 14 familial and 10 sporadic cases of SVAS, resulting in 7 novel mutations, including 5 frameshift and 2 donor splice site mutations, but found no *ELN* gene abnormality in the remaining 17 cases [21]. Therefore, less than half of the cases could be explained by *ELN* mutations, whereas it still remains unclear whether *ELN* could explain the remaining cases

* Corresponding author.

E-mail addresses: javauma@gmail.com (S. Hayano), yusukeokuno@gmail.com (Y. Okuno), makiko@fujita-hu.ac.jp (M. Tsutsumi), hinagaki@fujita-hu.ac.jp (H. Inagaki), love.rodin.love@gmail.com (Y. Fukasawa), kura@fujita-hu.ac.jp (H. Kurahashi), kojimas@med.nagoya-u.ac.jp (S. Kojima), ytakaha@med.nagoya-u.ac.jp (Y. Takahashi), ktachi@med.nagoya-u.ac.jp (T. Kato).

¹ This author takes responsibility for all aspects of the reliability and freedom from bias of the data presented and their discussed interpretation.

Abbreviations

SVAS	supravalvular aortic stenosis
WES	whole-exome sequencing
PPS	peripheral pulmonary stenosis
WBS	Williams-Beuren syndrome
FISH	fluorescence in situ hybridization
MLPA	Multiplex ligation-dependent probe amplification

with SVAS, or there are unidentified causative genes. In this study, whole-exome sequencing (WES) was performed with careful assessment of *ELN* mutations, including copy number analysis, to elucidate the genetic background of SVAS.

2. Methods

2.1. Sample collection

This study included seven families of Japanese ancestry with autosomal dominant inheritance of SVAS. There was no developmental delay or dysmorphic features suggestive of WBS or positive fluorescence in situ hybridization (FISH) on 7q11.23 in any family members. The vascular malformation (SVAS and PPS) was diagnosed if the sinotubular junction of the aorta was smaller than the diameter of the aortic annulus and significant pressure gradients were measurable by echocardiogram and/or angiographically [6]. Written, informed consent was obtained from patients or their parents, and whole blood or saliva was collected. Saliva samples were collected using an Oragene DNA self-collection kit (DNA Genotek, Ottawa, Canada). Genomic DNA was extracted from

whole blood or saliva using the QIAamp DNA Blood Mini kit (Qiagen, Hilden, Germany), according to the manufacturer's instructions. The study was approved by the Ethics Committee of the Nagoya University Graduate School of Medicine (approval number 2015-0032).

2.2. Whole-exome sequencing analysis

Exome capture was performed on each proband using SureSelect Human All Exon V5 (Agilent Technologies, Santa Clara, CA), according to the manufacturer's instructions. Generated libraries were sequenced on a HiSeq 2500 platform (Illumina, San Diego, CA). Sequence data were analyzed using an in-house pipeline [22]. Briefly, reads were aligned to UCSC build hg19 reference genome using the Burrows-Wheeler Aligner [23]. Picard tools (<http://broadinstitute.github.io/picard>) were utilized to remove PCR duplicates. Variants were called using VarScan2, where a variant allele frequency of >0.20 was used as a cutoff [24]. ANNOVAR was used together with in-house scripts to annotate genetic variants [25]. The average depth of coverage across the whole exome for each sample achieved was 111.14 (range 90.68 to 127.66), and the number of mutations found per sample ranged from 25,534 to 25,920.

2.3. Mutational analysis

Mutational analysis to define each variant's pathogenicity was essentially based on the latest release of the American College of Medical Genetics (ACMG) guideline [26]. Briefly, variants outside of coding regions and common variants with >1% minor allele frequency in the National Heart, Lung, and Blood Institute ESP (Exome Sequencing Project) 6500 [27], 1000 Genomes Project [28], ExAC (Exome Aggregation Consortium) [29], HGVD (Human Genetic Variation Database) [30], or the in-house database were excluded. Variants expected to cause the disorders (eg, missense variants with reported pathogenicity and nonsense, frameshift insertion/deletion, and splice-site variants on genes known to cause a disease by inactivation) were validated by Sanger sequencing using PrimeSTAR GXL DNA polymerase (Takara, Shiga, Japan) and the Big Dye Terminator 3.1 Cycle Sequencing Kit (Thermo Fisher Scientific Inc., Waltham, MA) with ABI PRISM 3130xL (Applied Biosystems, Foster City, CA). Primer sequences are listed in Table S1.

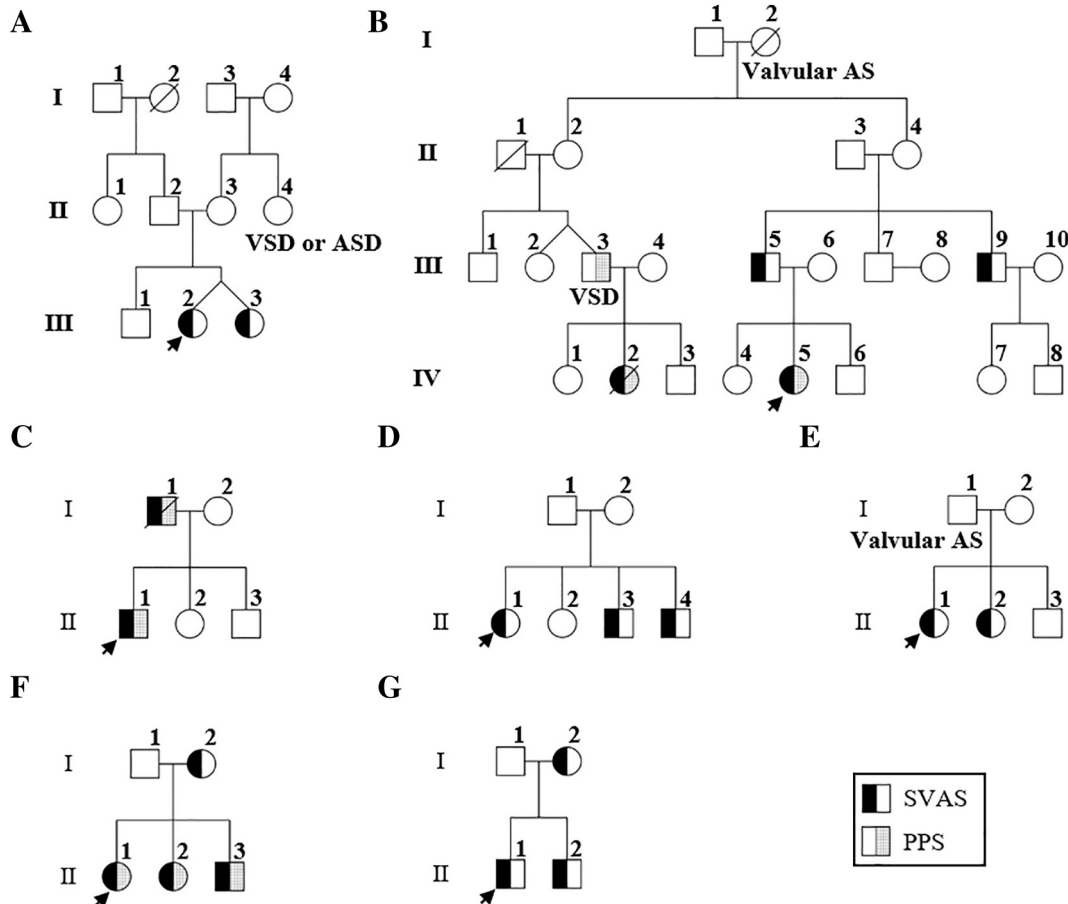


Fig. 1. Pedigree chart of families with familial supravalvular aortic stenosis. Arrows indicate probands for whom whole-exome sequencing was performed. SVAS, supravalvular aortic stenosis; PPS, peripheral pulmonary stenosis; VSD, ventricular septal defect; ASD, atrial septal defect; AS, aortic stenosis.

2.4. Copy number analysis

Copy number analysis was performed by comparing the number of reads conveying each exon normalized by the mean depth of the entire sample with that of unrelated normal DNA samples, as we have previously shown [22]. Exons of normalized coverage >3 standard deviations (SDs) or less than -3 SDs from the mean coverage of reference samples were considered to be candidates for copy number variants. Multiplex ligation-dependent probe amplification (MLPA) according to the manufacturer's protocol with the SALSA MLPA P029-WBS probemix (MRC Holland, Amsterdam, Netherlands), which includes 10 exons of the *ELN* gene (Exon 1, 3, 4, 6, 9, 16, 20, 26, 27 and 33), was performed to validate candidate exonic deletions detected in the *ELN* gene by WES analysis. MLPA analysis software Coffalyser (MRC Holland) was used to identify CNVs.

3. Results

WES-based detection of point mutations and copy number alterations was performed in seven families of Japanese ancestry with SVAS showing an autosomal dominant mode of inheritance (Fig. 1). Three heterozygous pathogenic mutations in *ELN* (c.370delT, p.Ser124Leufs*13 in family A, c.572-1G > A splice site mutation affecting the acceptor of exon 12 in family B, and c.218_219insTG, p.Gly74Valfs*49 in family C) were identified. All of these mutations were novel, and they were validated on all available family members by Sanger sequencing (Fig. S1). Mutations were present

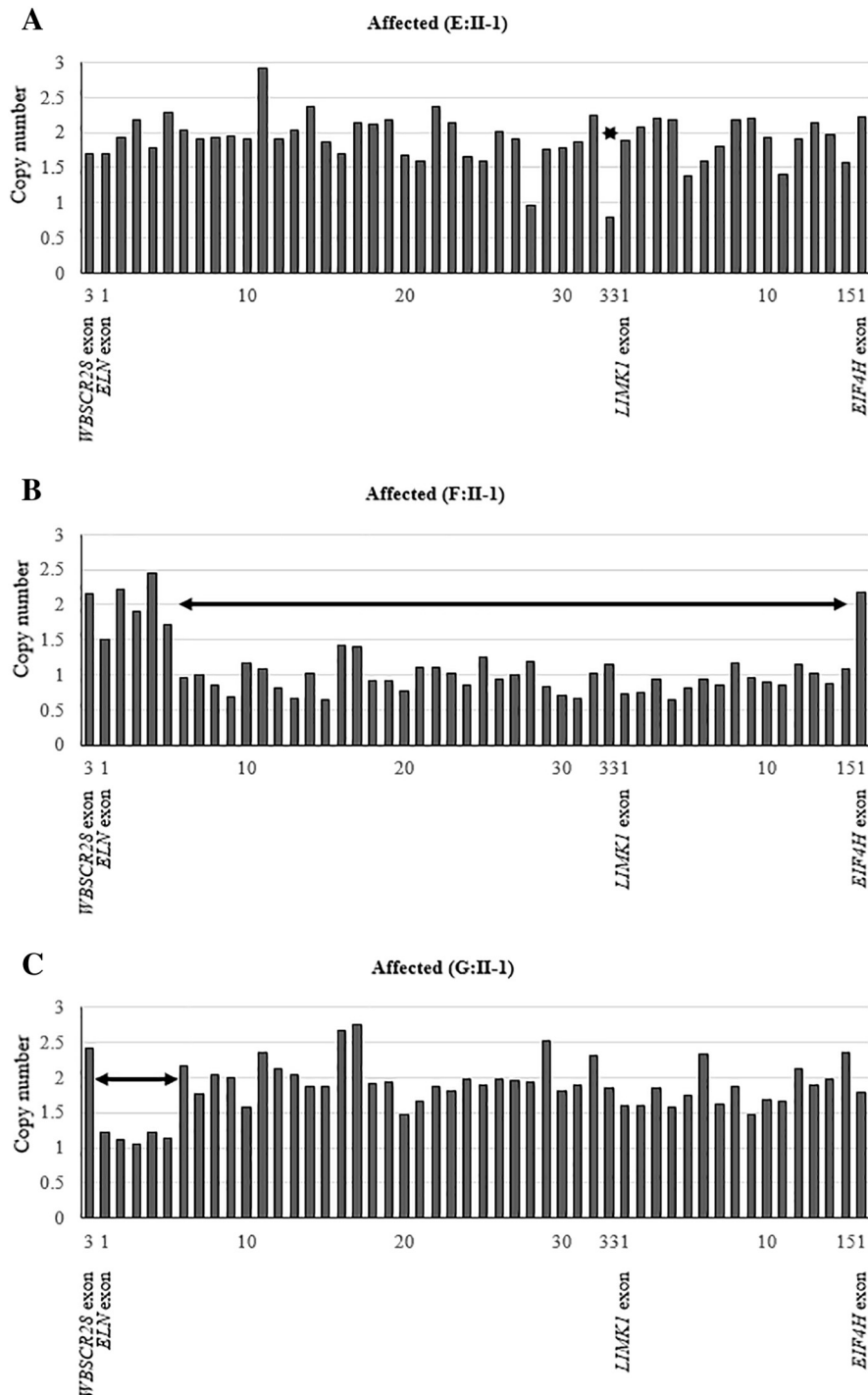


Fig. 2. Copy-number analysis The estimated copy number of each exon based on the number of reads in each exon in whole-exome sequencing. Each bar represents an exon, and the vertical axis represents the estimated copy number. Arrows indicate estimated deleted regions.

Table 1
Phenotype and segregation of *ELN* mutations.

Family	Subject	Phenotype	<i>ELN</i> mutation
A	II-2	–	–
	II-3	–	c.370delT, p.Ser124Leufs*13
	III-1	–	–
	III-2	SVAS	c.370delT, p.Ser124Leufs*13
B	III-3	SVAS	c.370delT, p.Ser124Leufs*13
	III-3	PPS, VSD	c.572-1G > A splice site
	III-5	SVAS	c.572-1G > A splice site
	III-6	–	–
	IV-4	–	–
	IV-5	SVAS, PPS	c.572-1G > A splice site
C	IV-6	–	–
	I-2	–	–
	II-1	SVAS, PPS	c.218_219insTG, p.Gly74Valfs*49
D	II-2	–	–
	II-3	–	c.218_219insTG, p.Gly74Valfs*49
E	II-1	SVAS	–
	I-1	Valvular AS	Microdeletion (exon 33)
	I-2	–	–
F	II-1	SVAS	Microdeletion (exon 33)
	II-2	SVAS	Microdeletion (exon 33)
	II-3	–	–
	I-1	–	–
G	I-2	SVAS	Microdeletion (exon 5–33)
	II-1	SVAS, PPS	Microdeletion (exon 5–33)
	II-2	SVAS, PPS	Microdeletion (exon 5–33)
	II-3	SVAS, PPS	Microdeletion (exon 5–33)
	II-2	SVAS	Microdeletion (exon 1–5)

All mutations were heterozygous. SVAS, supravalvular aortic stenosis; PPS, peripheral pulmonary stenosis; VSD, ventricular septal defect; AS, aortic stenosis.

in all patients and several family members without SVAS, indicating incomplete penetrance (Table 1).

Copy number aberrations in *ELN* were identified in three other families, all of which were deletions (exon 33 in family E, exons 5–33 in family F, and exons 1–5 in family G, Fig. 2). Such deletions were validated by MLPA (Fig. S2). All microdeletions showed complete cosegregation with clinical symptoms (Table 1).

In the remaining family D, no diagnostic mutations associated with SVAS could be identified in the proband (D:II-1) either by WES or MLPA (Table S2, Fig. S3).

4. Discussion

Pathogenic mutations or deletions in *ELN* gene were identified in six of seven families with autosomal dominant inheritance of SVAS, including three novel point mutations and three intragenic deletions. These findings suggest that intragenic deletions in *ELN* gene could explain the genetic cause in half of so-far unexplained cases with familial SVAS in Japan. Updated by these findings, a comprehensive list of reported pathogenic SVAS mutations is provided (Fig. 3) [7–9,12,17,20,21,31–38].

ELN encodes elastin, which is expressed in various tissues and organs, including smooth muscle cells of the great arteries, and contributes to tissue elasticity [39,40]. The molecular mechanism of the pathogenesis of SVAS is not fully elucidated. However, considering accumulating knowledge from patients and transgenic mice [18,19,21,41], it seems likely that mutations of *ELN* impair vascular elasticity, and increased shear stress in the vascular wall could result in SVAS [39,40].

The microdeletions of *ELN* gene shown in the present study were not identified with existing FISH probes for WBS. There are a few case reports showing that microdeletions of *ELN* gene are the cause of SVAS [8,9]. The present finding raises the necessity to investigate the

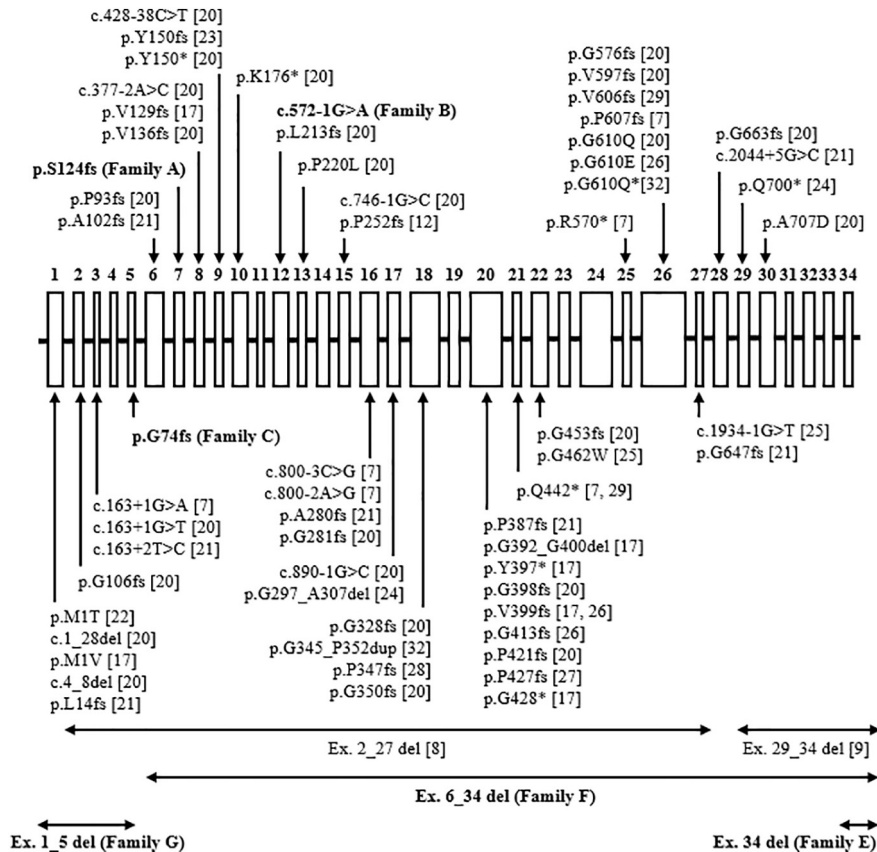


Fig. 3. *ELN* cDNA showing the exons and mutations detected. This figure summarizes previously reported and newly identified mutations for familial and sporadic SVAS. The numbers above open boxes indicate the exon numbers. The present findings are shown in bold letters.

exon-spanning deletions affecting *ELN* using MLPA, array-CGH, or other methods to establish sufficient coverage for its mutations.

The present analysis showed co-segregation of symptoms and *ELN* mutations in the majority of analyzed individuals. The three mutations identified in this study (c.370delT in family A, c.572-1G > A splice site in family B, and c.218_219insTG in family C) were highly pathogenic truncating mutations that result in premature stop codons (PTCs). A number of PTC mutations have actually been shown to be substrates of *ELN* mRNA insufficiency through nonsense-mediated decay in previous studies [17,21,35].

A highly variable phenotype within families with SVAS has been reported for large studies with many families with point mutations [20,21], and even for a family with apparently damaging 30 kb deletion involving multiple exons [7], ranging from asymptomatic mutation carrier to severe stenosis with multiple arteries. There were also two asymptomatic persons carrying *ELN* mutations (A:II-3 and C:II-3) in the present study. Factors affecting the variability of cardiovascular phenotypes in patients with *ELN* mutation are not yet fully understood, and there has as yet been no clear genotype-phenotype correlation reported for SVAS. Our comprehensive list of reported pathogenic SVAS mutations and deletions showed a universal distribution of variants over the entire *ELN* gene with no significant hotspot.

The primary mechanism for the pathogenesis of SVAS is proposed to be haploinsufficiency of *ELN*, as hemizyosity of *ELN* is established as the mechanism of SVAS in WBS [5]. Incomplete penetrance and a broad range in severity of cardiovascular phenotype are also seen in patients with WBS in whom one copy of *ELN* gene is totally lost [42,43]. Among possible causes affecting the severity of symptoms, the effect of the mutations in the remaining allele of *ELN* is very limited, as only two rare missense changes were identified through exon sequencing of 49 patients with WBS [44]. Currently, there is no definite explanation for the phenotypic variability associated with *ELN* mutations.

The present study showed that microdeletions of *ELN* gene could account for additional cases, around a half of previously unexplained cases, of familial SVAS, which would strengthen the causative role of *ELN* mutations in this disease entity. Therefore, quantitative genetic tests such as MLPA or array-CGH of *ELN* gene should be performed to genetically diagnose patients with familial SVAS to obtain satisfactory sensitivity. Further investigations of a larger cohort and so-far unexplained cases will be needed to elucidate the remaining molecular pathogenetic mechanisms of SVAS.

Supplementary data to this article can be found online at <https://doi.org/10.1016/j.ijcard.2018.09.032>.

Authors' contributions

All authors developed the concept and designed the research; S.H., Y.O., and M.T. performed the experiments; S.H., Y.O., M.T., H.I., H.K., and T.K. analyzed the data; all authors interpreted the results of the experiments; S.H., Y.O., and T.K. prepared the figures; S.H., Y.O., M.T., H.I., Y.F., H.K., S.K., Y.T., and T.K. drafted the manuscript; S.H., Y.O., and T.K. edited the manuscript; all authors approved the final version of the manuscript.

Source of funding

This work was supported by funding from the Morinaga Foundation for Health and Nutrition to Dr. Taichi Kato. The funders had no role in study design, data collection and analysis, decision to publish, or preparation of the manuscript.

Competing interests

The authors report no relationships that could be construed as a conflict of interest.

Acknowledgements

The authors would like to thank all of the clinicians and families who made this study possible with the provision of samples. The authors would also like to thank Dr. Shinsuke Kataoka (Department of Pediatrics, Nagoya University Graduate School of Medicine, Nagoya, Japan) for valuable assistance. The authors would also like to express their great appreciation to Drs. Sayaka Mii, Daichi Fukumi, Tameo Hatano (Department of Pediatrics, Japanese Red Cross Nagoya Daiichi Hospital, Nagoya, Japan), Takahiro Okumura (Department of Cardiology, Nagoya University Graduate School of Medicine), Kentaro Omoya, Takashi Kuwahara (Department of Pediatric Cardiology, Gifu Prefectural General Medical Center, Gifu, Japan), Naoki Ohashi, Hiroshi Nishikawa, Masaki Matsushima (Department of Pediatric Cardiology, Chukyo Hospital, Nagoya, Japan), Takaya Ota, Kenji Kuraishi, Nobuo Tsuchi (Department of Pediatric Cardiology and Neonatology, Ogaki Municipal Hospital, Ogaki, Japan), and Noriko Nagai (Department of Pediatrics, Okazaki City Hospital, Okazaki, Japan) for their assistance with the collection of our samples and data. The authors would like to thank the Division for Medical Research Engineering, Nagoya University Graduate School of Medicine for technical support in next-generation sequencing. The authors also acknowledge the assistance of the Human Genome Center, Institute of Medical Science, University of Tokyo (<http://sc.hgc.jp/shirokane.html>), for providing supercomputing resources.


References

- [1] A.K. Ewart, C.A. Morris, G.J. Ensing, J. Loker, C. Moore, M. Leppert, et al., A human vascular disorder, supravalvular aortic stenosis, maps to chromosome 7, *Proc. Natl. Acad. Sci. U. S. A.* 90 (1993) 3226–3230.
- [2] A.J. Beuren, C. Schulze, P. Eberle, D. Harmjan, J. Apitz, The syndrome of supravalvular aortic stenosis, peripheral pulmonary stenosis, mental retardation and similar facial appearance, *Am. J. Cardiol.* 13 (1964) 471–483.
- [3] R. Eisenberg, D. Young, B. Jacobson, A. Boito, Familial supravalvular aortic stenosis, *Am. J. Dis. Child.* 108 (1964) 341–347.
- [4] J.C. Williams, B.G. Barratt-Boyes, J.B. Lowe, Supravalvular aortic stenosis, *Circulation* 24 (1961) 1311–1318.
- [5] B.R. Pober, Williams–Beuren syndrome, *N. Engl. J. Med.* 362 (2010) 239–252.
- [6] J.M.Z.J. Frieland-Little, R.J. Gajarski, Aortic stenosis, in: H.D.S.R. Allen, D.J. Penny, T.F. Feltes, F. Cetta (Eds.), *Moss & Adams Heart Disease in Infants, Children, and Adolescents: Including the Fetus and Young Adult*, 9th ed. Wolters Kluwer, Philadelphia 2016, pp. 1085–1105.
- [7] D.Y. Li, A.E. Toland, B.B. Boak, D.L. Atkinson, G.J. Ensing, C.A. Morris, et al., Elastin point mutations cause an obstructive vascular disease, supravalvular aortic stenosis, *Hum. Mol. Genet.* 6 (1997) 1021–1028.
- [8] T.M. Olson, V.V. Michels, Z. Urban, K. Csiszar, A.M. Christiano, D.J. Driscoll, et al., A 30 kb deletion within the elastin gene results in familial supravalvular aortic stenosis, *Hum. Mol. Genet.* 4 (1995) 1677–1679.
- [9] A.K. Ewart, W. Jin, D. Atkinson, C.A. Morris, M.T. Keating, Supravalvular aortic stenosis associated with a deletion disrupting the elastin gene, *J. Clin. Invest.* 93 (1994) 1071–1077.
- [10] M.E. Curran, D.L. Atkinson, A.K. Ewart, C.A. Morris, M.F. Leppert, M.T. Keating, The elastin gene is disrupted by a translocation associated with supravalvular aortic stenosis, *Cell* 73 (1993) 159–168.
- [11] A.M. Jelsig, Z. Urban, V. Huchtagowder, H. Nissen, L.B. Ousager, Novel *ELN* mutation in a family with supravalvular aortic stenosis and intracranial aneurysm, *Eur. J. Med. Genet.* 60 (2017) 110–113.
- [12] A. Jakob, S. Unger, R. Arnold, J. Grohmann, C. Kraus, C. Schlensak, et al., A family with a new elastin gene mutation: broad clinical spectrum, including sudden cardiac death, *Cardiol. Young* 21 (2011) 62–65.
- [13] J. Katumba-Lunyanya, Two generations of identical twins with *ELN* deletion, *BMJ Case Rep.* 2009 (2009) (bcr06.2008.0036).
- [14] M. Martin, S. Secades, A.M. Plasencia, M.L. Rodriguez, C. Corros, A. Garcia-Campos, et al., Supravalvular aortic stenosis as a non-syndromic familial disease. Relevance of familial screening, *Int. J. Cardiol.* 172 (2014) 511–512.
- [15] G.M. Blue, E.P. Kirk, E. Giannoulatos, S.L. Dunwoodie, J.W. Ho, D.C. Hilton, et al., Targeted next-generation sequencing identifies pathogenic variants in familial congenital heart disease, *J. Am. Coll. Cardiol.* 64 (2014) 2498–2506.
- [16] T.M. Olson, V.V. Michels, N.M. Lindor, G.M. Pastores, J.L. Weber, D.J. Schaid, et al., Autosomal dominant supravalvular aortic stenosis: localization to chromosome 7, *Hum. Mol. Genet.* 2 (1993) 869–873.
- [17] Z. Urbán, V.V. Michels, S.N. Thibodeau, E.C. Davis, J.-P. Bonnefont, A. Munnich, et al., Isolated supravalvular aortic stenosis: functional haploinsufficiency of the elastin gene as a result of nonsense-mediated decay, *Hum. Genet.* 106 (2000) 577–588.
- [18] D.Y. Li, G. Faurly, D.G. Taylor, E.C. Davis, W.A. Boyle, R.P. Mecham, et al., Novel arterial pathology in mice and humans hemizygous for elastin, *J. Clin. Invest.* 102 (1998) 1783–1787.
- [19] D.Y. Li, B. Brooke, E.C. Davis, R.P. Mecham, L.K. Sorensen, B.B. Boak, et al., Elastin is an essential determinant of arterial morphogenesis, *Nature* 393 (1998) 276–280.

- [20] K. Metcalfe, A.K. Rucka, L. Smoot, G. Hofstadler, G. Tuzler, P. McKeown, et al., Elastin: mutational spectrum in supravalvular aortic stenosis, *Eur. J. Hum. Genet.* 8 (2000) 955–963.
- [21] L. Micale, M.G. Turturo, C. Fusco, B. Augello, L.A. Jurado, C. Izzi, et al., Identification and characterization of seven novel mutations of elastin gene in a cohort of patients affected by supravalvular aortic stenosis, *Eur. J. Hum. Genet.* 18 (2010) 317–323.
- [22] H. Muramatsu, Y. Okuno, K. Yoshida, Y. Shiraishi, S. Doisaki, A. Narita, et al., Clinical utility of next-generation sequencing for inherited bone marrow failure syndromes, *Genet. Med.* 19 (2017) 796–802.
- [23] H. Li, R. Durbin, Fast and accurate short read alignment with burrows-wheeler transform, *Bioinformatics* 25 (2009) 1754–1760.
- [24] D.C. Koboldt, Q. Zhang, D.E. Larson, D. Shen, M.D. McLellan, L. Lin, et al., VarScan 2: somatic mutation and copy number alteration discovery in cancer by exome sequencing, *Genome Res.* 22 (2012) 568–576.
- [25] K. Wang, M. Li, H. Hakonarson, ANNOVAR: functional annotation of genetic variants from high-throughput sequencing data, *Nucleic Acids Res.* 38 (2010) e164.
- [26] S. Richards, N. Aziz, S. Bale, D. Bick, S. Das, J. Gastier-Foster, et al., Standards and guidelines for the interpretation of sequence variants: a joint consensus recommendation of the American College of Medical Genetics and Genomics and the Association for Molecular Pathology, *Genet. Med.* 17 (2015) 405–424.
- [27] Exome Variant Server, NHLBI GO Exome Sequencing Project (ESP). Seattle, WA, <http://evs.gs.washington.edu/EVS/>, Accessed date: 22 August 2017.
- [28] C. Genomes Project, A. Auton, L.D. Brooks, R.M. Durbin, E.P. Garrison, H.M. Kang, et al., A global reference for human genetic variation, *Nature* 526 (2015) 68–74.
- [29] M. Lek, K. Karczewski, E. Minikel, K. Samocha, E. Banks, T. Fennell, et al., Analysis of protein-coding genetic variation in 60,706 humans, *bioRxiv*, 2015.
- [30] K. Higasa, N. Miyake, J. Yoshimura, K. Okamura, T. Niihori, H. Saitsu, et al., Human genetic variation database, a reference database of genetic variations in the Japanese population, *J. Hum. Genet.* 61 (2016) 547–553.
- [31] J.J. Louw, G. Verleden, M. Gewillig, K. Devriendt, Haploinsufficiency of elastin gene may lead to familial cardiopathy and pulmonary emphysema, *Am. J. Med. Genet. A* 158a (2012) 2053–2054.
- [32] X. Ge, Y. Ren, O. Bartulos, M.Y. Lee, Z. Yue, K.Y. Kim, et al., Modeling supravalvular aortic stenosis syndrome with human induced pluripotent stem cells, *Circulation* 126 (2012) 1695–1704.
- [33] S. Park, E.J. Seo, H.W. Yoo, Y. Kim, Novel mutations in the human elastin gene (ELN) causing isolated supravalvular aortic stenosis, *Int. J. Mol. Med.* 18 (2006) 329–332.
- [34] L. Rodriguez-Revena, C. Badenas, A. Carrio, M. Mila, Elastin mutation screening in a group of patients affected by vascular abnormalities, *Pediatr. Cardiol.* 26 (2005) 827–831.
- [35] Z. Urban, S. Riazi, T.L. Seidl, J. Katahira, L.B. Smoot, D. Chitayat, et al., Connection between elastin haploinsufficiency and increased cell proliferation in patients with supravalvular aortic stenosis and Williams-Beuren syndrome, *Am. J. Hum. Genet.* 71 (2002) 30–44.
- [36] J. Dedic, A.S. Weiss, J. Katahira, B. Yu, R.J. Trent, Z. Urban, A novel elastin gene mutation (1281delC) in a family with supravalvular aortic stenosis: a mutation cluster within exon 20, *Hum. Mutat.* 17 (2001) 81.
- [37] T. Boeckel, A. Dierks, A. Vergopoulos, S. Bähring, H. Knoblauch, B. Müller-Myhsok, et al., A new mutation in the elastin gene causing supravalvular aortic stenosis, *Am. J. Cardiol.* 83 (1999) 1141–1143 (a9–10).
- [38] M. Tassabehji, K. Metcalfe, D. Donnai, J. Hurst, W. Reardon, M. Burch, et al., Elastin: genomic structure and point mutations in patients with supravalvular aortic stenosis, *Hum. Mol. Genet.* 6 (1997) 1029–1036.
- [39] C. Stamm, I. Friehs, S.Y. Ho, A.M. Moran, R.A. Jonas, P.J. del Nido, Congenital supravalvular aortic stenosis: a simple lesion? *Eur. J. Cardiothorac. Surg.* 19 (2001) 195–202.
- [40] G. Merla, N. Brunetti-Pierri, P. Piccolo, L. Micale, M.N. Loviglio, Supravalvular aortic stenosis: elastin arteriopathy, *Circ. Cardiovasc. Genet.* 5 (2012) 692–696.
- [41] Z. Urban, J. Zhang, E.C. Davis, G.K. Maeda, A. Kumar, H. Stalker, et al., Supravalvular aortic stenosis: genetic and molecular dissection of a complex mutation in the elastin gene, *Hum. Genet.* 109 (2001) 512–520.
- [42] L. Li, L. Huang, Y. Luo, X. Huang, S. Lin, Q. Fang, Differing microdeletion sizes and breakpoints in chromosome 7q11.23 in Williams-Beuren syndrome detected by chromosomal microarray analysis, *Mol. Syndromol.* 6 (2016) 268–275.
- [43] A. Wessel, R. Pankau, D. Kececioglu, W. Ruschewski, J.H. Bursch, Three decades of follow-up of aortic and pulmonary vascular lesions in the Williams-Beuren syndrome, *Am. J. Med. Genet.* 52 (1994) 297–301.
- [44] M. Delio, K. Pope, T. Wang, J. Samanich, C.R. Haldeman-Englert, P. Kaplan, et al., Spectrum of elastin sequence variants and cardiovascular phenotypes in 49 patients with Williams-Beuren syndrome, *Am. J. Med. Genet. A* 161A (2013) 527–533.

Case Report

Exome-First Approach in Fetal Akinesia Reveals Chromosome 1p36 Deletion Syndrome

Masatake Toshimitsu ¹, Shinichi Nagaoka,¹ Shuusaku Kobori ¹, Maki Ogawa,¹
Fumihiko Suzuki,² Takema Kato,² Shunsuke Miyai,² Rie Kawamura,² Hidehito Inagaki,²
Hiroki Kurahashi,² and Jun Murotsuki ¹

¹Department of Maternal and Fetal Medicine, Miyagi Children's Hospital, Miyagi, Japan

²Division of Molecular Genetics, Institute for Comprehensive Medical Science, Fujita Health University, Toyoake, Japan

Correspondence should be addressed to Masatake Toshimitsu; toshitake1116@gmail.com

Received 13 February 2019; Revised 6 May 2019; Accepted 31 July 2019; Published 2 October 2019

Academic Editor: Irene Hoesli

Copyright © 2019 Masatake Toshimitsu et al. This is an open access article distributed under the Creative Commons Attribution License, which permits unrestricted use, distribution, and reproduction in any medium, provided the original work is properly cited.

Background. Fetal akinesia refers to a broad spectrum of disorders with reduced or absent fetal movements. There is no established approach for prenatal diagnosis of the cause of fetal akinesia. Chromosome 1p36 deletion syndrome is the most common subtelomeric terminal deletion syndrome, recognized postnatally from typical craniofacial features. However, the influence of chromosome 1p36 deletion on fetal movements remains unknown. **Case Report.** A 32-week-old fetus with akinesia showed multiple abnormalities, including fetal growth restriction, congenital cardiac defects, and ventriculomegaly. G-banding analysis using cultured amniocytes revealed 46,XY,22pstk+. Postnatal whole exome sequencing and subsequent chromosomal microarray identified a 3 Mb deletion of chromosomal region 1p36.33–p36.32. These results of molecular cytogenetic analyses were consistent with the fetal sonographic findings. **Conclusion.** Using the exome-first approach, we identified a case with fetal akinesia associated with chromosome 1p36 deletion. Chromosome 1p36 deletion syndrome may be considered for differential diagnosis in cases of fetal akinesia with multiple abnormalities.

1. Introduction

Fetal akinesia is a condition characterized by reduced or absent fetal movements independent of the etiologies [1–3]. A definitive diagnosis of the cause could be helpful for perinatal management, perinatal decision-making within local limits, and genetic counseling for future pregnancies [1]. Although next-generation sequencing (NGS) technologies have identified some underlying genetic mutations associated with fetal akinesia, some cases remain genetically unsolved [2, 3].

Chromosome 1p36 deletion syndrome (MIM# 607872) is the most common subtelomeric terminal deletion syndrome with a prevalence of 1 : 5000 newborns [4]. The typical clinical features of this syndrome include generalized hypotonia, severe developmental delay, seizure, growth restriction, microcephaly, congenital heart defects, flat nasal bridge, and midface hypoplasia [4]. It is classically diagnosed postnatally from

typical craniofacial features, although prenatal characteristic findings have been described [4, 5]. The recurrence risk depends on the mechanism of the deletion, such as *de novo* deletion or inheritance from one of the parents with balanced translocations [6].

Here, we present a case with fetal akinesia associated with chromosome 1p36 deletion syndrome, which was not suspected from prenatal clinical findings before genetic testing and was diagnosed postnatally by the exome-first approach.

2. Clinical Case

A 28-year-old nulliparous pregnant Japanese woman was referred for prenatal evaluation at 30 weeks of gestation because of abnormal ultrasound findings of fetal congenital

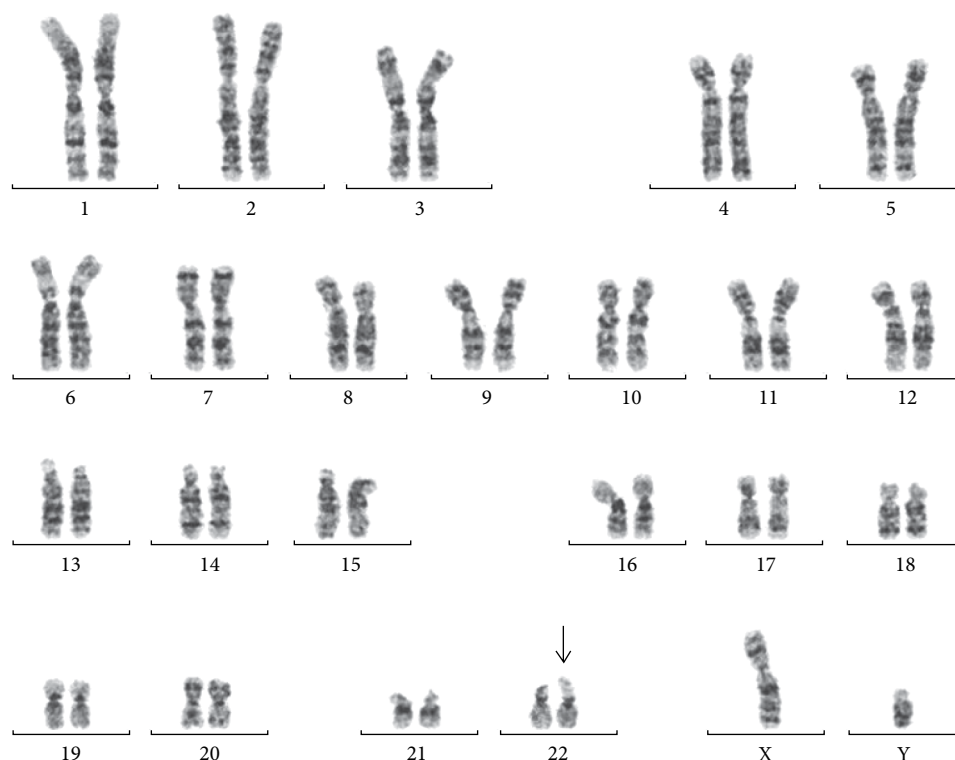
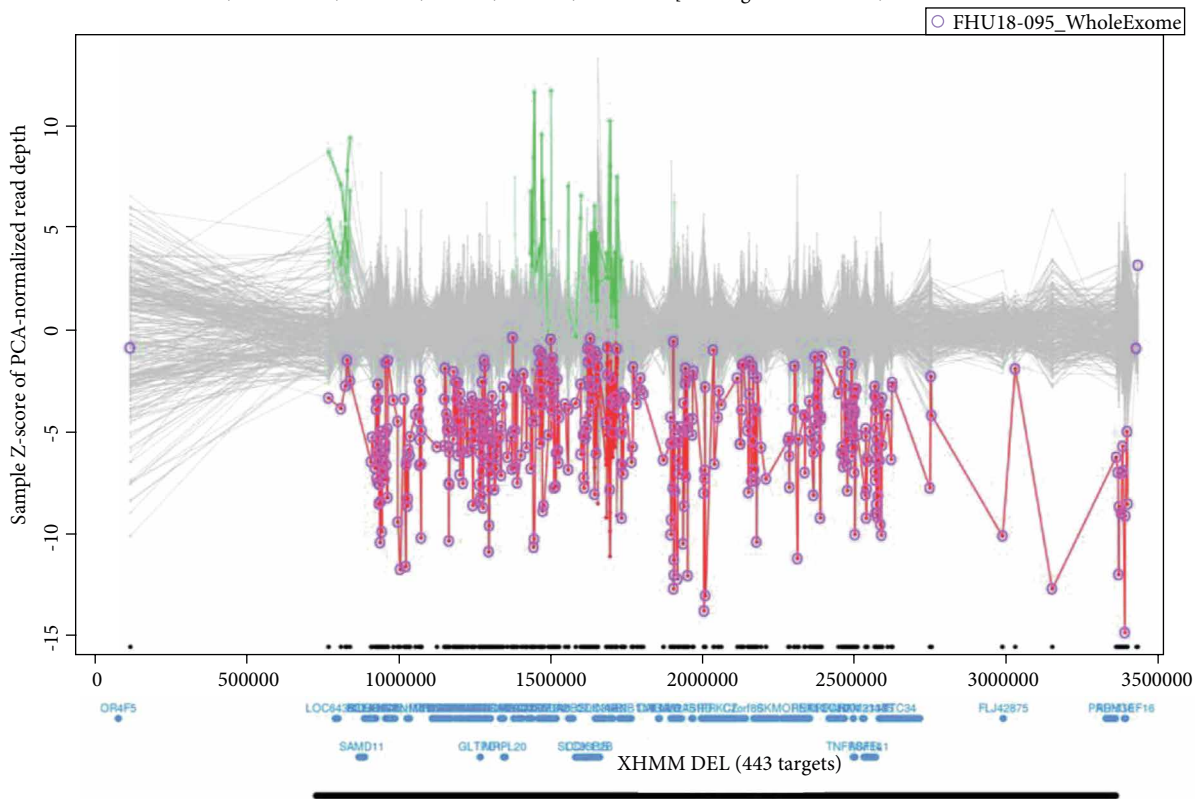


FIGURE 1: G-banding analysis of cultured amniocytes at 32 weeks and 6 days of gestation. The fetal karyotype was 46,XY,22pstk+. The arrow indicates 22pstk+.

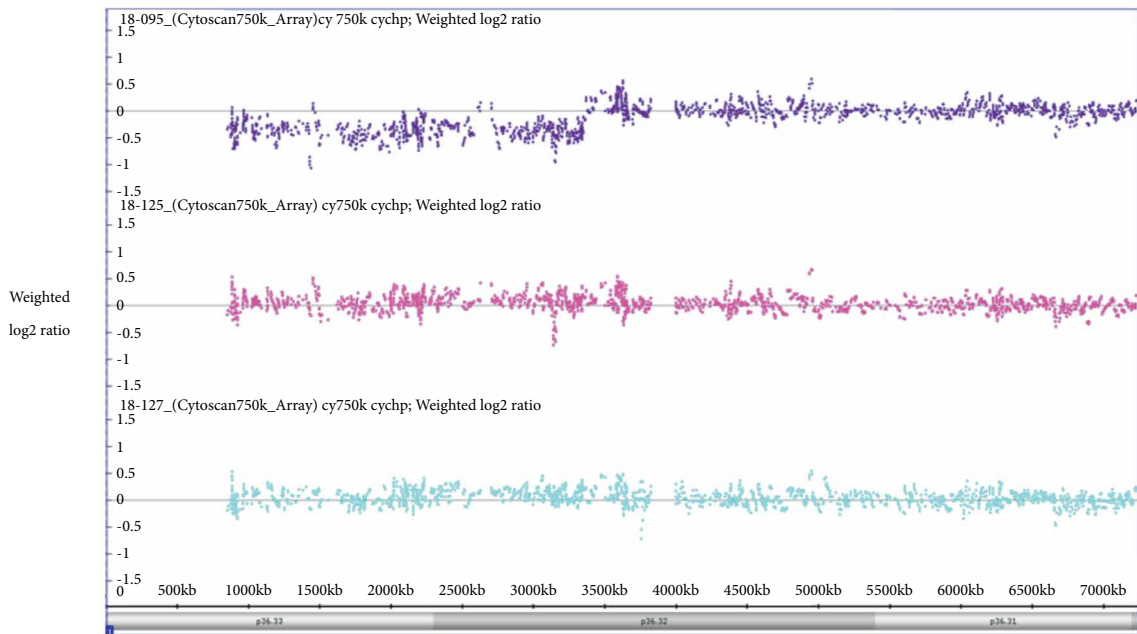
heart defects. The family history of the parents was unremarkable. Fetal ultrasonography at 30 weeks and 5 days of gestation showed vascular ring, Ebstein's anomaly, ventricular septal defect, and single umbilical artery. The estimated fetal body weight corresponded to the Japanese standard for the gestational age. Fetal ultrasonography showed vertex presentation of the moving fetus and the fetal stomach appeared to be normally dilated (Table 1). The pregnant woman had not felt any fetal movements since 31 weeks of gestation. At 32 weeks and 5 days of gestation, fetal ultrasonography showed absence of fetal movement with breech presentation, polyhydramnios, absent filling of stomach, and fetal growth restriction (FGR) (Table 1). However, abnormal Doppler findings regarding the fetal middle cerebral artery, umbilical cord artery, and ductus venosus were not observed. Clinical diagnosis of fetal akinesia was made at this point. At 32 weeks and 6 days of gestation, amniocentesis was performed to assess the possibility of chromosomal aberrations. Interphase fluorescence in situ hybridization (FISH) analysis on uncultured amniocytes for chromosome 13, 18, and 21 revealed two signals, respectively. At 34 weeks and 6 days of gestation, progression of polyhydramnios with maternal respiratory compromise occurred (Table 1) and 2300 mL of amniotic fluid was removed. G-banding analysis on cultured amniocytes revealed a karyotype of 46,XY,22pstk+ (Figure 1). After discussion with the parents about the prognosis of the fetus based on ultrasound findings, including fetal akinesia since 31 weeks of gestation, FGR, congenital heart defects, and left-sided pleural effusion that indicated severe phenotype with prenatal onset of genetic

disorders, perinatal palliative care was chosen. At 36 weeks and 3 days of gestation, fetal ultrasonography showed further progression of polyhydramnios with maternal compromise (Table 1), and 2000 mL of amniotic fluid was removed and labor was induced with oxytocin. The breech neonate was delivered vaginally at 36 weeks and 4 days of gestation with an Apgar score of 1 at 1 min and 1 at 5 min. Birth weight was 1839 g, length 45.5 cm, head circumference 31.8 cm, and chest circumference 23.5 cm. External examination revealed marked muscular hypoplasia of upper and lower extremities, extremely thin transverse palmar creases, joint contractures of lower extremities, hypertelorism, and deep-set ears. The neonate died within 2 h after birth due to respiratory failure. Therefore, we could not assess developmental profile after birth. In addition, permission for neonatal autopsy was not obtained from the parents. Clinical features of the neonate were not sufficient to diagnose a specific disease but suggested the possibility of genetic disorders, including diseases caused by either a single gene or a chromosomal defect. After genetic counseling and obtaining written consent from the parents, whole exome sequencing (WES) was performed with genomic DNA extracted from the placenta using the eXome Hidden Markov Model v1.0 (XHMM). Although the causative gene mutations related to the phenotype of the neonate were not identified, a 3 Mb deletion of chromosome 1p was suspected (Figure 2(a)). The suspected deleted region by the exome analysis using XHMM was further validated by chromosomal microarray (CMA). CMA analysis demonstrated monoallelic deletion located from positions 849466 to 3347420 on chromosome

OR4F5;LOC643837;SAMD11;NOC2L;KLHL17;PLEKHN1 [446 targets in 10⁷ bases,chr1:69382-33839591



(a)



(b)

FIGURE 2: Postnatal molecular cytogenetic analyses. (a) Whole exome sequencing analysis using the eXome Hidden Markov Model (XHMM). XHMM analysis using WES data detected the copy number loss located within 1p36.33–p36.32, suggesting a 3 Mb deletion (black bar). *x* axis shows the physical position, and *y* axis shows the Z score of the principal component analysis that was normalized to read depth. Purple circles connected by red lines represent values of the placenta to WES. Gray dots with gray connected lines indicate the results of normalized read depth. Copy number losses (red dots) without gains (green dots) on chromosome 1p36 were detected in the placenta. (b) Chromosomal microarray (CMA) analysis using Cytoscan 750k Array. CMA analysis results for the copy number log₂ ratio of chromosome 1p region for the placenta (purple), father (pink), and mother (blue). CMA analysis demonstrated a 3 Mb heterozygous deletion within 1p36.33–p36.32 in the placenta. The fetus had arr[hg]1p36.33–p36.32 (849466_3347420)x1. There were no copy number variations in the parents detected by CMA.

TABLE 1: Prenatal findings of the present case.

GA (Weeks + days)	30 + 5	32 + 5	33 + 3	34 + 6	35 + 5	36 + 3
EFBW (g) (SD)	1353 (-1.2)	1545 (-1.75)	1566 (-2.0)	1694 (-2.27)	1881 (-2.0)	1865 (-2.4)
AFI	9.7	24.4	30.47	48.0	33.2	39.8
Stomach	+	absent	absent	absent	absent	absent
Fetal movements	+	absent	absent	absent	absent	absent
Fetal presentation	Vertex	Breech	Breech	Breech	Breech	Breech
Ventriculomegaly (mm)	4.4	8.2	10	14.2	15	N/A
Others		CPCs		PE	PE	PE

GA, gestational age; EFBW, estimated fetal body weight; AFI, amniotic fluid index; CPCs, choroid plexus cysts; PE, pleural effusion; SD, standard deviation; N/A, not available.



FIGURE 3: Fluorescence in-situ hybridization (FISH) analysis of cultured amniocytes. FISH showed two 1p31.3 region specific signals (blue) and one 1p36.33 region specific signal (green), indicating 1p36 deletion. The arrow indicates 1p36.33 region specific signal. The arrowhead indicates 1p31.3 region specific signal.

1p36.33–p36.32 (Chr1:849466–3347420) including 76 genes, which is known as chromosome 1p36 deletion syndrome (Figure 2(b)). Among 76 genes, the gene *SKI*, which is known to contribute to the phenotype of chromosome 1p36 deletion syndrome, is included [4, 7]. These results were consistent with the prenatal sonographic findings and the neonate was diagnosed with chromosome 1p36 deletion syndrome. In addition, CMA analysis revealed no additional copy number variations (CNVs), which suggested *de novo* deletion rather than inheritance from the parents. After genetic counseling for future pregnancies, the parents decided against genetic carrier screening. Postnatal sub-telomeric FISH analysis on cultured amniocytes revealed a terminal deletion of chromosome 1p (Figure 3).

3. Discussion

In this report, we present a case of fetal akinesia associated with chromosome 1p36 deletion syndrome diagnosed postnatally by the exome-first approach. To our knowledge, this is

the first report describing a case with chromosome 1p36 deletion syndrome presenting with fetal akinesia.

Fetal akinesia is a condition characterized by reduced or absent fetal movement [1–3]. Prenatal sonographic findings of fetal akinesia include lack of extremity motions, persistent abnormal posture of the extremities, polyhydramnios due to decreased fetal swallowing, thorax hypoplasia due to absent fetal breathing, and fetal hydrops [1]. However, these prenatal ultrasound findings are nonspecific to identify the cause, and as yet there is no established approach for prenatal diagnosis of fetal akinesia. Fetal akinesia can result from primary defects at any point along the motor system pathway from the central nervous system to the skeletal muscle cell, which cause diseases such as spinal muscular atrophy, congenital myasthenic syndromes, and congenital muscular dystrophies [1–3]. In addition, a differential diagnosis should include a trisomy 18, metabolic dysfunction such as pyruvate dehydrogenase deficiency, maternal antibodies against acetylcholine receptor, and maternal infections such as cytomegalovirus and toxoplasmosis [1, 8]. A family history is helpful because some diseases are inherited [1–3]. Although a definitive diagnosis helps parents with perinatal decision-making, it would not be possible to do so based on sonographic findings alone. Prenatal sonography could provide sufficient information about a severity of the fetus for parents.

In the present case, while fetal movements and a normal fluid-filled stomach were seen until second trimester, these were absent during the third trimester. In addition, multiple fetal abnormalities such as congenital heart defects, FGR, ventriculomegaly, choroid plexus cysts, and single umbilical artery were found through fetal sonography. Based on these fetal sonographic findings, we performed amniocentesis to rule out trisomy 18. Although the amniocytes showed a normal karyotype, perinatal palliative care was performed based on the prenatal sonographic findings. WES was performed postnatally to assess the possibility of autosomal recessive inherited diseases, including those of neuromuscular origin. As a result, chromosome 1p36 deletion was incidentally identified by quantitative WES analysis usingXHMM.

Chromosome 1p36 deletion syndrome causes severe developmental delay, hypotonia, seizure, growth restriction, brain anomalies, and congenital heart defects [4]. Although brain anomalies, FGR, and congenital heart defects in a fetus can be detected using prenatal sonographic examination and indicate the possibility of chromosome 1p36 deletion syndrome [5, 9–11], there is significant phenotypic variation

among affected individuals [12]. This phenotypic variation is due, at least in part, to the genetic heterogeneity seen in 1p36 deletions, which include deletions of varying lengths located throughout the 30 Mb of DNA that comprise chromosome 1p36 [6, 12]. In addition, the terminal 1p36 deletion can be missed using conventional G-banding analysis because of the low level of resolution and light staining of the region [5, 11]. In this regard, CMA analysis or subtelomeric FISH may be required to identify chromosome 1p36 deletion [5, 11]. In the present case, a 3 Mb deletion of 1p36 was not seen prenatally in the cultured amniocyte karyotype (Figure 1). Given the WES and CMA findings, the cultured amniocyte karyotype was reanalyzed and the deletion was still not seen. In Japan, the use of sub-telomeric FISH or CMA analysis for prenatal screening are not considered due to legal constraints. However, given the implications for prognosis and higher rate of hypotonia and severe developmental delay, molecular prenatal diagnosis, specifically for deletion of 1p36, should be considered in the setting of a fetal akinesia.

In the present case, the 76 deleted genes included the *SKI* gene that is responsible for the 1p36 deletion phenotype and is one of the candidate genes involved in hypotonia [4, 7]. However, there are no reports of the association between fetal akinesia and 1p36 deletion within a segment from 849466 to 3347420. Four genes *AGRN*, *B3GALT6*, *ATAD3A*, and *PEX10*, which were also among the 76 genes, cause recessive syndrome with hypotonia. As no mutations were detected in the four genes in the nondeleted allele, fetal akinesia may not result from the unmasking of recessive diseases. Therefore, we did not speculate that a deletion located from positions 849466 to 3347420 on chromosome 1p36.33–p36.32 resulted in fetal akinesia, which may present a more severe phenotype with prenatal onset of chromosome 1p36 deletion syndrome. Trio whole genome sequencing is helpful to search other causes of fetal akinesia. Further molecular analyses are essential to clarify this point.

In regard to diagnostic approach for the present case, we performed exome-first approach postnatally following prenatal G-banding analysis. Although the CMA-first approach is still widely used to detect CNVs, WES is becoming available to detect CNVs, leading to an appropriate clinical diagnosis [13]. The advantage of using exome sequencing for a combined analysis of not only single nucleotide variants but also CNVs is to increase the analysis resolution and detection rate with one single test. Therefore, in postnatal testing, WES may be advantageous to screen genetic abnormalities as a first-choice diagnostic approach before performing CMA in undiagnosed syndromic individuals suspected of having either single gene defects or CNVs, such as the present case [13]. After WES analysis, CMA analysis with or without FISH is necessary to accurately determine the range of the region of genomic imbalance for accurate cytogenetic diagnosis.

In conclusion, we propose that chromosome 1p36 deletion syndrome, which may be missed using conventional G-banding karyotype with amniocytes, be considered for differential diagnosis in cases of fetal akinesia and prompt molecular cytogenetic analysis if necessary. As a practical approach to the diagnosis of the cause of fetal akinesia, a detailed anomaly scan should be performed with karyotyping

and if unremarkable, exome-first approach may be offered postnatally.

Conflicts of Interest

The authors declare that they have no conflicts of interest.

References

- [1] A. Hellmund, C. Berg, A. Geipel, A. Müller, and U. Gembruch, "Prenatal diagnosis of fetal akinesia deformation sequence (FADS): a study of 79 consecutive cases," *Archives of Gynecology and Obstetrics*, vol. 294, no. 4, pp. 697–707, 2016.
- [2] G. Ravenscroft, E. Sollis, A. K. Charles, K. N. North, G. Baynam, and N. G. Laing, "Fetal akinesia: review of the genetics of the neuromuscular causes," *Journal of Medical Genetics*, vol. 48, no. 12, pp. 793–801, 2011.
- [3] S. J. Beecroft, M. Lombard, D. Mowat et al., "Genetics of neuromuscular fetal akinesia in the genomics era," *Journal of Medical Genetics*, vol. 55, no. 8, pp. 505–514, 2018.
- [4] V. K. Jordan, H. P. Zaveri, and D. A. Scott, "1p36 deletion syndrome: an update," *The Application of Clinical Genetics*, vol. 8, pp. 189–200, 2015.
- [5] P. M. Campeau, N. Ah Mew, L. Cartier et al., "Prenatal diagnosis of monosomy 1p36: a focus on brain abnormalities and a review of the literature," *American Journal of Medical Genetics Part A*, vol. 146A, no. 23, pp. 3062–3069, 2008.
- [6] M. GajECKa, K. L. Mackay, and L. G. Shaffer, "Monosomy 1p36 deletion syndrome," *American Journal of Medical Genetics Part C: Seminars in Medical Genetics*, vol. 145C, no. 4, pp. 346–356, 2007.
- [7] N. Okamoto, Y. Toribe, T. Nakajima et al., "A girl with 1p36 deletion syndrome and congenital fiber type disproportion myopathy," *Journal of Human Genetics*, vol. 47, no. 10, pp. 556–559, 2002.
- [8] L. Winters, E. Van Hoof, L. De Catte et al., "Massive parallel sequencing identifies RAPSN and PDHA1 mutations causing fetal akinesia deformation sequence," *European Journal of Paediatric Neurology*, vol. 21, no. 5, pp. 745–753, 2017.
- [9] G. H. Seo, J. H. Kim, J. H. Cho et al., "Identification of 1p36 deletion syndrome in patients with facial dysmorphism and developmental delay," *Korean Journal of Pediatrics*, vol. 59, no. 1, pp. 16–23, 2016.
- [10] C. P. Chen, M. Chen, Y. N. Su et al., "Chromosome 1p36 deletion syndrome: prenatal diagnosis, molecular cytogenetic characterization and fetal ultrasound findings," *Taiwanese Journal of Obstetrics and Gynecology*, vol. 49, no. 4, pp. 473–480, 2010.
- [11] D. Lissauer, S. A. Larkins, S. Sharif, L. MacPherson, C. Rhodes, and M. D. Kilby, "Prenatal diagnosis and prenatal imaging features of fetal monosomy 1p36," *Prenatal Diagnosis*, vol. 27, no. 9, pp. 874–878, 2007.
- [12] C. F. Rocha, R. B. Vasques, S. R. Santos, and C. L. Paiva, "Mini-Review: Monosomy 1p36 syndrome: reviewing the correlation between deletion sizes and phenotypes," *Genetics and Molecular Research*, vol. 15, no. 1, 2016.
- [13] M. Watanabe, Y. Hayabuchi, A. Ono et al., "Detection of 1p36 deletion by clinical exome-first diagnostic approach," *Human Genome Variation*, vol. 3, no. 1, 2016.



2 The involvement of U-type dicentric chromosomes in the formation 3 of terminal deletions with or without adjacent inverted duplications

4 Takema Kato¹ · Hidehito Inagaki¹ · Syunsuke Miyai¹ · Fumihiko Suzuki¹ · Yuki Naru¹ · Yasuko Shinkai¹ ·
5 Asuka Kato¹ · Kazuo Kanyama¹ · Seiji Mizuno² · Yukako Muramatsu³ · Toshiyuki Yamamoto⁴ · Mitsuhsa Shinya^{5,6} ·
6 Yukiko Tazaki^{5,6} · Sayuri Hiwatashi^{5,6} · Toshiro Ikeda^{5,6} · Mamoru Ozaki⁷ · Hiroki Kurahashi^{1,2}

7 Received: 7 April 2020 / Accepted: 22 May 2020
8 © Springer-Verlag GmbH Germany, part of Springer Nature 2020

9 Abstract

10 An inverted duplication with a terminal deletion (inv-dup-del) is one of the complex constitutional structural rearrangements
11 that can occur in a chromosome. Although breakages of dicentric chromosome have been suggested, the precise mechanism
12 of this is yet to be fully understood. In our present study, we investigated the genomic structure of 10 inv-dup-del cases to
13 elucidate this mechanism. Two recurrent 8p inv-dup-del cases harbored a large copy-number-neutral region between the
14 duplication and deletion in common. Although the other non-recurrent cases did not appear to have this copy-number-
15 neutral region, refined sequencing analysis identified that they contained a small intervening region at the junction between
16 the inverted and non-inverted segment. The size of this small intervening region ranged from 1741 to 3728 bp. Combined
17 with a presence of microhomology at the junction, a resolution of the replication fork stalling through template switching
18 within the same replication fork is suggested. We further observed two cases with mosaicism of the dicentric chromosome
19 and various structural rearrangements related to the dicentric chromosome. Refined analysis allowed us to identify different
20 breakpoints on the same chromosome in the same case, implicating multiple rounds of U-type formation and its breakage.
21 From these results, we propose that a replication-based mechanism generates unstable dicentric chromosomes and that their
22 breakage leads to the formation of inv-dup-dels and other related derivative chromosomes.

23 Introduction

24 An inverted duplication with a concomitant terminal deletion
25 (inv-dup-del) is one of the common complex chromosomal
26 rearrangements (CCRs) that arises in humans (Weckselblatt
27 and Rudd 2015). Inv-dup-del rearrangements develop mainly
28 in two successive steps. The first of these is the formation
29 of a symmetric dicentric chromosome, which is unstable
30 during mitosis because two functional centromeres can act
31 bidirectionally. The formation of this unstable intermediate
32 leads to anaphase bridging, followed by asymmetric break-
33 age between the two centromeres in a subsequent mitotic
34 division. Finally, it forms a stable large monocentric chro-
35 mosome with an inverted duplication contiguous to a distal
36 deletion and a small monocentric chromosome with a dele-
37 tion (Zuffardi et al. 2009).
38

Two possible mechanisms are currently proposed for the
formation of a dicentric chromosomal structure, the inter-
mediate product of the inv-dup-del rearrangement (Zuffardi
et al. 2009). One is a non-allelic homologous recombina-
tion (NAHR)-based mechanism. NAHR between segmen-
tal duplications with an inverted orientation produces a
dicentric chromosome, and it induces breakage between the
two centromeres during mitotic division. One of the repre-
sentative NAHR-mediated inv-dup-dels is chromosome 8p
inv-dup-del, which is mediated by homologous recombina-
tion between olfactory receptor-gene clusters (Shimokawa
et al. 2004; Yu et al. 2010; García-Santiago et al. 2015).
Since many 8p inv-dup-dels have been reported in unrelated
families, those that are NAHR-mediated are thought to arise
recurrently. In addition, NAHR between inverted repeats
within the olfactory receptor-gene clusters induces benign
polymorphic pericentric inversions. Meiotic recombination
within the inverted segment in heterozygotes of polymorphic
pericentric inversions produces a dicentric chromosomal
structure that serves as an intermediate of the inv-dup-dels
(Giglio et al. 2001).

A1 ✉ Hiroki Kurahashi
A2 kura@fujita-hu.ac.jp

A3 Extended author information available on the last page of the article

59 Another proposed mechanism for the generation of dicen-
60 tric chromosomal structures is a U-type exchange for the
61 formation of a sporadic inv-dup-del (Ballif 2003; Rowe et al.
62 2009; Yu and Graf 2010). This is based on a replication-
63 based mechanism involving template-switching between
64 sister chromatids. When a DNA replication fork encoun-
65 ters a replication block caused by different types of DNA
66 damage, DNA synthesis may stall and a DNA end will then
67 emerge. Break-induced replication then initiates at the site
68 of microhomology on the opposite strand forming a U-type
69 exchange between sister chromatids. Single stranded DNA
70 nearby can be a potential template for strand switching and
71 is usually present during lagging strand synthesis; it appears
72 in the uncoupling of helicase and polymerase even during
73 leading strand synthesis. Strand switching can facilitate a
74 DNA synthesis restart, which continues to the next fork or
75 as far as the telomere leading to the formation of dicen-
76 tric chromosomes. This series of events leading to an inv-
77 dup-del rearrangement is consistent with the concepts of
78 replication fork stalling and template switching (FoSTeS)
79 and microhomology-mediated break-induced replication
80 (MMBIR) (Zhang et al. 2009a, b). This pathway can lead to
81 a non-recurrent inv-dup-del rearrangement in a sequence-
82 independent manner.

83 In our present study, we further elucidated the mecha-
84 nism of dicentric chromosome formation, and the secondary
85 structural rearrangements that consequently arise, by analyz-
86 ing the breakpoint junction sequence of 10 cases of inv-dup-
87 del representing 9 different chromosome regions. Breakpoint
88 sequences found in common among the non-recurrent cases
89 suggested the involvement of the replication-based mecha-
90 nism in the formation of the dicentric chromosome. In addi-
91 tion, we obtained evidence of dynamic structural changes
92 from the dicentric chromosome to the terminal deletion with
93 or without adjacent inverted duplication during cell culture
94 of samples from miscarriage fetuses. Taken together, we
95 hypothesized from our present data that the replication stall
96 model for the formation of a dicentric chromosome followed
97 by a breakage-fusion-bridge (BFB) cycle is required for the
98 generation of an inv-dup-del rearrangement.

99 Materials and methods

100 Ethical statement

101 This study was approved by the Ethical Review Board for
102 Human Genome Studies at Fujita Health University. We
103 obtained informed consent from all of the participating
104 patients. All genetic experiments were carried out in accord-
105 ance with the relevant guidelines and regulations.

Subjects

106 We analyzed 10 patients harboring an inv-dup-del that had
107 been identified by initial standard chromosome banding and
108 subsequent cytogenetic microarray. The karyotypes of the
109 inv-dup-dels are summarized in Table 1. The breakpoints of
110 the inv-dup-dels in 2 patients (cases 9 and 10) were almost
111 identical and located at 8p, suggesting that they are recur-
112 rent. Two patients had a mosaic ring shaped chromosome
113 (cases 3 and 8). Case 5 harbored an inv-dup-del with an
114 additional triplication. Case 10 showed an inv-dup-del on
115 8p with an additional duplication of 8q. In addition, to better
116 understand the development of inv-dup-del rearrangement
117 from an intermediate dicentric chromosome, we analyzed
118 2 miscarriage fetuses (cases 11 and 12), whose karyotype
119 showed mosaic isodicentric chromosomes. 120

Copy-number-analysis by cytogenetic microarray analyses

121 Genomic DNA samples were isolated from peripheral
122 blood, cultured cells or chorionic villi using a Gentra Pure-
123 gene Tissue Kit (Qiagen, Hilden, Germany). To identify the
124 extent of the copy-number-alterations of the inv-dup-del, we
125 employed a CytoScan HD, 750 k Array (Affymetrix, Santa
126 Clara, CA) or Human Genome CGH Microarray (Agilent,
127 Santa Clara, CA) in accordance with the manufacturer's
128 instructions. Regions of copy-number-alteration were visu-
129 alized using Chromosome Analysis Suite 3.2 (Affymetrix)
130 or Genomics Workbench 7.0 (Agilent). 131 132

Copy-number-analysis by next generation sequencing (NGS)

133 In cases 11 and 12, we performed copy-number-analysis by
134 NGS. The isolation and purification of genomic DNA from
135 cultured cells or chorionic villi was carried out using a Gen-
136 tra Puregene Tissue Kit (QIAGEN). Genomic DNA samples
137 were diluted and amplified by whole-genome amplification
138 using SurePlex (Illumina, San Diego, CA). One nanogram
139 of each whole-genome amplified DNA sample was prepared
140 for NGS analysis. Shallow whole-genome sequencing was
141 performed for comprehensive copy-number-analysis using
142 the VeriSeq PGS Kit MiSeq (Illumina). The sequencing data
143 were analyzed using BlueFuse Multi Software (Illumina). 144 145

Breakpoint characterization by NGS

146 To identify the breakpoint junctions in our sporadic inv-
147 dup-del study cases, we carried out NGS analysis of
148 each patient's genomic DNA. Mate-pair whole-genome
149

Table 1 Patients information with inv-dup-dels

Sample no.	Chromosome	Karyotype	Genomic coordinates from microarray analysis	Copy-number-neutral region	Size (bp)	Microhomology (bp)
1	4p	-	arr[GRCCh37]4p16.3(71552_664410)X1.4p16.3p14(703668_36230853)X3	chr4:689,203-690,943	1741	3
2	4q	der(4)(pter→q37;q4.3::q34.3→31.3)	arr[GRCCh37]4q31.23q34.2(151058587_177382551)x3.4q34.2q35.2(177383079_190957473)x1	chr4:177,383,829-177,387,559	3728	2
3	9p	r(9)(:::p24→q44.3::)[27]45,XY,-9 [3]	arr[GRCCh37]9p24.3p24.1(203861_8216831)x1.9p24.1p21.1(8216910_31620128)x3	chr9:8,215,737-8,218,461	2725	0
4	9p	add(9)(p24)	arr[GRCCh37]9p24.3p23(214367_11573590)X1.9p23p13.1(12048553_39156954)X3	chr9:11,712,793-11,715,125	2333	- 4
5	10q	add(10)(q25.1)	arr[GRCCh37]10q26.12q26.3(122328262_132082817)X3-4.10q26.3(132942513_135404523)X1	chr10:132,878,450-132,880,484, chr10:122,306,763-122,307,064	2035, 303	2
6	11q	-	arr[GRCCh37]11q23.1q24.1(111612172_121578675)X3.11q24.1q25(121829034_134868407)X1	chr11:121,765,738-121,767,908	2167	3
7	18p	add(18)(p11.2)	arr[GRCCh37]18p11.32p11.31(14,316-3,458,388)x1.18p11.31p11.21(3,572,316-14,733,870)x3	chr18:3,492,546-3,494,355	1810	3
8	21q	r(21)[27]45,XX,-21 [2]/46,XX,?dic r(21) [1]	arr[GRCCh37]21q21.1q22.13(16832706_44518076)x3.21q22.3(44526182_48097372)x1	chr21:44,524,195-44,526,196	2001	0
9	8p	der(8)(p12→p23.1::p23.1→qter)	arr[GRCCh37]8p23.3p23.1(158048_6981988)x1.8p23.1p11.22(11945855_39451389)x3			
10	8p	der(8)(8qter→8q24.2::8p11.2→8p23.1::8p23.1→8qter)	arr[GRCCh37]8p23.3p23.1(158048_6999114)x18p23.1p11.22(12560781_39078328)x3.8q24.2.21q24.3(129285242_146295771)x3			

sequencing was performed to determine the breakpoints of the inverted duplication in the dicentric chromosome. Since the breakpoint junctions can have palindromic (inverted repeated) characteristic sequences, we generated mate-pair long libraries of 9 kb to minimize the loss of palindromic DNA molecules at the breakpoint junction during library preparation. These 9-kb mate-pair libraries were prepared using a Nextera Mate Pair Library Preparation Kit (Illumina) in accordance with the manufacturer's protocol. The libraries were sequenced with 101 bp-paired-end reads on a HiSeq 1500 platform (Illumina). Sequence reads were trimmed adapter sequences using NxTrim and mapped with BWA 0.7.10 against hg19 (Li and Durbin 2010). Subsequently, discordantly mapped paired-reads were extracted to detect chromosomal structural rearrangements using BreakDancer (Fan et al. 2014). Putative breakpoints produced by inverted duplications, triplications and terminal deletions were confirmed by visual inspection of NGS data using Integrative Genomics Viewer (IGV) (Thorvaldsdottir et al. 2013). The nucleotide sequences of the breakpoint junctions of the inverted duplications and triplications were determined by breakpoint-specific PCR and Sanger sequencing using an ABI3130xl sequencer (Life Technologies, Foster City, CA). The length of the inverted sequence homology at the between copy-number-gain and -loss was searched using a YASS sequence similarity search (Noe and Kucherov 2005). Default parameter setting was used for this analysis.

Product of conception karyotyping

Products of conception (POC) were analyzed for chromosome abnormalities using standard cell culture followed by Giemsa banding.

Results

Copy-number variation features in recurrent and non-recurrent inv-dup-dels

We employed a cytogenetic microarray to characterize the 10 inv-dup-del rearrangements in our study cohort. The copy-number-profile detected by SNP microarray showed a clear difference between the cases involving 8p23.1 (cases 9 and 10) and others (Fig. 1). The two 8p23.1 cases harbored a large copy-number-neutral region between the copy-number-gain and -loss regions (~ 5 Mb). The endpoints of these copy-number-neutral regions were found to be almost identical between the two subjects and located within the olfactory receptor (OR) gene clusters. In contrast, none of the eight sporadic inv-dup-del cases showed

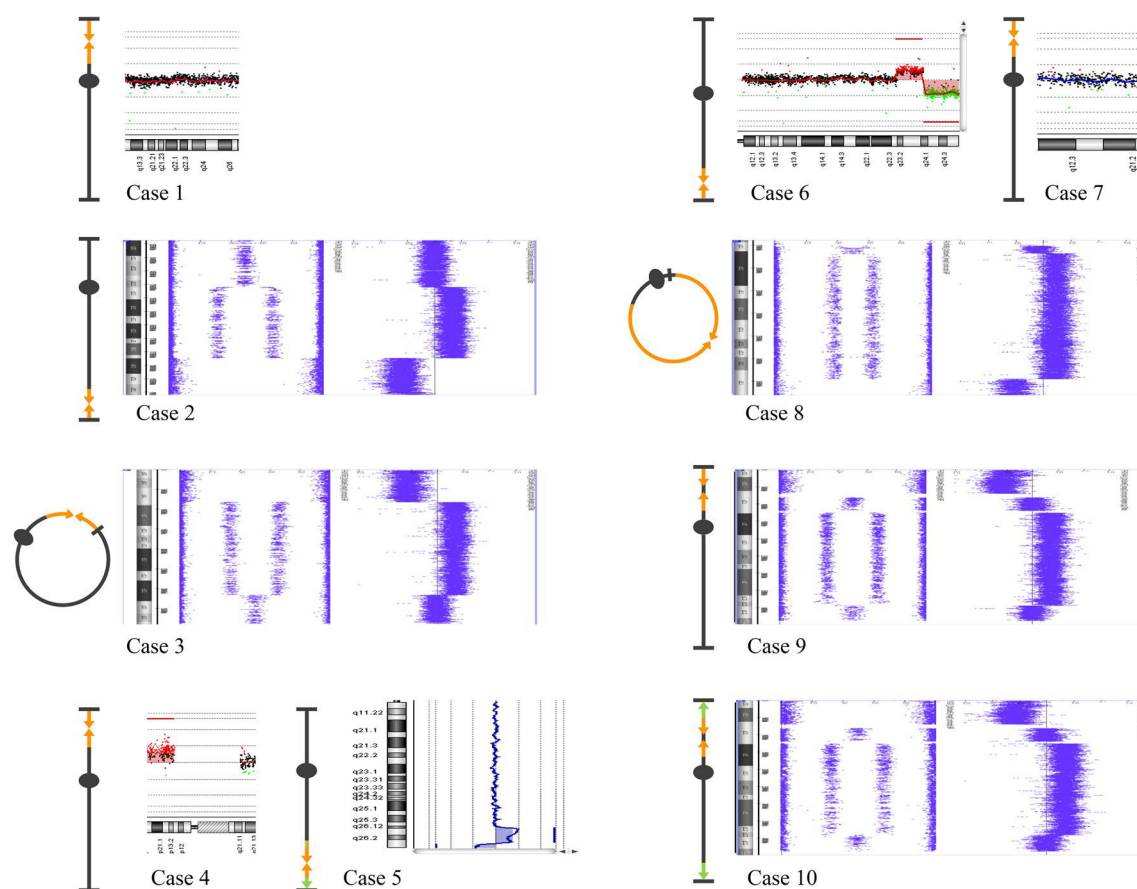


Fig. 1 Copy-number-profile of the inv-dup-dels determined by microarray. Copy-numbers were determined using an Affymetrix CytoScan microarray and visualized with ChAS software (Case 2, 3, 8, 9, 10). The upper blue plots show the signal for the weighted log 2 ratio. The lower plots indicate the B allele frequency. Copy-numbers were also determined using an Agilent CGH microarray and visual-

ized with Genomics Workbench (Case 1, 4, 5, 6, 7). The log 2 ratio of the genomic copy-number is also plotted and indicated by horizontal lines. Illustrative diagrams of chromosomal structure are shown at the left. Inverted duplications are shown by arrows with orange color. Other rearrangements are shown with green color

196 any detectable copy-number-neutral regions between the
197 copy-number-gain and -loss (cases 1–8; Fig. 1).

198 Breakpoint analysis of the non-recurrent 199 inv-dup-dels

200 Whole genome sequencing of the 9-kb mate-pair library
201 was performed to further analyze the breakpoints in our
202 eight study cases with non-recurrent inv-dup-del structures.
203 The inverted duplication structures were confirmed in each
204 case by the presence of a junction for the inverted orienta-
205 tion of the two copy-number-gain regions. The DNA frag-
206 ment incorporating the junction manifested a characteristic
207 volcano-like pattern in the mapping of the discordant reads
208 (Fig. 2). Some cases had telomeric repeat sequences at the
209 proximal end of the inverted duplication, i.e. mapped at the
210 proximal end of the copy-number-gain regions, reflecting
211 telomere healing of the breakage (data not shown). In the
212 case of ring chromosomes, the proximal end of the inverted

duplication possibly contained a 9q subtelomeric repeat
213 sequence (case 3) or 21q repetitive sequence (case 8), sug-
214 gesting that ring formation was another healing pathway
215 for the breakage (data not shown). Based on the fact that
216 inverted and non-inverted segment was fused in head-to-
217 head orientation and the chromosome end-like sequence
218 appeared at the other end of the inverted segment, the inv-
219 dup-del structures were confirmed in these cases.

220 Although high-resolution microarray did not detect
221 an intervening copy-number-neutral region between the
222 inverted and non-inverted segment, refined analysis of the
223 breakpoint junction sequences identified a small copy-num-
224 ber-neutral region at the junction in all of the cases with
225 a non-recurrent inv-dup-del (Fig. 2, red arrows). The size
226 of the copy-number-neutral regions ranged from 1741 to
227 3728 bp (Fig. 3, Table 1). Microhomologies from 1 to 3 bp
228 were found at breakpoint junctions between inverted and
229 non-inverted segment in 5 cases, but none were evident in 3
230

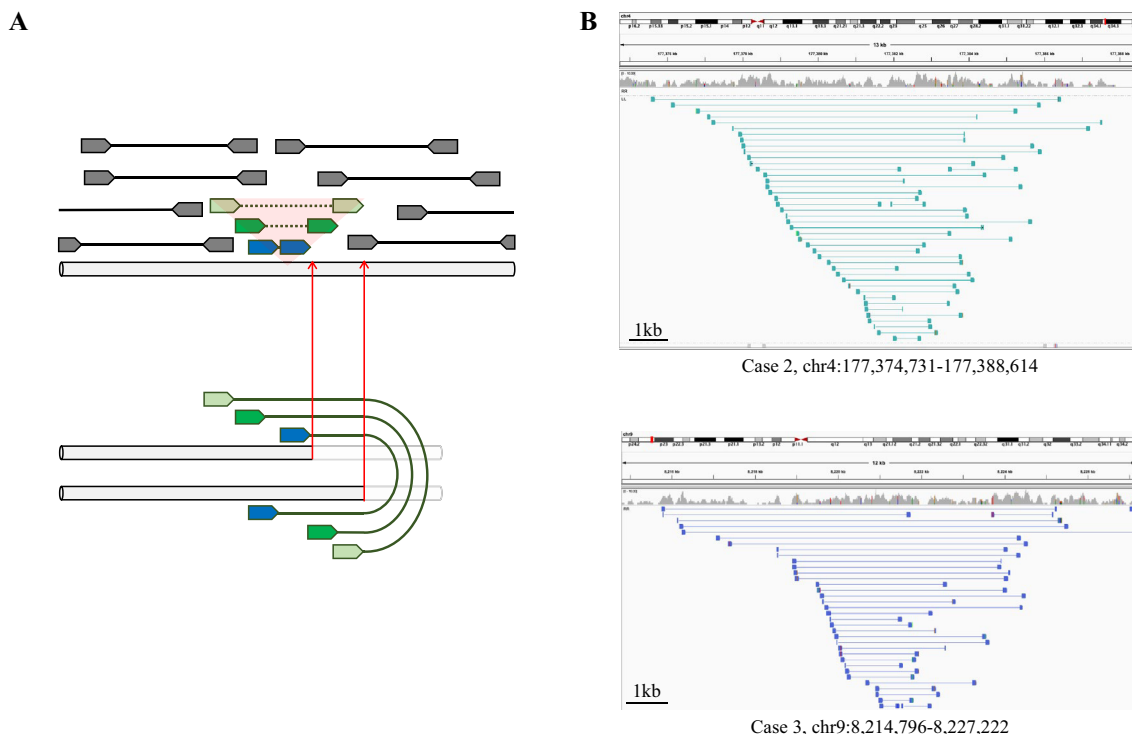
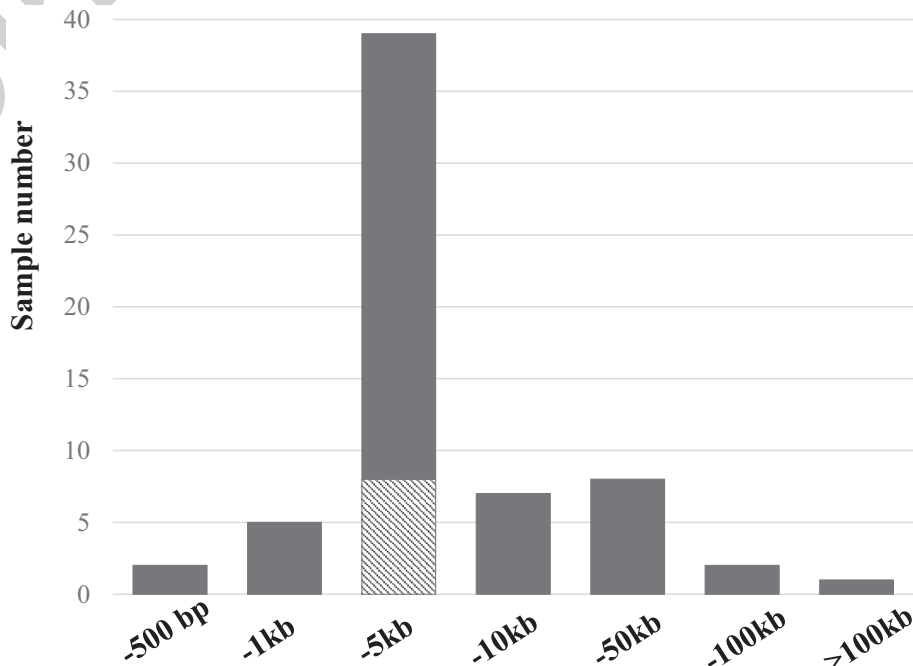


Fig. 2 Discordant reads at the junction of the dicentric chromosome. **a** Strategy for determining mate-pair sequences. The upper panel provides a schematic of the reference human genome structure. The lower panel depicts the assumed structure of the inverted duplication. Gray reads show normal paired-end reads, which were mapped in the forward and reverse direction to the reference genome. Green colored

reads indicate discordant reads, which were mapped in the same orientation. Red arrows indicate the putative breakpoints. **b** Mapping of mate-pair sequences on the reference human genome sequence. The region around the breakpoint of dicentric chromosome was shown using IGV browser. A characteristic volcano-like pattern could be observed

Fig. 3 Distribution of the lengths of the intervening copy-number-neutral regions. Bars indicate the number of analyzed cases in studies published from 2003 to 2014 (black bar) 4,5,15,16 and in this current study (hatched bar)

AQ1



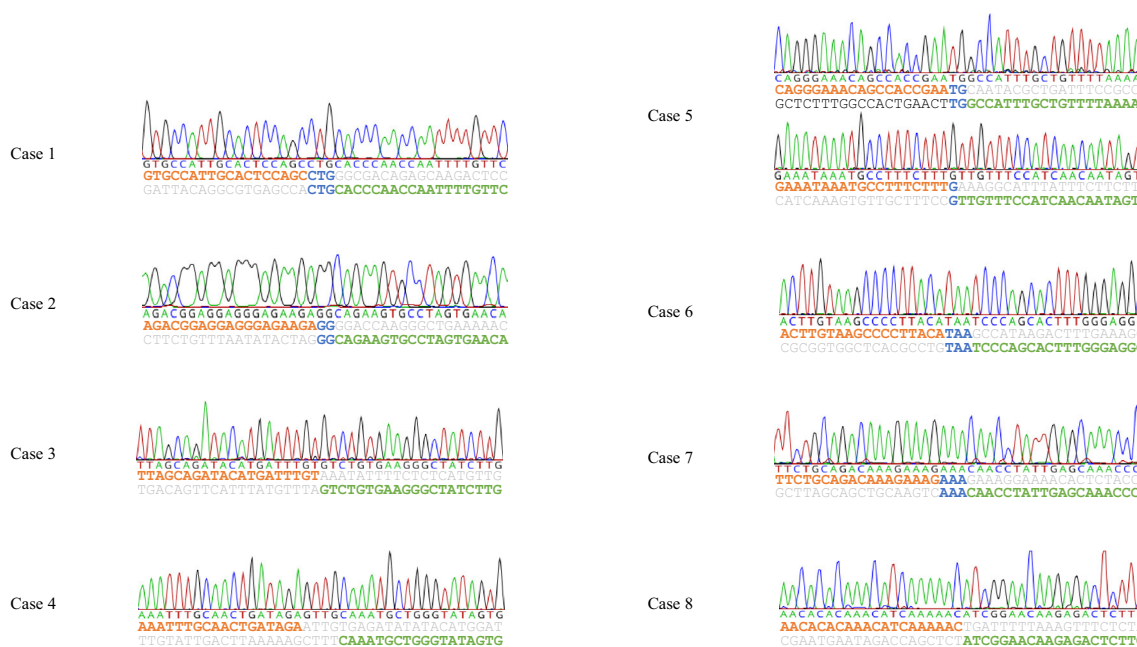


Fig. 4 Junction sequences of fold-back chromosomes. The orange and green characters indicate the plus and minus strands, respectively. Blue characters indicate homologous nucleotides. Gray characters indicate unknown nucleotide insertions

231 cases with the remaining subject carrying a 4 bp microinsertion
232 (Fig. 4, Table 1).

233 To investigate whether the initial formation of the dicentric
234 chromosome in our study subjects was caused by an inverted
235 repeat sequence at the breakpoint, we conducted
236 sequence similarity analysis around the breakpoint region.
237 Sequences with high similarity were found as expected in
238 the inverted orientation at the proximal and distal end of
239 the copy-neutral-region in the two recurrent 8p inv-dup-del
240 cases (case 9 and 10), suggesting that the breakpoints were
241 located within the olfactory receptor-gene clusters (Fig. 5).
242 In contrast, significant inverted repeat sequences were not
243 observed in any of the other inv-dup-del cases (cases 1–8).
244 It is likely that the inverted duplications were generated in
245 these eight individuals through repeat-independent, micro-
246 homology-based mechanisms, such as FoSTeS/MMBIR or
247 microhomology-mediated end joining (MMEJ).

248 Breakage of the dicentric chromosome to form 249 an inv-dup-del rearrangement

250 We additionally analyzed two fetal loss cases for which
251 molecular cytogenetic analysis revealed evidence of dicentric
252 chromosomes leading to inv-dup-del formation. Case
253 11 underwent a miscarriage after 8 gestational weeks. Kar-
254 yotyping of her POC sample revealed that all clones har-
255 bored add(13)(q22). Furthermore, derivative chromosome
256 13 showed a mirror structure. NGS chromosome analysis

257 further revealed a copy-number-gain adjacent to a deletion
258 on chromosome 13 (Fig. 6a). Based on these results, we con-
259 cluded that the derivative chromosome was an isodicentric
260 chromosome 13 (idic(13)). When we used uncultured POC
261 cells for NGS copy-number-analysis, we identified an inv-
262 dup-del pattern on the chromosome 13 which was likely to
263 have derived from a breakage of idic(13). Intriguingly, the
264 endpoint of the deletion of the two samples did not show
265 concordance. If the inv-dup-del was a breakage product of
266 idic(13), the deletion endpoint should be concordant, but the
267 position of the deletion endpoint in inv-dup-del was more
268 proximal (see “Discussion”).

269 Case 12 (Fig. 6b) underwent a stillbirth at gestational
270 week 34 due to multiple fetal anomalies. We analyzed three
271 independent cultures of her POC sample. Karyotyping
272 from one of the cultures revealed a 46,XX,del(15)(q26.1)
273 [46]/46,XX,psu idic(15)(q26.3) mosaicism [8]. To analyze
274 for a possible breakage of the idic(15) chromosome, we
275 performed an SNP array of the same sample. We observed
276 a stepwise copy-number-loss on chromosome 15q. It was
277 likely that the distal breakpoint corresponded to the idic(15)
278 breakpoint whilst the proximal breakpoint corresponded to
279 a terminal deletion endpoint or inv-dup-del endpoint. We
280 performed karyotype analysis of another culture which
281 revealed 46,XX,add(15)(q26.1)[24]/46,XX,del(15)(q26.1)
282 [19]/46,XX,psu idic(15)(q26.3)[14]. As was the case with
283 the first culture, an SNP array indicated a stepwise copy-
284 number-loss on chromosome 15q. The distal breakpoint was

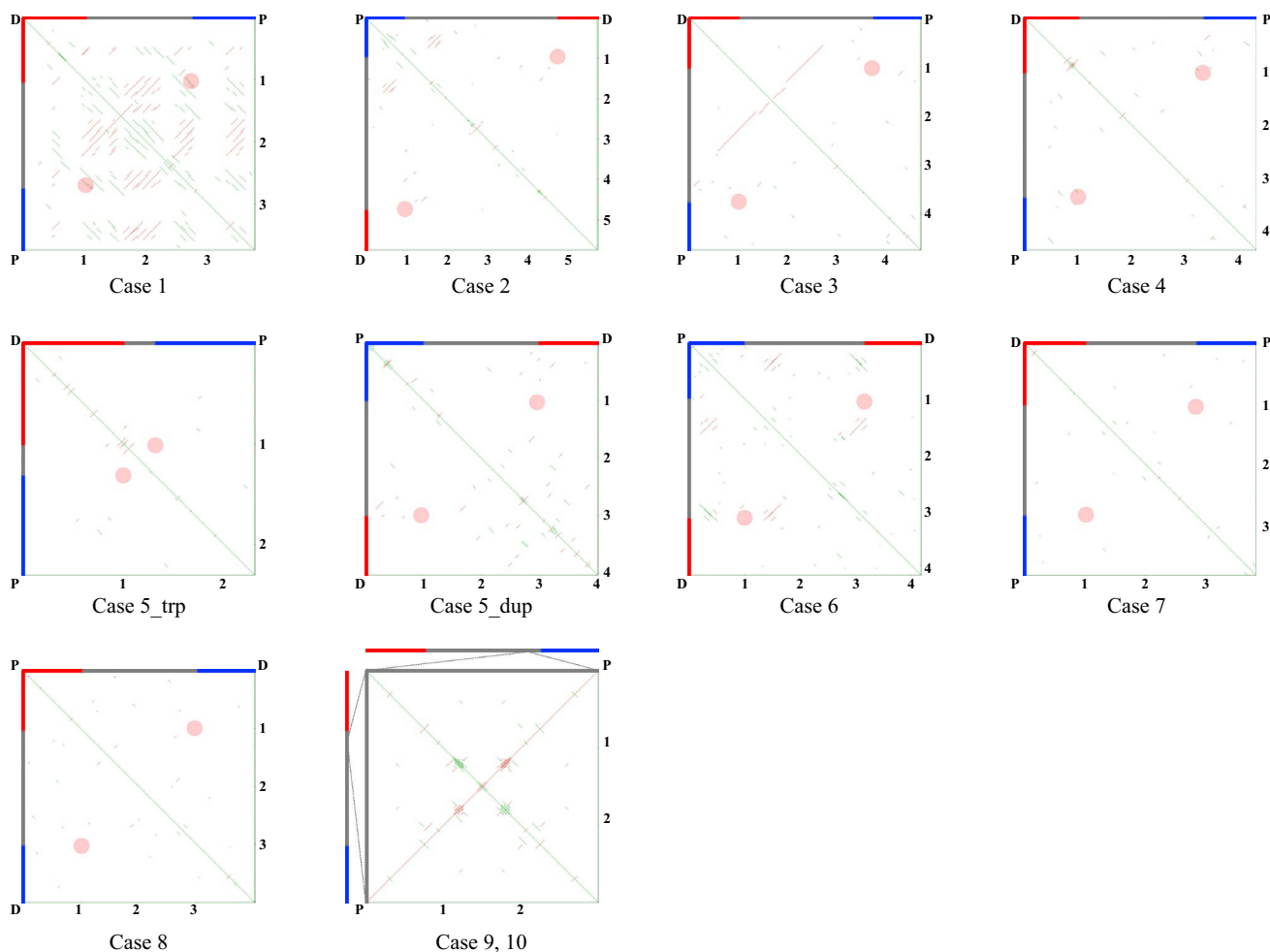


Fig. 5 Sequence similarity analysis of the small intervening regions in our case subjects. Intervening regions which covered ± 1 kb around the copy-number-neutral region are schematically represented on both axes. Black bars indicate copy-number-neutral regions, while blue and red bars indicate copy-number-gain and -loss, respectively. We defined the default parameter values for this analysis. Green line indicates a direct repeat and pink line denotes an inverted repeat. Pink

circles indicate sequence similarities between the proximal and distal breakpoints. With regard to cases 9 and 10, parts of the two olfactory receptor-gene cluster regions (REPD[hg19]chr8:7,466,506-7,468,005 and REPP[hg19]chr8:12,466,006-12,467,505) were merged and used for this analysis. P, proximal side; D, distal side. The scale represents size in 1 kb

285 found to be identical to that of the first culture, whilst the
 286 position of the proximal breakpoint differed (see “**Discus-**
 287 **sion**”). In addition, a copy-number-gain of chromosome
 288 17q was observed, suggesting that the add(15)(q26.1) was
 289 der(15)t(15;17)(q26;q21). We also performed SNP array
 290 analyses of a frozen uncultured sample for case 12, which
 291 indicated a copy-number-gain on chromosome 9q in addition
 292 to a stepwise copy-number-loss of chromosome 15q,
 293 which might be derived from a line with 46,XX,der(15)
 294 t(9;15)(q34;q26). In summary, the unstable idic(15) chro-
 295 mosome may be susceptible to DNA breakage, leading not
 296 only to inv-dup-del rearrangement, but also to a terminal
 297 deletion such as del(15)(q26.1), or other unbalanced trans-
 298 locations like der(15)t(15;17)(q26;q21) or der(15)t(9;15)
 299 (q34;q26).

Discussion

We conducted our current molecular cytogenetic study to
 clarify how an inv-dup-del rearrangement is generated. We
 carried out the breakpoint junction analysis of dicentric
 chromosomes and a follow-up survey of secondary rear-
 rangements that arose due to these dicentric chromosomes.

Involvement of a replication-based mechanism in the formation of a U-type dicentric chromosome

SNP microarray data showed a significant difference
 between recurrent and non-recurrent inv-dup-dels. Recur-
 rent inv-dup-dels harbor large copy-number neutral region
 between the copy-number-gain and -loss. In contrast,

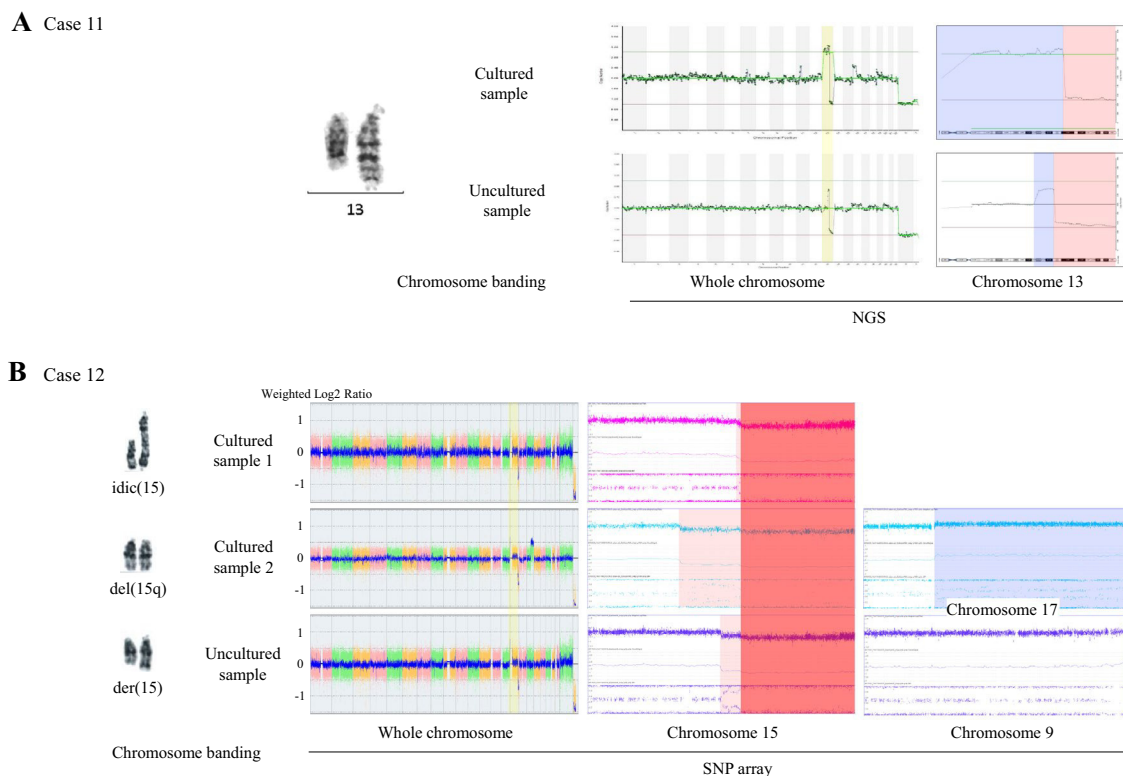


Fig. 6 Chromosome conformation changes during cell culture. Various chromosome analyses of cases 11 and 12 indicating that dicentric chromosomes in both subjects led to secondary structural rearrangements. **a** Case 11 harbors a chromosomal abnormality on chromosome 13. The upper panel shows a cultured sample and the lower panel shows an uncultured sample. Chromosome 13 was painted with a yellow signal. Copy-number-alterations are indicated in blue

(copy-number-gain) and red (copy-number-loss). **b** Case 12 harbors chromosomal abnormalities on chromosomes 9, 15 and 17. The upper and middle panels show cultures of sample 1 and 2, respectively. The lower panel shows an uncultured sample. Chromosome 15 was painted with a yellow signal. Copy-number-alterations are indicated in blue (copy-number-gain) or red (copy-number-loss). In cultured sample 2, chromosome banding revealed three different karyotypes

312 non-recurrent sporadic inv-dup-dels do not have copy-number
 313 neutral region. This implicates mechanism leading to
 314 the formation of a dicentric chromosome might be differ-
 315 ent. The endpoints of copy-number-neutral regions were
 316 located within the OR gene clusters. This suggested that the
 317 repetitive nature of OR gene clusters was involved in the
 318 development of the recurrent inv-dup-dels in cases 9 and
 319 10. NAHR between the OR genes may possibly underlie
 320 the most common recurrent inv-dup-del (Giglio et al. 2001;
 321 García-Santiago et al. 2015). Although we used high-res-
 322 olution microarray in our current study, any sporadic inv-
 323 dup-del cases were not able to detect copy-number-neutral
 324 regions between the copy-number-gain and -loss. It was
 325 previously proposed that a symmetrical U-type exchange is
 326 the underlying mechanism leading to non-recurrent dicentric
 327 chromosome formation (Rowe et al. 2009). In our current
 328 study however, when we analyzed junction sequences at
 329 a nucleotide resolution, asymmetrical dicentric structures
 330 with an intervening sequence were observed. The presence
 331 of microhomologies or microinsertions at the fusion points
 332 of inverted and non-inverted segments (Fig. 4) indicated that

the inverted duplications were generated through repeat-
 independent, microhomology-based mechanisms, such as
 FoStES/MMBIR or microhomology-mediated end joining.

In a previous report, Hermetz et al., proposed a fold-
 back model for the formation of dicentric chromosomes
 via a double-strand break (DSB) repair pathway (Hermetz
 et al. 2014). In this model, a DSB undergoes resection,
 which generates a long 3' single-stranded DNA (ssDNA)
 overhang. This in turn promotes intrastrand pairing to the
 short inverted repeat via a homology-based mechanism lead-
 ing to the formation of a dicentric chromosome. Notably
 however, we did not observe any homology between both
 ends of the intervening copy-number-neutral region at the
 boundary of the inverted and non-inverted segments in our
 current cases (Fig. 5). Further, the size of the intervening
 sequence showed a unique distribution, ranging from 1 to
 5 kb in our analyzed cases. When we increased the num-
 ber of inv-dup-del cases using data from previous studies in
 which where the breakpoints of inv-dup cases were analyzed
 at a nucleotide resolution (Ballif 2003; Bonaglia et al. 2008;

333
 334
 335
 336
 337
 338
 339
 340
 341
 342
 343
 344
 345
 346
 347
 348
 349
 350
 351
 352

Rowe et al. 2009; Hermetz et al. 2014), the size of the intervening sequence peaked at 1–5 kb (Fig. 3).

Uncoupling of the helicase and polymerase leads to a single-stranded DNA in the leading strand, which when stalled can produce an uncoupled nascent lagging strand under certain conditions. Such single-stranded DNA can be up to 3–5 kb in length, depending on the nature of the replication fork block (Lopes et al. 2006). It is likely that the tight distribution of these sizes may reflect a resolution of the replication fork block through template switching within the same replication fork. Interestingly, when we increased our current sample number by including prior data from the literature, another low-pitched distribution curve appeared up to 100 kb (Fig. 3). This possibly reflects a resolution of the stalled replication fork by an adjacent fork which may be distant in a genomic sense but in close proximity within the nucleus. We are thus proposing a replication stall model as a mechanism of formation for U-type dicentric chromosomes.

371 **Dicentric chromosome instability results** 372 **in secondary rearrangements**

In general, dicentric chromosome breakages would produce two reciprocal products: inv-dup-del chromosomes and terminal deletion chromosomes. We observed in our present series that two POC samples had a mosaicism of cells with dicentric chromosomes and inv-dup-del or other rearrangements associated with the dicentric chromosome. This suggested that the formation of the dicentric chromosome and other related rearrangements including the inv-dup-del were sequential events. The breakage of an unstable dicentric chromosome leads to the formation of not only an inv-dup-del chromosome and terminal deletion chromosome after stabilization through telomere healing of the broken ends, but also results in various structural rearrangements via stabilization by telomere capture.

Interestingly, our SNP microarray analysis of case 11 indicates that the endpoint of the deletion of the possible inv-dup-del was more proximal to that of the idic(13) chromosome. This suggested that the inv-dup-del chromosome might have originated from a terminal deletion chromosome reciprocal of the inv-dup-del chromosome derived from a breakage of idic(13). The terminal deletion chromosome might form a U-type dicentric chromosome leading to the second inv-dup-del chromosome having the proximal deletion endpoint. Likewise, SNP microarray data for case 12 indicated a more proximal endpoint of der(15) to that of the idic(15). This also suggested that the der(15) chromosome might have been generated in the second round of breakage of the dicentric chromosome. Dicentric chromosome must be stable and segregate to daughter cells correctly since one of the centromeres is functionally silenced (Stimpson

et al. 2010). However, just after the formation of a U-type dicentric chromosome, both of the centromeres might be still active and the dicentric chromosomes are therefore unstable, leading to secondary rearrangements into various derivative chromosomes (Soler et al. 2003; Chabchoub et al. 2007; Schlade-Bartusiak et al. 2013; Pedurupillay et al. 2014). Hence, we can observe multiple clones with different derivative chromosomes.

Finally, in case 12, two types of translocation chromosomes related to the idic(15) chromosome were observed. In general, an unbalanced translocation would originate from segregation of the one of the translocation chromosomes from a balanced translocation carrier. However, our current results suggest that if the unbalanced translocation arises as de novo, it might originate from breakage of dicentric chromosome followed by telomere capture using the other chromosomal end.

In summary, a dicentric chromosome is so unstable that it leads to the generation of an inv-dup-del chromosome, as well as a reciprocal terminal deletion through telomere healing and also an unbalanced translocation via telomere capture.

Acknowledgements We thank the patients and their families for participating in this study. This study was supported by a Grant-in-Aid for Scientific Research from the Ministry of Education, Culture, Sports, Science, and Technology of Japan (17K11259 to T.K., 15H04710 and 24390085 to H.K.) and from the Ministry of Health, Welfare and Labor (16ek0109067h0003 to H.K.).

Author contributions TK—participated in the design of the study, carried out the molecular biology work, and drafted the manuscript. HI—participated in the design of the study, carried out the molecular biology work. SuM—participated in the design of the study, carried out the molecular biology work. FS—participated in the design of the study, carried out the molecular biology work. YN—participated in the design of the study, carried out the molecular biology work. YS—participated in the design of the study, carried out the molecular biology work. AK—participated in the design of the study, carried out the molecular biology work. KK—participated in the design of the study, carried out the molecular biology work. SeM—participated in the design of the study. YM—participated in the design of the study. TY—participated in the design of the study. MS—participated in the design of the study. TY—participated in the design of the study, carried out the molecular biology work. SH—participated in the design of the study. TI—participated in the design of the study. MO—participated in the design of the study. HK—Coordinated and conceived the study, being involved in the critical revision of the manuscript for important intellectual content.

Funding Authors must give full details about the funding of any research relevant to their study, including sponsor names and explanations of the roles of these sources in the preparation of data or the manuscript.

Data availability All data analyzed during this study are included in this published article.

456 **Compliance with ethical standards**457 **Conflict of interest** The authors declare no competing interests.458 **Ethical approval** This study was approved by the Ethical Review Board
459 for Human Genome Studies at Fujita Health University. The written
460 informed consent was obtained from patients. All experiments were
461 carried out in accordance with the relevant guidelines and regulations.462 **Informed consent** We have obtained consent to participate in the study.
463 We have obtained consent to publication in the study.464 **References**

- 465 Ballif BC (2003) Monosomy 1p36 breakpoint junctions suggest pre-
466 meiotic breakage-fusion-bridge cycles are involved in generating
467 terminal deletions. *Hum Mol Genet* 12:2153–2165. <https://doi.org/10.1093/hmg/ddg231>
- 468 Bonaglia MC, Giorda R, Massaglia A et al (2008) A familial inverted
469 duplication/deletion of 2p25.1–25.3 provides new clues on the
470 genesis of inverted duplications. *Eur J Hum Genet* 17:179–186.
471 <https://doi.org/10.1038/ejhg.2008.160>
- 472 Chabchoub E, Rodriguez L, Galan E et al (2007) Molecular charac-
473 terisation of a mosaicism with a complex chromosome rearrange-
474 ment: evidence for coincident chromosome healing by telomere
475 capture and neo-telomere formation. *J Med Genet* 44:250–256.
476 <https://doi.org/10.1136/jmg.2006.045476>
- 477 Fan X, Abbott TE, Larson D, Chen K (2014) BreakDancer: Identifi-
478 cation of genomic structural variation from paired-end read
479 mapping. *Curr Protoc Bioinformatics* 45:15.6.1–11. <https://doi.org/10.1002/0471250953.bi1506s45>
- 480 García-Santiago FA, Martínez-Glez V, Santos F et al (2015) Analysis
481 of invdupdel(8p) rearrangement: clinical, cytogenetic and molecu-
482 lar characterization. *Am J Med Genet* 167A:1018–1025. <https://doi.org/10.1002/ajmg.a.36879>
- 483 Giglio S, Broman KW, Matsumoto N et al (2001) Olfactory receptor-
484 gene clusters, genomic-inversion polymorphisms, and common
485 chromosome rearrangements. *Am J Hum Genet* 68:874–883. <https://doi.org/10.1086/319506>
- 486 Hermetz KE, Newman S, Conneely KN et al (2014) Large inverted
487 duplications in the human genome form via a fold-back mech-
488 anism. *PLoS Genet* 10:e1004139–e1004214. <https://doi.org/10.1371/journal.pgen.1004139>
- 489 Li H, Durbin R (2010) Fast and accurate long-read alignment with
490 Burrows-Wheeler transform. *Bioinformatics* 26:589–595. <https://doi.org/10.1093/bioinformatics/btp698>
- 491 Lopes M, Foiani M, Sogo JM (2006) Multiple mechanisms control
492 chromosome integrity after replication fork uncoupling and
493 restart at irreparable UV lesions. *Mol Cell* 21:15–27. <https://doi.org/10.1016/j.molcel.2005.11.015>
- 494 Noe L, Kucherov G (2005) YASS: enhancing the sensitivity of DNA
495 similarity search. *Nucleic Acids Res* 33:W540–W543. <https://doi.org/10.1093/nar/gki478>

- Pedurupillay CRJ, Misceo D, Gamage TH et al (2014) Post-zygotic
breakage of a dicentric chromosome results in mosaicism for
a telocentric 9p marker chromosome in a boy with develop-
mental delay. *Gene* 533:403–410. <https://doi.org/10.1016/j.gene.2013.09.090>
- Rowe LR, Lee J-Y, Rector L et al (2009) U-type exchange is the
most frequent mechanism for inverted duplication with terminal
deletion rearrangements. *J Med Genet* 46:694–702. <https://doi.org/10.1136/jmg.2008.065052>
- Schlade-Bartusiak K, Tucker T, Safavi H et al (2013) Independent
post-zygotic breaks of a dicentric chromosome result in mosai-
cism for an inverted duplication deletion 9p and terminal dele-
tion 9p. *Eur J Med Genet* 56:229–235. <https://doi.org/10.1016/j.ejmg.2013.01.013>
- Shimokawa O, Kurosawa K, Ida T et al (2004) Molecular characteriza-
tion of inv dup del(8p): analysis of five cases. *Am J Med Genet*
128A:133–137. <https://doi.org/10.1002/ajmg.a.30063>
- Soler A, Sánchez A, Carrió A et al (2003) Fetoplacental discrepancy
involving structural abnormalities of chromosome 8 detected
by prenatal diagnosis. *Prenat Diagn* 23:319–322. <https://doi.org/10.1002/pd.590>
- Stimpson KM, Song IY, Jauch A et al (2010) Telomere disruption
results in non-random formation of de novo dicentric chro-
mosomes involving acrocentric human chromosomes. *PLoS*
Genet 6:e1001061–e1001119. <https://doi.org/10.1371/journal.pgen.1001061>
- Thorvaldsdottir H, Robinson JT, Mesirov JP (2013) Integrative Genom-
ics Viewer (IGV): high-performance genomics data visualiza-
tion and exploration. *Brief Bioinform* 14:178–192. <https://doi.org/10.1093/bib/bbs017>
- Weckselblatt B, Rudd MK (2015) Human structural variation: mech-
anisms of chromosome rearrangements. *Trends Genet*. <https://doi.org/10.1016/j.tig.2015.05.010>
- Yu S, Graf WD (2010) Telomere capture as a frequent mechanism for
stabilization of the terminal chromosomal deletion associated with
inverted duplication. *Cytogenet Genome Res* 129:265–274. <https://doi.org/10.1159/000315887>
- Yu S, Fiedler S, Stegner A, Graf WD (2010) Genomic profile of copy
number variants on the short arm of human chromosome 8. *Eur J*
Hum Genet 18:1114–1120. <https://doi.org/10.1038/ejhg.2010.66>
- Zhang F, Carvalho CMB, Lupski JR (2009a) Complex human chro-
mosomal and genomic rearrangements. *Trends Genet* 25:298–307.
<https://doi.org/10.1016/j.tig.2009.05.005>
- Zhang F, Khajavi M, Connolly AM et al (2009b) The DNA replication
FoSTeS/MMBIR mechanism can generate genomic, genic and
exonic complex rearrangements in humans. *Nat Genet* 41:849–
853. <https://doi.org/10.1038/ng.399>
- Zuffardi O, Bonaglia M, Ciccone R, Giorda R (2009) Inverted dupli-
cations deletions: underdiagnosed rearrangements?? *Clin Genet*
75:505–513. <https://doi.org/10.1111/j.1399-0004.2009.01187.x>

Publisher's Note Springer Nature remains neutral with regard to
jurisdictional claims in published maps and institutional affiliations.

Affiliations

Takema Kato¹ · Hidehito Inagaki¹ · Syunsuke Miyai¹ · Fumihiko Suzuki¹ · Yuki Naru¹ · Yasuko Shinkai¹ · Asuka Kato¹ · Kazuo Kanyama¹ · Seiji Mizuno² · Yukako Muramatsu³ · Toshiyuki Yamamoto⁴ · Mitsuhsa Shinya^{5,6} · Yukiko Tazaki^{5,6} · Sayuri Hiwatashi^{5,6} · Toshiro Ikeda^{5,6} · Mamoru Ozaki⁷ · Hiroki Kurahashi^{1,2}

Takema Kato
takema@fujita-hu.ac.jp

Hidehito Inagaki
hinagaki@fujita-hu.ac.jp

Syunsuke Miyai
smiyai@fujita-hu.ac.jp

Fumihiko Suzuki
fsuzuki@fujita-hu.ac.jp

Yuki Naru
y.naru@ovus.co.jp

Yasuko Shinkai
y.shinkai@ovus.co.jp

Asuka Kato
asukak@fujita-hu.ac.jp

Kazuo Kanyama
kanyamk@labcorp.com

Seiji Mizuno
seiji_mizuno@aichi-colony.jp

Yukako Muramatsu
murayuka@med.nagoya-u.ac.jp

Toshiyuki Yamamoto
yamamoto.toshiyuki@twmu.ac.jp

Mitsuhsa Shinya
m-shinya@m3.kufm.kagoshima-u.ac.jp

Yukiko Tazaki
tazaki-y@m.kufm.kagoshima-u.ac.jp

Sayuri Hiwatashi
sayuri1030@yahoo.co.jp

Toshiro Ikeda
ikedam2@m2.kufm.kagoshima-u.ac.jp

Mamoru Ozaki
m-ozaki@kanazawa-med.ac.jp

¹ Division of Molecular Genetics, Institute for Comprehensive Medical Science, Fujita Health University, 1-98 Dengakugakubo, Kutsukake-cho, Toyoake, Aichi 470-1192, Japan

² Department of Clinical Genetics, Central Hospital, Aichi Developmental Disability Center, Kasugai, Kasugai, Japan

³ Department of Pediatrics, Nagoya University Graduate School of Medicine, Nagoya, Japan

⁴ Institute of Medical Genetics, Tokyo Women's Medical University, Shinjuku, Japan

⁵ Genetic Counseling Room, Kagoshima University Hospital, Kagoshima, Japan

⁶ Department of Obstetrics and Gynecology, Faculty of Medicine, Kagoshima, Japan

⁷ Division of Genomic Medicine, Department of Advanced Medicine, Medical Research Institute, Kanazawa Medical University, Uchinada, Japan